Identification of Intoxicated Driving Using Steering Wheel Signals and Improving Lateral Control in Semi-autonomous and Autonomous Vehicles

by

Mehran Shirazi

M.Sc., Isfahan University of Technology, 2009

B.Sc., Isfahan University of Technology, 2006

Thesis Submitted in Partial Fulfillment of the
Requirements for the Degree of
Doctor of Philosophy

in the
School of Mechatronic Systems Engineering
Faculty of Applied Sciences

SIMON FRASER UNIVERSITY

Summer 2018

Approval

Name:	**Mehran Shirazi**
Degree:	**Doctor of Philosophy**
Title:	**Identification of Intoxicated Driving Using Steering Wheel Signals and Improving Lateral Control in Semi-autonomous and Autonomous Vehicles**
Examining Committee:	**Chair: Krishna Vijayaraghavan** Associate Professor
	Ahmad Rad Senior Supervisor Professor, Mechatronic Systems Engineering
	Mehrdad Moallem Supervisor Professor, Mechatronic Systems Engineering
	Gary Wang Supervisor Professor, Mechatronic Systems Engineering
	Carlo Menon Internal Examiner Professor
	Mo Jamshidi External Examiner Lutcher Brown Endowed Chair and Professor Department of Electrical and Computer Engineering University of Texas at San Antonio
Date Defended/Approved:	August 22, 2018

Abstract

The studies reported in this thesis focus on specific problems in detection of intoxicated driving, improving the performance of the vehicle when an intoxicated driver is controlling the vehicle, and designing autonomous lateral controllers.

In the first phase of this study, we apply system identification techniques on the steering wheel control behavior of the driver to present two models to describe the behaviors of sober and drunk drivers. Then we use these models and online identification methods to detect intoxicated driving from steering wheel data and vehicle lateral position.

In the second part of this thesis, we present the idea of improving the steering action of intoxicated drivers by adding serial and parallel controllers to the system while the driver is in the loop. In the first proposed algorithm, the steering signal coming from the steering wheel is fed to a serial controller. The output of the controller becomes the actual steering of the car. In the second suggested algorithm, the output of an independent lateral controller is added to the control signal generated by the human driver.

In the third phase, several look-ahead lateral controllers are designed to maintain the vehicle in the center of the lane when the driver is removed from the system. Among the designed controllers are a novel, simple fused neural-network controller, introduced by our group, and a recently introduced robust adaptive controller which applies $\mathcal{L}_1$ adaptive control theory on vehicles for the first time. The designed controllers are tested in challenging scenarios including wind gusts, road banking, icy roads, vehicle parameter uncertainties, and measurement noise, all present at the same time.

Finally, longitudinal controllers are studied, designed, and combined with the previously designed lateral controllers to complete the control subsystem of autonomous vehicles.

Keywords: Driver Modeling; Intoxicated Driving Detection; Driver Assistance Systems; Lateral Control; Longitudinal Control; $\mathcal{L}_1$ Adaptive Control

To my best friend, dear Zhila

Acknowledgements

I wish to express my sincere appreciation to those who have contributed to this thesis and supported me in one way or the other during this amazing journey.

First, I would like to thank my senior supervisor, dear Professor **Ahmad Rad**, for giving me the opportunity to be part of his team and start a PhD program in SFU, for supporting me, for letting me experience and do research on anything I liked, for being nice, caring and understanding, for all the Friday morning meetings where we had great discussions on research and life, for all the priceless advice, for being a different professor and letting me be a different graduate student, for everything I learned from him, for editing my papers and thesis, for his patience, motivation, and enthusiasm, for his guidance, and for everything he has done for me in all these years.

Dear Professor **Gary Wang**, thank you very much for being so nice to us. You had a great positive influence on our lives. We can never be thankful enough for all you did for us. We will always consider you as part of our family. Academia lacks profs like you. You are a great human being, and you are one of my role models. It was a great honor to have you in my supervisory committee. Thank you very much for your great feedback and comments. They definitely improved the quality of this work.

Dear Professor **Carlo Menon**, you might not know how much you helped me shape my career, and find what I enjoy the most in life, which is teaching. I will be forever thankful to you. Thank you very much for teaching me how to teach, for giving me teaching opportunities, for encouraging and supporting me, for all the time you spent to talk to me during your busy schedule, for all your nice words during last 8 years which gave me hope and motivation, and for being awesome! You are my other role model.

Dear Professor **Mehrdad Moallem**, you are one of the best professors I have met in my life. I always wished I could find an opportunity to work with you. I consider myself very lucky that I found the opportunity to be in the same committee meetings with you, where I learned a lot about that aspect of academia from you. Thank you! I always

admire your attitude towards others. You are very respectable and professional, and you deserve to have the highest positions in the university.

Dear Professor **Mo Jamshidi**, thank you very much for accepting to be my external examiner, for reviewing my dissertation promptly, for giving valuable feedback, and for participating in the defense session even though you were on vacation. I will always be proud that you were my examiner.

Dear Dr. **Krishna Vijayaraghavan**, thank you very much for accepting to be the chair of my defense session, and for your comments at the end of the session.

Friedrich Nietzsche says "Was mich nicht umbringt macht mich stärker." I would like to thank Dr. G. who did everything he could to destroy my career and my life. He almost succeeded, but he did not. Although he used many different methods to harass me for years, and consequently I became depressed and even suicidal for a while, I got up again with the help of the other lovely people mentioned here, and now I feel way happier and stronger than ever. I thank you, Dr. G, for this. By the way, you are a failure as a human being.

Dear Professor **Mehrdad Saif**, getting to know you was a great privilege. Thank you very much for supporting the students who wanted to be treated fairly. Also, thanks a million for the message you sent me after you moved to Windsor. That message made me feel more determined to defend the rights of graduate students and assured me that I was on the right track.

Dear Dr. **Atousa Hajshirmohammadi**, thank you very much for letting us stay at your place when we arrived in Canada, and for all the kindness of you and your family. You were the first person we talked to the night we came to Vancouver, and you were so nice that it felt like home here from that very first night.

I would like to thank professors in Isfahan University of Technology, especially dear Dr. **Saeed Hosseinnia**, dear Dr. **Farid Sheikholeslam**, dear Dr. **Maryam Zekri**, and dear Dr. **Yadollah Zakeri** who inspired me to continue my studies in Control Theory. I also thank Dr. **Mahmoud Modarres Hashemi** who gave me many great

opportunities as the representative of students. We had great conservations which prepared me for getting more serious leadership roles.

I also thank the **anonymous reviewers** of our papers for their useful suggestions. Special thanks to reviewer #2 for the very candid critical insights. You are the best example to demonstrate how negative feedback can improve the performance (quality) of a system (paper).

Dear Dr. **Javier Sanchez-Medina**, you are an awesome professor and friend. You were always very kind to me and helped me learn a lot about intelligent transportation and its history. I enjoyed every single podcast we made together. Thank a lot for giving me the opportunity. You kindly offered me accommodation during ITSC. Although I could not attend that conference (which will remain one of my regrets forever), I will never forget your kindness.

Dear **Winnie Lu**, you are a fantastic GPA. I can never thank you enough for the things you did for me. Most importantly, you helped me a lot when many unexpected problems happened before my defense. I will never forget it, my savior angel. I wish you the best wherever you go.

Dear **Jennifer Coffey**, thank you very much for all your help during my studies. You were always very patient, and always found the best solutions for the problems very quickly. We missed you when you left the department. However, you were too good for MSE.

PhD students often talk about loneliness during the course of their study, but this is something which I never experienced in Vancouver. A heartfelt thanks to all my friends who made the PhD experience something special for me.

Dear (soon to be a doctor) **Prabjit**, my thesis writing buddy, thank you very much for all those long days at the library. I do not know when I would have finished writing this 200-page thesis if we did not write together. Thank you very much for all the motivation you gave to me, and for making the dreaded writing phase of PhD so enjoyable.

My dear friends and labmates, dear **Mehdi**, dear **Kamal**, dear **Muhammad**, dear **El-Fituri**, and dear **Ethan**, thank you very much for all the great times we had together, for all the ups and downs, for the happy and the sad days, for fighting with the mice in the lab together (and yes we won!), for our discussions and debates about research (and evolution :-D), for supporting each other, and for the fun group lunches.

Dear **Maryam** and **Hamid**, I am so blessed and lucky to have you as friends. You have been like two angels in my life. You were always there for me when I needed a friend. Whenever I felt down and sad, you called me and visited me. I really cannot find appropriate words to thank you two. I just hope I can find the opportunity to show my appreciation for everything you did for me.

Dear **Sanam** and **Bamdad**, you and your parents were like family to us. I hope I can return your favors. You two always cheered me and cared for me. You helped me overcome PhD blues. Thank you very much! Bamdad jan, our chitchats over lunch, and our gym sessions made my PhD years much more pleasant.

Dear **Azadeh** and **Majid**, you were like my siblings. You are the sweetest friends anyone can wish for. Thank you very much! My life became much more beautiful since you came to Canada. Dear **Farzaneh** and **Ali**, thank you very much for being such wonderful friends, for the movie nights, for the hikes, for the "mingling", for the get-togethers, and for the book club. You know I really like you, right? Dear **Samaneh** and **Yaser**, you were my first friends in SFU, thank you very much for making so many good memories, from the beginning to now. I really appreciate all the things you did for me.

Dear **Haleh** and **Mohammad**, there were many times that I felt frustrated during these years, and every single time a text or call from you reminded me what lovely friends I have. Dear **Shabnam** and **Payam**, when I was about to give up, your words of encouragement, sharing your experiences, and showing me the light at the end of the tunnel made me hopeful again. Also, in the darkest days of my life, I received very kind messages from you. Thank you! Dear **Mohammad Kargar,** thank you very much for caring for me from thousands of kilometers away. Our quarter-century friendship is very valuable for me. Dear **Golnoosh** and **Ali**, thank you very much for everything especially

the time you called and we went to Eagle Bluffs. That was just what the doctor ordered in those days. Dear **Pourkaveh brothers**, thank you and your families for creating unforgettable memories for me.

The list of my friends that I want to thank is very long. I am happy for having all of you in my life. Thank you, **Shabnam, Mojtaba, Sara, Amir, Rose, Hesam, Ita, Nima, Sama, Masood, Faranak, Pooya, Behnaz, Peyman, Negin**, and **Saeed** for all our gatherings, hikes, camping, parties, and for your kind words all during my PhD.

Dear **Somayyeh**,

❼❽❾ ❿❽❺❹❼❽ ❻❽ ❻❶❾ ❽❾❼❽❺❽❿❽❼❼ ❼❼ ❿❽❻❾❼ ❽❼❶❼ ❼❼ ❼❼ ❷❽ ❾❺ ❽❽❽❼ ❼❶ ❽❾❽ ❽❽❿❻❸❶❼❽❸❺ ❼❽❾ ❽❽❿❼ ❽❺❽ ❿❸❽❽❼❽❿❼ ❽❾❼❼❽❺❽ ❽❺❺❻❺❽ ❽❻❶❸❽ ❽❽❷❽ ❘ ❽❹ ❽❽❽❸ ❿❻ ❽❽❼❼❺ ❽❺❽ ❸ ❶❽❷❺ ❼❽❽❼ ❸❽ ❹❽❼ ☒❽❽❺❷ ❺❻❶ ❷❽❾❺ ❹❶❽❽ ❽❻❾ ❺❻❶❾ ❸❼❿❽ ❽❽❷❼❽❽ ❽❻❾ ❺❻❶❾ ❿❶❼❼❻❾❼ ❽❺❽ ❽❻❾ ❹❽❷❼❺❽ ❼❽❼❼ ❸❽❿❼ ❽❽❸ ❹❻❺❼❽❿ ❻❽ ❹❺ ✓❽❧ ❿❻ ❹❶❽❽ ❽❶❺.

Finally, I want to express my deep and sincere gratitude to my family for their continuous and unparalleled love, help and support:

My dear **Leila** and **Sima**, I thank you and **your parents** very much. I always cherish having you in my life. You were always so kind and supportive. I love all of you very much!

I am very grateful to my brothers dear **Mohammad**, dear **Hamed**, and dear **Mahan** who have provided me with emotional support in my life. I would have never ended this journey without having you in my life. My nephew, dear **Ali**, thank you very much for the letter you wrote to me when you were nine, and I was leaving Iran. I have read that letter hundreds of times, and my heart was filled with love every single time.

Words cannot express the feelings I have for **my parents** for their constant unconditional support. My hard-working parents have sacrificed their lives for my siblings and me and provided unconditional love and care. Thank you very much for encouraging me to continue my studies and doing whatever you could do to support me

to reach my goal, both emotionally and financially. You are absolutely the best parents in the world.

Finally, I would like to acknowledge the most important person in my life, **Zhila**. You have been a constant source of strength and inspiration. There were times during the past few years when everything seemed hopeless, and I didn't have any hope. I can honestly say that it was only your determination and constant encouragement that ultimately made it possible for me to finish this project. There are no words to convey how much I appreciate what you have done for me. These past several years have not been an easy ride, both academically and personally. I truly thank you for sticking by my side, even when I was sad and depressed. I owe you my life, my love!

Table of Contents

List of Tables

List of Figures

Chapter 1.

Introduction

The second decade of the twenty-first century will probably be remembered as the years of emerging disruptive technologies that triggered another industrial revolution with an irreversible impact on human societies across the world. These game changers have challenged the status quo and are envisioned to force paradigm shifts in all aspects of our daily life. Driverless cars are at the center of these disruptors, and their further developments will be closely intertwined with other disruptive innovations including but not limited to AI, cloud computing, wireless, and the Internet of Things. Driverless cars are expected to revolutionize the land mobility, redefine the role of human drivers, and reshape the road and traffic infrastructure. The research on these autonomous vehicles is ongoing and diverse. There are still many open and coupled questions that ought to be addressed among which are –in no particular order of priority, appropriate and cost-effective sensor technologies, power technologies, sensors technology, machine intelligence and perception, advanced driver assistance systems, road and traffic sign detection, situation awareness and assessment, scene understanding, self-diagnosis, design of lower level control systems, vehicle-2-vehicle communication, vehicle-2-road infrastructure communication, planning, localization and mapping, detection of other road users (moving and stationary objects), guaranteed safe driving, passenger comfort, legal issues and liabilities, and regulations. The list is exhaustive and clearly indicates the scope of complexity and multidimensionality of the area.

The central premise of this dissertation is to address selected questions within the context of advanced driver assistance systems and study the lower level control systems. In particular, we study detection and overriding intoxicated drivers and design of lateral control system that is essential for autonomous or semi-autonomous vehicles. We have predominately adopted the model-based control theory as the backbone of the studies undertaken in this project and suggest that it has much to offer for the overall operation of an autonomous vehicle.

1.1. Research Motivation

The rationale for autonomous vehicles is multi-faceted; yet enhancing road safety is often referred to as one of the main objectives in designing intelligent transportation systems. In average, every thirty seconds, one person dies somewhere in the world due to a car crash. The cost of accidents in the USA is estimated to be about 300 billion dollars annually [1], i.e., about 2% of its GDP. Conservative estimates suggest that a high proportion of fatalities and injuries due to traffic accidents involve impaired drivers. It is projected that these figures could be increased by 65% in the next 20 years unless novel driving risk reduction methods are leveraged [2].

Among all fatal traffic accidents, 95% are caused by human errors [3]. The three major causes of these human errors, often referred to as the "Big Three", are alcohol, drowsiness, and inattention [4]. Statistics show that 25% of fatal accidents in Europe [5], 32% in the US [6], and 38% in Canada [7] are caused by drunk drivers.

Educating drivers, especially young drivers, through extensive advertising campaigns in media against impaired driving and detecting drunk drivers on the road via visual observations by police are the only two main preventive measures to eliminate or alleviate the problem; the outcome is less than impressive. The U.S. National Highway Traffic Safety Administration (NHTSA) has conducted 3 field studies, involving hundreds of officers and about 12,000 enforcement stops, to find typical driving behaviors of intoxicated drivers [8]. The results of this study indicate that drunk drivers have difficulty in vigilance, judgment, braking, and maintaining desired lateral position and speed [8]. Therefore, these behaviors are used as the most important cues for officers to detect Driving While Intoxicated (DWI) motorists, stop them, and perform a Breathalyzer test.

Even though the mentioned cues can be noticed in most of the alcohol-induced drivers, knowing these cues is not enough to identify intoxicated drivers [6]. The main reason is the small number of available petrol officers compared to the enormous number of cars and roads. The other reason is that poor weather conditions, darkness, and obstacles can prevent detecting intoxicated driving patterns. As an example, a study by

Centre for Disease Controls and Prevention (CDC) shows that about 99% of drunk drivers in the US are not detected by officers because of the aforementioned reasons [9]. Even the detected drivers might have been driving for a long distance before they get noted. Based on the premise that every single death or injury due to impaired driving could be avoidable, the main motivation of the first phase of this project is to propose and design a system that can detect the state of an impaired driver based on his/her handling of the car. It is envisaged that ultimately an intelligent car detects whether or not its driver is impaired.

There have been attempts to identify impaired drivers via on-board sensor-based condition monitoring techniques in recent years. A survey that reviews many of these condition monitoring systems is available in [10]. In these systems, data is gathered using vehicle-based sensors; then it is processed to determine the impairment level of the driver. Based on the signals they use, the driver monitoring systems available in the literature, which will be reviewed in Chapter 2, can be classified into three categories [11]:

1) Systems which use signals containing physiological measures of the driver such as electroencephalogram (EEG), eye movement, eye gaze data, eyelid aperture, pulsation waves, heart rate, perspiration, breath, etc.[4, 12-15]. These signals contain rich information that can lead to the detection of impaired drivers. However, except for eye tracking systems which are non-invasive, the rest require either wearable devices, or active participation of the driver.

2) Systems which use signals containing vehicle information such as its speed, its lateral position, etc. [6, 16-18]. Although collecting these signals is easier than driver physiological signals, they usually do not carry sufficient information by themselves.

3) Systems which use vehicle inputs (driver outputs) such as accelerator and brake pedals, steering wheel, etc.[11, 19]. These signals are available in most of the new cars, especially the ones equipped with drive-by-wire-systems.

Systems in the first category are expected to play an important role to detect DWI in the next few years as the technology matures and prices become more competitive. In addition, most of the condition monitoring systems in the other two categories consider driver impairments such as fatigue, distraction, and drowsiness. Only a few (e.g., [11] and [6]) have specifically considered intoxicated motorists. Even these few studies have considered a single signal from one of the two aforementioned categories (categories 2 and 3). However, a signal from the third category might be affected by other variables from the second one (and vice versa). Therefore, studying only one of these signals is insufficient for detection of alcohol-induced drivers.

The scope and flow of this thesis include four phases as shown in Figure 1.1. The organization of the thesis, the summary of each chapter, and the original contributions of this study are presented in the next sections of this chapter.

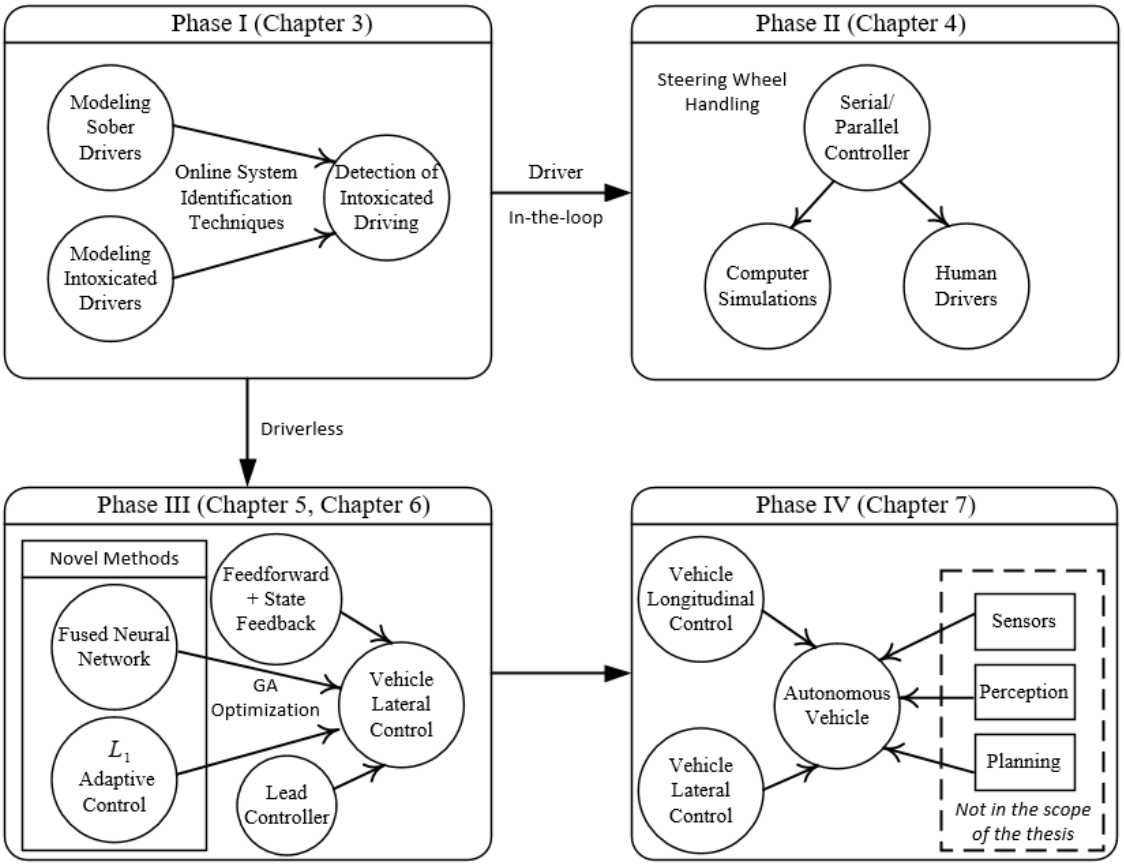

Figure 1.1. Thesis scope and flow

The research reported in Chapter 3 is related to classes two and three as outlined above. We rely on system identification based on input and output signals from the driver to estimate the state of the driver. In particular, we propose a method to overcome these shortcomings through considering the lane-keeping task of the drivers and focusing on two signals: lateral preview error (from category 2) and steering wheel (from category 3), to

1) Present two models to describe the lane keeping behavior of sober and drunk drivers

2) Perform online identification on the driver to detect drunk driving by comparing the current model of the driver with the obtained models in the previous part

Detecting drunk driving concludes the first phase of this study. In the second phase, we try to improve the handling of the vehicle when it is being driven by an impaired driver. Modern technology has tried to reduce the risk of car accidents using various means which can be categorized into two classes: passive and active [20]. Passive methods, like seatbelts and airbags, can only reduce the injury, but active methods, like advanced driver assistance systems (ADAS), are meant to assist the driver in preventing the accidents. Since more than 95% of the fatal accidents are caused by human error [3], driver assistance systems are expected to have a significant role in reducing the risk of traffic accidents. Different causes of accidents and the effect of different advanced driver assistance systems are discussed in [21].

Although much progress has been made in developing these ADASs, the suggestion that these systems are not yet reliable and might even lead to driver distraction has been around. For example, the warning systems used in the cars are visual, auditory or haptic [22]. If the driver is looking away, fixed front displays in front of him will not attract his/ her attention so it will not be useful. In addition, side screen displays can take the driver's attention off the road which can be dangerous. Auditory or haptic warning systems cannot transmit enough information in a short time. Moreover, drivers might not

appreciate repetitive warning messages when they already have noticed an imminent danger [23].

On the other hand, although the main goal of a driver assistance system is to reduce the physical and mental workload of the driver and therefore to improve safety, however, if the workload is less than a certain amount, the driver would be disengaged from driving.

The main idea of the second phase of this thesis, explained in Chapter 4, is to design either a series or a parallel controller to the human control loop to assist in steering the vehicle. In the serial assisting controller system, when the driver turns the steering wheel, the steering signal is fed to a controller instead of the steering column of the car. The output of the controller is the actual value of the steering signal which acts on the wheels. This control system can be readily implemented using a steer-by-wire system [24]. In the parallel assisting controller, the output of an independent lateral controller is added to the driver's steering signal so that the poor performance caused by driver impairment is compensated.

In the third phase of the thesis, we study, design, and evaluate several lateral controllers. Vehicle lateral control is an integral part of the autonomous and intelligent vehicle control systems. The primary goal of the lateral control, also referred to as steering control, is to navigate a car along the desired path (lane keeping/following). In addition, performing lane change maneuvers, avoiding obstacles and collisions in emergency situations are also directly related to vehicle lateral control.

Data from the Federal Highway Administration (FHWA) suggests that crashes caused by lane deviation account for about 53 percent of all fatal crashes [25]. More than half a million road accidents are due to improper lane changing executions [26] which makes it one of the dangerous driving maneuvers on highways. In emergency obstacle avoidance cases, less experienced drivers have difficulty performing evasive maneuvers and stabilizing the vehicle afterward. Advanced Driver Assistance Systems are expected to alleviate the number of these types of accidents by assisting the drivers in lane-

keeping, lane changing, and emergency collision avoidance tasks. Also, driverless cars also need to have high-performance steering control systems.

The vehicle lateral controller should be able to maintain the car in the center of the lane in the presence of disturbances and uncertainties. In addition, the parameters of the vehicle dynamics are not constant and depend on the car speed, weather, road, and tire conditions. Therefore, the system should be able to follow the reference road trajectory by compensating the effects of all uncertainties, noises, disturbances, and parameter variations.

As lateral control is central to driving, it has been extensively studied. A literature survey on the most important methods used for this task is presented in Chapter 2. The literature review discusses the significance and importance of lateral control in autonomous vehicles. However, the problem presents additional challenges when external disturbances, uncertainties, and parameter variations are considered. These complexities are less considered in the literature. Therefore, it is envisaged that a robust adaptive control is an excellent candidate to address these problems successfully.

Less than a decade ago, $\mathcal{L}_1$ adaptive control was introduced by Hovakimyan and Cao [27-29]. The following properties of this controller make it a suitable choice for the vehicle lateral control problem. The key features of this control architecture are guaranteed robustness and fast adaptation. These ensure that the control system is robust to variations in the uncertainty and parameters of the system as well as demonstrating an acceptable performance. The $\mathcal{L}_1$ control algorithm also ensures uniformly bounded transient response and steady-state tracking. This is achieved by proper formulation of the control objective in a way that the uncertainties of the system can be compensated for within the bandwidth of the control channel [27]. In this algorithm, the decoupling of adaptation and robustness is made possible by building the robustness specifications in the problem formulation, which increases the speed of adaptation. In other words, employing $\mathcal{L}_1$ adaptive control addresses fast adaptation which is beneficial for both robustness and performance. One of the crucial steps in this algorithm is selecting the

underlying filter structure. This task can be addressed using classical and robust control techniques.

Within the above context, the contribution of Chapter 6 of this study is two folds: (1) The algorithm will guarantee stability and performance in trajectory (lane center) tracking in the presence of model uncertainties, wind disturbance, road banking angle, and icy roads, assuming there is no sensor failure; (2) The proposed controller will rapidly adapt to variations in the parameters of the system model and compensate for the effects of unknown disturbances. Also, since this method is adaptive, it is a suitable choice for vehicle lateral control problem in the presence of parameter variations. Lastly, because of its guaranteed robustness, $\mathcal{L}_1$ adaptive controller is an appropriate controller for handling vehicle lateral model uncertainties and disturbances such as the wind, slippery roads, and road banking angles.

In the fourth and the last phase of this dissertation, we design longitudinal controllers, add it to the lateral control systems designed before, and implement the integrated controller on the driving simulator. This completes the control system module of driverless cars. In order to have a completely autonomous driving vehicle, sensors, perception, and planning modules should be designed and added to the system, which is not within the scope of this study.

1.2. Organization of the Thesis

In Chapter 2, we present an overview of the literature related to driver modeling, safety methods regarding intoxicated driving, and lateral control systems. Driver assistance systems and vehicle safety systems are used to improve the driving performance of the driver. We also show through our selective literature review that one of the important requirements in designing such systems is the driver mathematical model. We will see that although different models of sober drivers are available in the literature, to the best of our knowledge, the steering behavior of intoxicated drivers has not been previously reported.

In Chapter 3, we apply system identification techniques and present two models to describe the lateral control behavior of sober and drunk drivers. We also introduce a novel method to detect alcohol-induced driving. The proposed method not only is useful in detecting alcohol-induced driving but also can be used as a measure to evaluate the performance of the driver. It can also detect any other impairment that might have a similar effect as alcohol on driving behavior.

In Chapter 4, the idea of improving the steering action of the driver by serial and parallel controllers is presented and studied. The performances of the suggested algorithms are studied and compared using computer simulations and human-in-the-loop experiments using the driving simulator and actual human drivers.

In Chapter 5, we design several lateral control systems including a state-feedback controller which is accompanied by a feedforward controller. We also use a preview error algorithm to design a lead compensator that increases the stability margins of the system significantly. In addition, we introduce a novel, simple neural-network controller, which was recently developed by our group. We use genetic algorithm to optimize the neural network weights for designing a lateral controller.

In Chapter 6, the recently introduced $\mathcal{L}_1$ adaptive control algorithm is utilized to design a controller for the lateral dynamics of the vehicle. We consider challenging conditions in the simulation scenarios of this chapter, which include icy roads, strong wind gusts, road banking angle, curves, and drastic variations in vehicle model parameters. The robustness of $\mathcal{L}_1$ adaptive control makes it possible to control the vehicle when all these disturbances and uncertainties are present in the system.

In Chapter 7, we design a control system for vehicle cruise (speed) control. In addition, we investigate different strategies to be considered for adaptive cruise control of the autonomous vehicle in our project and decide which is the most appropriate one to select considering the available sensors and current limitations. We also consider the transition between speed control and vehicle following modes. The conditions when the vehicle should apply the brake to avoid a collision are also investigated. Finally, we implement the designed control algorithms on a high-quality driving simulator. We show

that both longitudinal and lateral controllers can make the vehicle follow the desired trajectories in various scenarios satisfactorily.

In Chapter 8, we summarize the research accomplished in this thesis. The conclusions and outcomes of the thesis based on theoretical studies, simulation results, and experimental evaluations are given in this chapter. Finally, tentative suggestions for the future direction of this research work are included.

1.3. Original Contributions and Publications

The summary of the original contributions and publications at the time of writing this thesis follows:

- Using system identification techniques to derive two mathematical models to describe the steering wheel handling behavior of sober and intoxicated drivers, published in IEEE Intelligent Transportation Systems Conference in 2012 [30]

- Introducing a novel method to detect intoxicated driving, published in IEEE Transaction on Intelligent Transportation Systems in 2014 [31]

- Designing a human-in-the-loop vehicle lateral serial controller, published in IEEE International Conference on Mechatronics in 2011 [32]

- Designing parallel assisting lateral controller, a paper to be submitted to IEEE Transaction in Intelligent Transportation Systems in 2018.

- Contributing to development of a new fused neural network controller (introduced by our group) and designing vehicle lateral controller based on it, published in the Journal of Applied Soft Computing in 2012 [33]

- Designing $\mathcal{L}_1$adaptive control for vehicle lateral dynamics, published in IEEE Transaction on Intelligent Vehicles in 2017 [34]

- Designing an integrated autonomous vehicle control system and implementing it, done as part of an NSERC research project for an industrial partner in 2013, published as a report.

Chapter 2.

Literature Review

In the 1960's, the Bureau of Public Roads (BPR) of the Department of Commerce in the United States, the predecessor to Federal Highway Administration (FHWA), started the earliest research and development program to improve the efficiency and safety of highway-based transportation [35]. The core of this program was an effort to apply the evolving electronic communications and control systems theory to vehicle/highway operations. Later, several similar programs were conducted around the world, the most important of which were in the US, Europe, and Japan. The main goals of these programs were to improve safety, mitigate congestion, reduce environmental pollution, increase energy efficiency, and improve travel comfort.

In the mid-1980s in the US, a group (named Mobility 2000) consisting of universities, federal and state governments, and private companies started working together and discussed possible technologies that could change the future of transportation [36]. These discussions resulted in forming of Intelligent Vehicle Highway Systems (IVHS), that was later renamed to Intelligent Transportation Systems (ITS) America, which has continually conducted many transportation projects since the 1990s. One of the most famous transformation research programs initiated in that period was Partners for Advanced Transit and Highways (PATH) in California [37].

Almost parallel and at the same time as the US, the Commission of European Communities (CEC) initiated similar projects in Integrated Road Transport Environment (IRTE) and Road Transport Informatics (RTI). Two important projects conducted under the European Advanced Transport Telematics (ATT) in 1989 were DRIVE I and DRIVE II [38]. The European vehicle industry started the PROgraM for European Traffic with Highest Efficiency and Unprecedented Safety (PROMETHEUS) in 1985. Later, several other intelligent transportation programs such as Cybercar and PReVENT were launched in Europe [39].

In the last few decades, significant advances have been made in the field of intelligent transportation. However, the scope of research in this field is multifaceted, and a thorough literature review is neither intended nor feasible within the constraints of this dissertation. An overview of the research topics related to intelligent vehicles is shown in Figure 2.1. Here, the key objective is to provide a succinct coverage of the key related topics within the scope of the research undertaken in this project in order to set the scene for the next chapters. Hence, the literature review presented here covers advanced driver assistance systems, driver behavior modeling, detection of intoxicated driving, and lateral control systems.

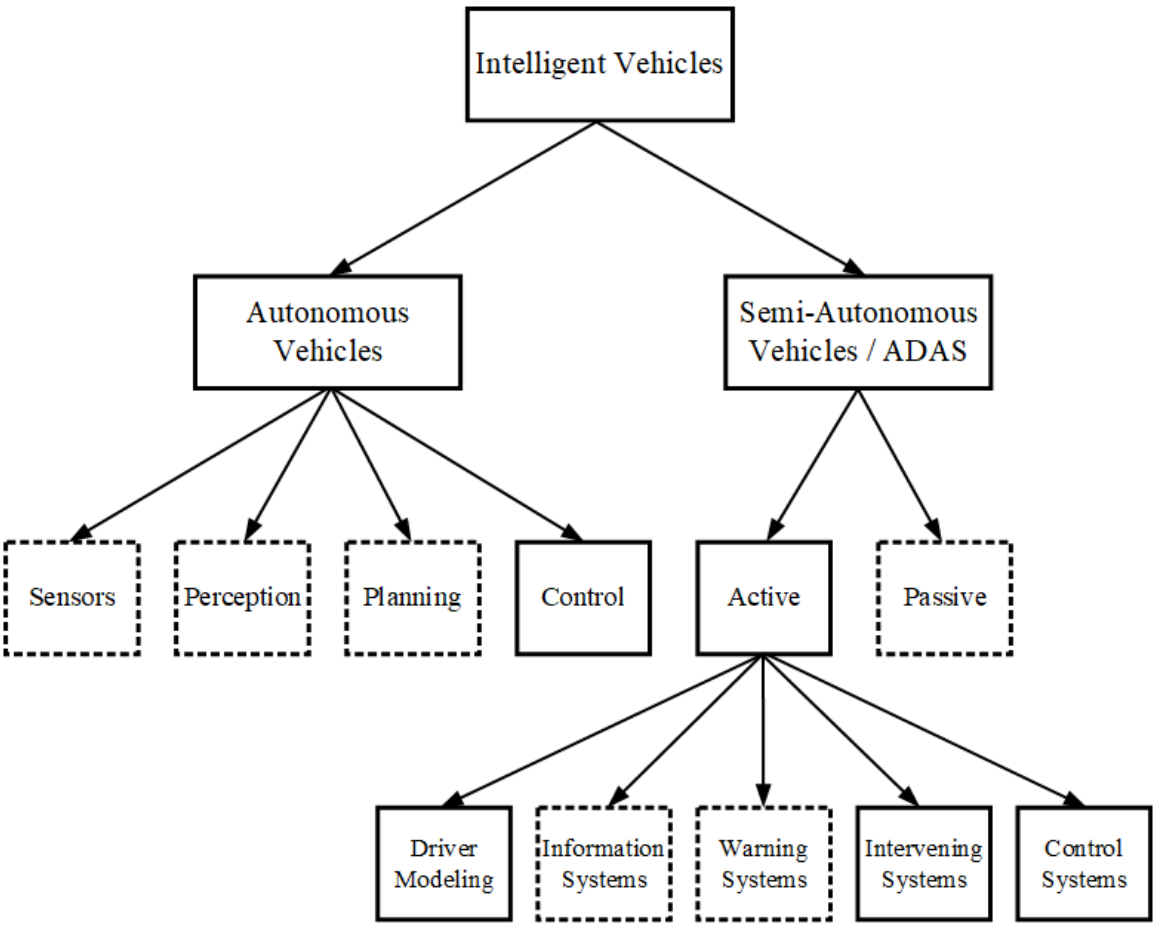

Figure 2.1. An overview of the field of intelligent vehicles. The sections shown by dashed rectangles are not within the scope of this dissertation.

The chapter is organized as follows: some basic definitions used in this field and throughout this thesis are reviewed in section 2.1. Classification of advanced driver assistance systems and reviewing some commercially available ones are done in the next

section. The issues in driver modeling are discussed in section 2.3. The available safety methods regarding intoxicated driving are reviewed in section 2.4. Finally, the chapter is concluded with a review of available lateral control systems.

2.1. Some Basic Definitions and Concepts

Oxford dictionary defines “intelligence” as “the ability to acquire and apply knowledge and skills”. However, applying this definition to vehicles and transportations systems raises the expectations too high and far from reality. For several decades, the ultimate goal of researchers in the field of artificial intelligence has been to design intelligent machines. Although the progress towards this goal has been considerable, the success in demonstrating real human-like intelligence has been limited. A more realistic and practical definition of an *intelligent vehicle* is a vehicle that helps the drivers to perform their driving tasks more safely and effectively, or performs some aspects of driving autonomously [40].

The word *autonomous* refers to machines that can perform a task without guidance from a human operator. The range of such a task is vast and can be anything from placing a part at the desired location to piloting an airplane and driving a vehicle. Therefore, performing a task autonomously involves having a specific goal, sensing, perceiving the conditions, analyzing and planning for action, and finally executing the task [40]. In the case of vehicle driving, these steps for the goal of autonomous driving translate to

(I) employing sensors for detecting the surrounding environment,

(II) perceiving the current situation including traffic lights, traffic signs, or obstacles and other vehicles on the current path,

(III) analyzing the conditions, making decisions to react to the current situation, considering the desired destination and the required route to reach there, and considering all of these goals for planning the desired vehicle trajectories,

(IV) executing the necessary steering, accelerating, or braking tasks to follow the trajectories planned in part (III).

The above steps, in addition to comparison to manual driving, are shown schematically in Figure 2.2. More details on different parts of this figure will be given in Chapter 7. The sensing, perception, and planning subsystems are not within the scope of this study, as it will be further explained in Chapter 7.

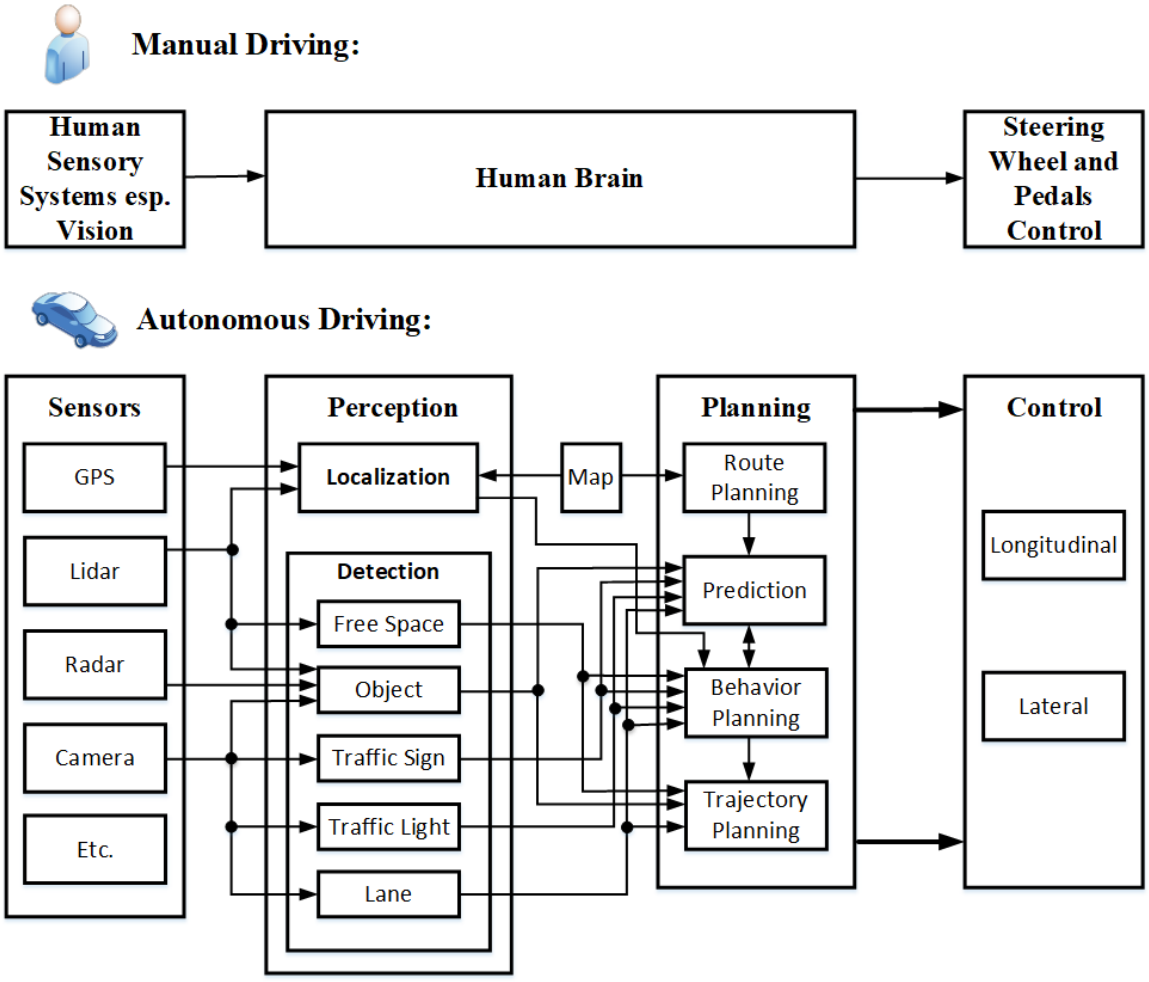

Figure 2.2. Different parts of the autonomous driving system

As mentioned in Chapter 1, about 95% of accidents are caused by human error [41]. Therefore it is not surprising that the idea of driverless cars has a long story. The dream started to appear in science fictions in the 1920s, the more realistic concept was presented in General Motor's Futurama New York World's Fair in the 1930s, and it seemed a real possibility in the 1980s. At this time, the road to driverless cars was paved

by works such as [42]. The most notable early results were obtained in (1) the previously mentioned PROMETHEUS project where the VaMP driverless car drove 95% of its 1600 km path autonomously in 1994 [43], and in (2) Carnegie Mellon University (CMU) Navlab where the autonomous vehicle in the No Hands Across America project drove 98% of the 5000 km road across the US autonomously in 1995 [44].

The next important milestone in developing autonomous vehicle technology was the first Defense Advanced Research Projects Agency (DARPA) Grand Challenge in 2004 [45]. The goal was for autonomous vehicles to navigate a 240-kilometer off-road route as fast as possible without any human intervention during the race. Eliminating human assist in critical moments proved to be the main challenge, and none of the 15 vehicles could finish the route. The challenge was repeated in 2005 [46]; this time 5 out of 23 teams arrived at the finish line, and Stanley [47] from Stanford University was the winner. Later, in 2007, DARPA Challenge was held in a simulated urban environment. Six vehicles finished the course demonstrating the advancements in fully driverless urban driving [48].

Several events and challenges regarding driverless cars were held since the DARPA challenges. Some of the noteworthy examples include VisLab Intercontinental Autonomous Challenge (VIAC) which was a 16,000 km (from Italy to China) driverless challenge with no human intervention held in 2010 [49], Hyundai Autonomous Challenge in 2010 [50], China Intelligent Vehicle Future Challenges (IVFC) from 2009 to 2017 [51], and the autonomous journey on a historic route of Bertha Benz [52]. Recently, the research on this topic has accelerated rapidly in both academia and industry. Waymo (Google) self-driving car [53] and Tesla Autopilot system [54] are two of the commercial products that have received significant media attention recently.

The field of intelligent transportation and the term intelligent vehicle are not limited to autonomous driving. *Advanced Driver Assistance Systems* (ADAS) refers to vehicle driving tasks that an intelligent vehicle assists the drivers to perform more safely and effectively. The term *driver assistance,* which is usually used interchangeably,

includes ADAS but also refers to all the other in-vehicle driver support systems, such as navigation, too [40].

In summary, driving tasks are supported by intelligent vehicles at different levels of automation. The highest level of automation is called *driverless* where all aspects of driving are performed without the intervention of the human driver. In the intermediate levels of automation (*semi-autonomous*), the intelligent vehicle assists the human driver in various aspects of driving as needed and acts as a copilot. In the lower levels of automation, the vehicle acts as an informational assistant and warns the driver when necessary. Examples of such systems will be given and explained in more details in section 2.2. The Society of Automotive Engineers (SAE), an automotive standardization body, published a classification based on six different levels of driving automation systems [55]. This classification system is mainly based on the required level of human attentiveness and intervention, rather than the capabilities of the vehicle [56]. The summary of these levels of automation based on SAE taxonomy are shown in Table 2.1.

Table 2.1. Autonomy levels based on SAE taxonomy

SAE Level	Name	Execution of Steering, Acceleration, and Brake	Monitoring of Driving Environment	Fallback Performance of Dynamic Driving Task	System Capability (Driving Modes)
Human driver monitors the driving environment					
0	No Automation	Human driver	Human driver	Human driver	n/a
1	Driver Assistance	Human driver and system	Human driver	Human driver	Some driving modes
2	Partial Automation	System	Human driver	Human driver	Some driving modes
Automated driving system monitors the driving environment					
3	Conditional Automation	System	System	Human driver	Some driving modes
4	High Automation	System	System	System	Many driving modes
5	Full Automation	System	System	System	All driving modes

In this dissertation, Chapter 3 and Chapter 4 are related to SAE levels 1 to 3, and Chapters 5 to 7 can be applied in levels 1 to 5 of autonomy.

2.2. Advanced Driver Assistance Systems (ADAS)

Advances in microelectronics have encouraged automotive industry to integrate sensors, actuators, microcomputers, and information processing for the engine, drivetrain, suspension, and brake systems. The first developments in this regard were cruise control systems and digitally controlled combustion engines in the 1970s. Electronic braking and advanced vehicle handling were then introduced to reduce the risk of driving. A historical survey on these developments is reported in [57]. These were the first advanced driver assistance systems introduced which reduced the number of accidents by assisting the driver.

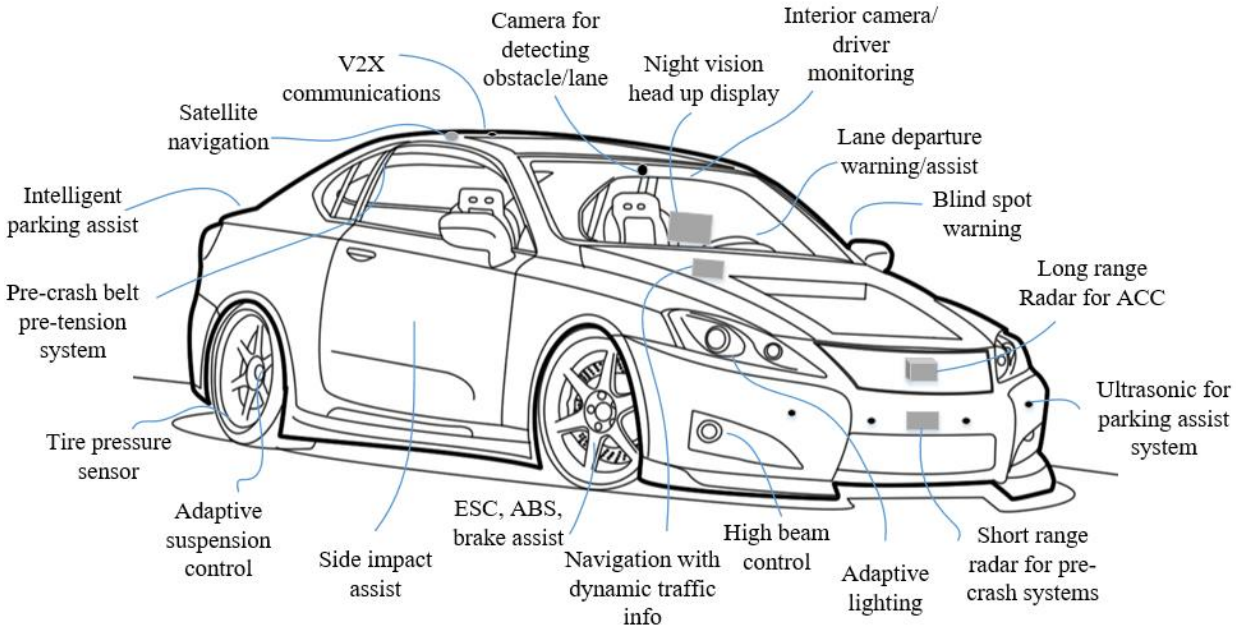

Figure 2.3. Illustration of some commercially available advanced driver assistance systems

Some of the most famous and effective systems developed at this stage (the 1980s and the 1990s) are anti-lock braking systems (ABS) [58], traction control system, brake assist, and electronic stability control (ESC) [59]. Meantime, active steering systems, active roll stabilization, and active suspension systems were developed to improve

vehicle lateral stability and driver comfort [60]. Many of the proposed ADASs are currently commercially available. Some of these systems are shown in Figure 2.3.

The field of research on advanced driver assistance system is wide and includes a broad range of algorithms and technologies. Here, we briefly categorize them based on the hierarchical levels of the driving task. More information about them can be found in [61-65].

1) *Driver information systems* which help the driver in the highest level of driving task. In these systems, no control or intervention by ADAS occurs, and the driver is the only controller of the vehicle. However, the driver assistance gives additional information to the drivers and increases their situation awareness [66]. Some of the examples that fit into this category include GPS navigation system, adaptive light control, and night vision head-up display.

2) *Driver warning systems* which assist the driver in the second level of driving task which is maneuvering. These systems are among active safety systems which are always monitoring vehicle, road and driver conditions and give an alarm to the driver when there is an imminent danger. Then, it is up to the driver to perform the correct action and avoid the danger. Some of the systems that fit in this category are lane departure warning, forward collision warning, driver drowsiness warning, parking assistant, intersection collision warning, and blind spot warning systems [67].

3) *Intervening systems* which assist the driver actively in the control level of the driving. These systems can take over control the car in some specific tasks. Although these tasks can be performed automatically be these ADASs, the driver should be alert to take other tasks of the driving. Some examples are adaptive cruise control (ACC) [68], intelligent speed adaptation [69], and lane keeping systems [70].

4) *Integrated passive and active safety systems* which increase the safety by integrating passive and active systems (see Table 2.2). In the normal driving conditions, the system informs the driver about potential dangers. In the next step, some warnings are sent to the driver to alert him/her. If the driver still does not respond and time to collision is reduced to a few seconds, ADAS overtakes and tries to avoid the accident. In addition, emergency braking systems can reduce the severity of the accident. At about 500ms to crash, seat belt pre-tensioners can be activated [71], and at about 10ms before the accident, airbag deployment can be optimized [72]. Automatic emergency call system (eCall) can be activated after the accident [73].

5) *Fully automated systems* are beyond driver assistance and completely eliminate the driver from the control loop. Autonomous vehicles which can drive automatically have been the topic of intense research. Although these systems can greatly improve road safety [74], full autonomy is at least a decade away. The main reasons are the high cost of sensors used by driverless cars, such as Lidar receivers, and also the need to map all roads with centimeter-precision.

Table 2.2. Integrated safety systems including both passive and active systems which cooperate before, during, and after an accident

	Preventive and Active Safety					Passive Safety		
	Inform	Support		Intervene		Safety systems soft level	Safety systems hard level	Rescue systems
	Foresighted driving	Warning	Assistance	Pre-crash systems	C R A S H	Minor accidents	Major accidents	Post-crash
Examples	Night vision [75] Route navigation [76] Incident warning [77] Cooperative systems [78, 79]	Blind spot [80] Forward collision warning [81] Lane departure warning [82] Speed warning [83]	Electronic Stability Control [84] Brake assist [85] Collision avoidance [86]	Reversible restraints[87] Emergency braking [88] Adaptive seatbelt adjustment system [89]		Pedestrian airbag systems [90, 91] Intelligent restraint systems [92]	Vehicle crashworthiness [93] Airbags [94] Smart materials (energy absorption) [95]	eCall system [96] Emergency vehicle automatic dispatch system [97]
	Normal driving	Collision avoidance		Collision mitigation		Human protection		Injury treatment
	60-10 s before	10-2 s before	2-1 s before	1-0 s before		0-100 ms after		100 ms–60 s after

The research in this field is very broad, so we only presented the most significant developments. More comprehensive reviews can be found in [61, 63, 64, 98-104].

2.3. Driver Modeling

Understanding the behavior of drivers and attempts to derive mathematical models for human operators has been an important research topic in many different disciplines in the last five decades. The first significant results in this regard were obtained during aircraft pilot studies [105-108]. For example in [107], the following transfer function was proposed for any human operator in pursuit tasks:

$$G(s) = \frac{(a_1 s + a_0)e^{-s\tau}}{b_2 s^2 + b_1 s + b_0} \qquad (2\text{-}1)$$

where a_1 is related to the anticipatory behavior of human and τ is the inherent delay in human tracking tasks. Later in the seventies, specific research on the human driver of automobiles was conducted [109-112]. The main result of the investigations in this decade suggested that the model of the driver could not be clearly decoupled from the

model of the vehicle. In other words, vehicle and driver constitute a complex combined system which cannot be split. Some survey papers on the results obtained in driver modeling up to the nineties were reported [113-115].

The human sensory and neuromuscular system has some limitations which are usually considered in the driver models. These limitations are explained comprehensively in [116]. The most important ones among these limitations are transport delay, threshold properties, rate-limiting properties, signal noise in sensory inputs and output responses, and visual acuity abilities.

Further progress in modeling human driver was made when engineers started to work with scientists from other disciplines such as psychology and physiology, e.g. [117-119]. The main characteristics that these scientists suggested that should be considered in deriving a driver model can be categorized into three groups. The first group contains general characteristics of human beings such as input channels of the driver (visual, vestibular and kinesthetic, tactile, and auditory) which have different effects on driver behavior in different scenarios. Other characteristics to be considered are perception, processing, neuromuscular dynamics, preview, anticipation, adaptation, learning, path planning, and speed adjustments. Further information about these characteristics can be found in [120]. The second group consists of properties regarding the experience, age, sex, and willingness to take and accept risks of the driver. Finally, features like emotions, tiredness, concentration, and stress are other factors which should be considered while modeling the human driver.

A look back to early research in this area, when Kondo [121] in Japan started to model the driver, might be helpful to illustrate some of the roots to which many later models up to now (although not always directly) are obliged [122]. In that study, a bicycle model was considered for the vehicle, which has a constant longitudinal model, and the driver steers in a way that at a point in a definite distance ahead, he/she would like to coincide with the sight point. In other words, from a control theory point of view, the driver would like to reduce Δy_p, at a distance L ahead of the vehicle (Figure 2.4).

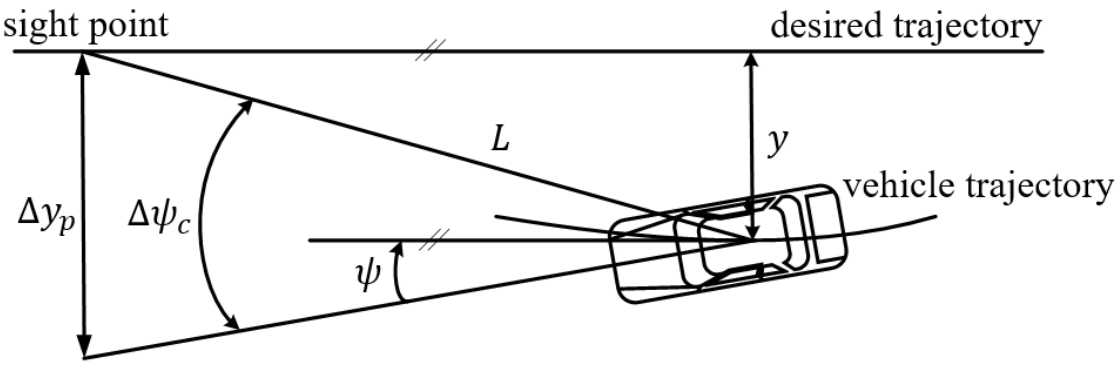

Figure 2.4. Kondo's shaft driver model

This study was the first work which used the well-known preview tracking structure. The general structure of these kinds of models is shown in Figure 2.5. In this structure *P(s)* is the preview strategy of the driver, *H(s)* represents control properties of the driver, *G(s)* is the transfer function(s) of the vehicle, and *B(s)* shows the feedback function.

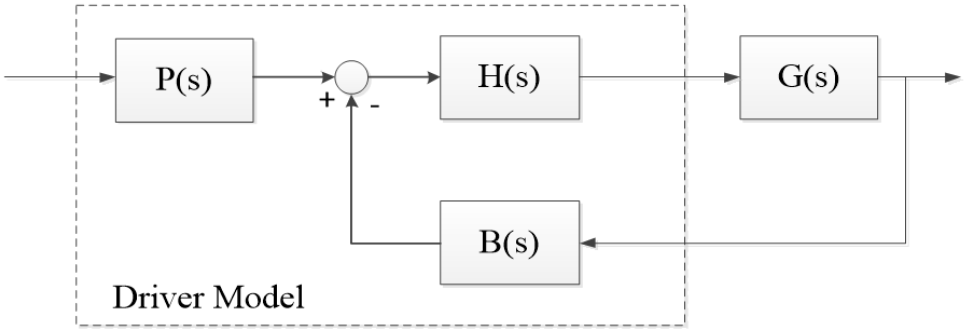

Figure 2.5. General structure of preview tracking driver models

In Kondo's shaft model we have

$$\Delta y_p(t) \approx y(t) + L\psi(t) = y(t) + T_p v\psi(t) \approx y(t + T_p) \qquad (2\text{-}2)$$

where the preview time is $T_p = L/v$. In order to show it in the format of Figure 2.5, we can determine $B(s) = e^{T_p s}$ and $y_p = \Delta y_p$.With $P(s) = e^{T_p s}$ and $H(s) = K$, a simple proportional control is composed for Kondo's shaft model in Figure 2.4 with $\delta_s(s) = Ke^{T_p s}y(s)$ for desired $y_0 = 0$.

In some papers, for small values of $\psi(t)$, $v\psi(t)$ in the above equation is replaced by $\dot{y}(t)$, therefore $B(s) = 1 + T_p s$ [123, 124]. Some others have used Taylor series expansion for $y(t + T_p)$ and used the following second order prediction function [115, 125, 126]:

$$B(s) = 1 + T_p s + \frac{1}{2} T_p^2 s^2 \qquad (2\text{-}3)$$

One of the most popular driver models used by many scientists is the McRuer model [127] where

$$H(s) = \frac{K(T_L s+1)}{(T_I s+1)(T_N s+1)} e^{-\tau_r s} \qquad (2\text{-}4)$$

was used for the tracking behavior of human. In this model, *P(s)* and *B(s)* of Figure 2.5 are neglected. The parameters in the above transfer function can be categorized into two groups. The first group are related to human characteristics: neuromuscular delay time T_N and reaction time τ_r. The second group of parameters (K, T_L, and T_I) depend on the controlled system (vehicle) and are independent of the human driver. Later, McRuer modified this model and presented the 'precision model' [128].

One effective way of describing human regulation task (e.g., driving) is the 'crossover model' [111, 129]. In this model, the open-loop transfer function of the combined system of driver *H(s)* and vehicle *G(s)* is presented by

$$H(s)G(s) = \frac{\omega_c}{s} e^{-\tau_r s} \qquad (2\text{-}5)$$

in the vicinity of the crossover frequency ω_c. Transport delay is shown by τ_r as before. The main problem of this model is the fact that it is valid only near the crossover frequency and it does not tell anything about the other frequencies, especially the low frequency where most of the human driving tasks occur. Some information about crossover frequencies and phase margins for different driving scenarios are given in [126].

Two-level driver model from Donges [130] is another famous driver model which was used and modified by many other scientists later, for example [131-134]. This model consists of an anticipatory open-loop layer and a compensatory closed-loop one. The parameters of this model can be selected to meet the required characteristics of the crossover model [125]. This model is extended to a three-layer model in [132].

In a major class of human driver models, the goal of the driver is minimizing tracking errors in an interval of the future path ahead. These tracking errors can be several different variables such as lateral deviation from the center of the road, heading angle, etc. and their cause is usually the difference between previewed and desired path and the predicted motion of the car. One of the most cited models in this category is the preview/prediction model [135] which uses optimal control theory and is the basis of many software packages including Carsim and Trucksim.

Another class of controllers used for representing human driver is fuzzy logic. Since it is shown that fuzzy logic can be used to resemble human thinking and perception for making a decision [136], some scientists have expressed human driving behaviors with fuzzy logic linguistic terms [137, 138]. A self-organizing technique for fuzzy logic human driver model is presented in [139] to have more accurate fuzzy reasoning rules. The inputs of the fuzzy controller are lateral deviation of the vehicle in single and double lane change maneuvers and yaw velocity. Some other fuzzy logic driver models are introduced in [140-142].

Neural Networks (NNs) were also used in several driver models. In [143], a visual data processing method for the road ahead of the vehicle was developed using NNs. In this model, the curvature of the road is the only variable which affects the steering wheel angle, which is the output of the driver model. Time delays of sensor data are also used as input of NN in [144] to obtain steering wheel angle. Similar methods were used in [145-147] to obtain an NN model for the human driver. The longitudinal behavior of the driver is also modeled using NNs in [148]. The task of this model is to follow a given velocity profile.

2.4. Safety Methods Regarding Intoxicated Driving

As mentioned in Chapter 1, although the number of alcohol-related accidents is very high, the most important method for detecting drivers, and therefore preventing accidents, is only performing visual observations by patrol officers. Intoxicated drivers have difficulty in performing various tasks related to driving, including maintaining the desired lateral position, speeding, braking, vigilance, and judgment [149]. Therefore, these behaviors are used as some guidelines for identifying drivers under the influence of alcohol. But since usually only 1% of drunk drivers are identified and arrested using this method [9], some other methods need to be established to prevent accidents related to drunk driving.

The research on developing devices for detecting drivers with high alcohol level started in the nineties [150, 151]. Most of the more recent methods proposed in the literature, for improving road safety regarding drunk driving, are drunk driver detection techniques [4-6, 12, 152-157]. For example, in the method proposed by [152], the driver is constantly monitored, and face detection techniques are combined with alcohol detection systems to guarantee the uniqueness of the driver. A dynamic Bayesian network is used in [153] to consider blood alcohol concentration (BAC), eye movement, and head movement simultaneously to detect intoxicated drivers. Oxygen level in driver's breath [154], water-cluster-detecting method [12], biological sensor obtained from driver's seat and frequency time series analysis [4], vehicle maneuvers detected by accelerometer and orientation sensors in mobile phones [6], electric alcohol nose sensor [155], vehicle trajectories [156], and driver's perspiration [157] are also used to detect intoxicated drivers.

Many lane departure warning systems are also available which aim to prevent the crashes caused by driver inattention, intoxication or fatigue. Some of these systems are presented in [158-162]. In [163], a non-standard safety technology, which assists impaired drivers to improve the driving safety is presented. Sometimes a driver drives the vehicle with some actions that might not cause an accident immediately but may show that he/she is intoxicated, tired or drowsy. In this situation, this non-standard safety

system determines if the driver is physiologically impaired based on the information of vehicle, road and other objects before the driver causes an accident.

A summary of studies in the last half a century on the effects of alcohol on driver performance is given in [164]. Comprehensive experimental and epidemiological studies are available in this report. The relationships between alcohol and fatigue, aggression, and the degree of injury are also investigated. Specific studies on the effects of different blood alcohol concentrations (BAC) and breath alcohol concentrations (BrAC) on driving behavior are presented in [165] and [7], respectively. The effects of age, gender and drinking practice characteristics on alcohol impairment of the drivers are also looked into in [165].

2.5. Lateral Control Systems

Vehicle lateral control is an integral part of autonomous and intelligent vehicle control systems. The primary goal of the lateral control, also referred to as steering control, is to navigate a car along the desired path (lane keeping/following). In addition, performing lane change maneuvers, avoiding obstacles and collisions in emergency situations are also related to vehicle lateral control.

2.5.1. Lateral Referencing Systems

In order to implement the lateral control algorithms, we need to measure the position of the vehicle with respect to the road (reference). This task can be done using various referencing systems. One of the earliest methods available in literature was laying a wire along the center of the lane [166] in the 1960's. The wire was excited with an alternating current. This amplitude-sensing technique, employed by General Motors Corporation/Radio Corporation of America worked satisfactorily at low speeds (up to 55 km/h) provided no ferrous material were located under or on the road. In order to increase the robustness to ferrous materials, phase-sensing approaches were replaced later in the mid-1970's [167]. In 1977, FHWA banned the use of wire-reference systems because of operations and maintenance considerations. This incident led to a search for referencing systems with only passive devices in the roadbed or along the road.

Various referencing systems have been proposed in the last four decades, all of which can be categorized into *look-down* and *look-ahead* systems. The look-down systems measure the lateral error at a place within the vehicle boundaries. The most famous example of look-down referencing systems is magnetometer [168]. Discrete permanent magnets were used in [169] for implementing lateral control algorithms. Guldner *et al.* employed magnetic markers to code road information [170]. The magnet binary coding in that study could also code information such as road geometry, lane change permit, merge/diverge, and Kilometer-post.

In contrast to look-down systems, look-ahead systems try to mimic human driving behavior by measuring lateral error at a distance ahead of the vehicle. One of the earliest methods presented in this category was a forward-looking chirp monopulse [171] developed at Ohio State University. In this method, a frequency selective surface (FSS) strip is installed at the center of the lane, so that the radar chirp can identify the vehicle lateral error. This technique could also provide the distance to the preceding vehicle by detecting the echo of the radar pulse.

The most commonly used look-ahead referencing systems are machine vision systems which employ cameras and image processing techniques [172, 173]. The main advantage of visual guidance techniques is the minimal infrastructure modification they require. Vision-based systems can be employed not only for lateral control of the vehicle but also for its situation awareness. They were also used for designing active safety systems such as Emergency Lane Assist (ELA) [174]. Another advantage of camera-based systems is in the lane change maneuver where they can continuously provide the reference signal, which is impossible in systems with magnetic markers or FSS. On the other hand, the main disadvantage of computer vision based systems is their dependency on light and weather conditions. Enhancing image processing techniques to improve the robustness of such systems is ongoing research [175-178].

2.5.2. Lateral Control Algorithms

As lateral control is central to driving, it has been extensively studied [40]. The research on lateral control has been reported by many government-funded programs,

industrial sector, and academia [63]. Currently, research on designing reliable and effective lateral control system for both autonomous vehicles and active safety systems in manually driven cars is ongoing.

Steering assistance is available in many vehicles in various forms including lane-keeping support systems [179]. The differences in these systems are mainly due to the controller algorithm, which will be explained later, or the control signal. The control signal in these systems is either (1) steering angle or (2) steering torque [179, 180]. Whereas most of the practical available lane-keeping systems have used steering torque as the control signal [181-183], many researchers in academia have selected steering angle as the control signal for lateral control [180].

In practice, various sensors can measure the lateral error of vehicle position. These sensors, which are usually accompanied by a signal processor to estimate the lateral position of the vehicle with respect to the lane, include differential global positioning systems [184], cameras [185, 186], and magnetometers [168].

Another major part of the lateral control system is performing lane change maneuvers [187]. This maneuver is performed in four steps: sense, perceive, decide, and act. A combination of sensors including camera, Radar, Laser, and infrared is usually required for this task [188]. Various algorithms have been proposed by researchers for performing lane change maneuvers. A review of many of these techniques is presented in [189].

Active driver-assistance systems of the vehicle related to its lateral movement are increasingly being used in commercial vehicles. Although there are still many problems that need to be addressed, these active systems are being improved rapidly and can already perform many fully autonomous tasks including parking, lane changes, and obstacle avoidance [190]. A comprehensive list of such active safety systems is presented in [174].

A vast range of control algorithms has been used for all different task of lateral control mentioned above. Among the methodologies employed are linear quadratic

control (LQ) [191], lead-lag control [192], optimal preview control [193], sliding mode control [194], virtual curvature method for lane change [188], extended Kalman filter [195], and genetic algorithm [196]. Some researchers have tried to imitate human steering behavior using fuzzy logic controllers [197], artificial neural networks [33], and also by using the neuromuscular dynamics [198].

In the last decade, following the implementation and excellent performance of model predictive controllers (MPC) in various industrial projects [199], many researchers and companies in automotive industries have started using this algorithm for the lateral control of autonomous vehicles. For example, MPC was used for double change maneuver in [200]. Lee and Yoo designed a controller using MPC algorithm using sideslip angle and vehicle velocity [201]. In 2010, Anderson et al. applied MPC to plan optimal vehicle trajectories to keep the vehicle in a safe corridor [202].

Less than a decade ago, $\mathcal{L}_1$ adaptive control was introduced by Hovakimyan and Cao [27-29]. In Chapter 6, we employ this algorithm for vehicle lateral control problem. In recent years, this algorithm was applied to control some industrial and military systems. The first and most notable application of $\mathcal{L}_1$ adaptive control was in flight control for aircraft, missiles, and spacecraft [203-206]. These flight tests included different sources of un-modeled dynamics and unknown and variable parameters. Current flight tests are being performed on a prototype commercial jet at NASA. Other than Unmanned Aerial Vehicles (UAV), this algorithm has also been used successfully in drilling systems [207], anesthesia delivery [208], wind turbines [209], and some other industrial systems [27].

Chapter 3.

Detection of Intoxicated Drivers via Steering Behaviour: A System Identification Approach

Impaired driving is known to be among the leading causes of death and injury on the roads [4]; however, as discussed in the previous chapter, the existing measures to address this menace appear to be insufficient. In this chapter, we present a novel method that not only mathematically models the behavior of drivers; also detects intoxicated driving. The algorithm lays a foundation that can be implemented in future cars to derive personalized models of the drivers and to detect intoxicated driving as well as other reckless driving styles.

In this study, we consider the vehicle information and driver input signals to study the behaviors of drivers in performing lateral control task. We rely on system identification techniques based on the input and output signals from the driver to estimate his/her state. In particular, we propose a method to overcome the current shortcomings of intoxicated driver detection, explained in Chapter 2, by considering the lane-keeping task of the drivers and focusing on two signals: the lateral preview error and the steering wheel angle. We employ these two signals to:

1. Present and evaluate two models to describe the lane keeping behavior of sober and drunk drivers
2. Perform online identification on the driver to detect drunk driving by comparing the current model of the driver with the obtained models in the previous part

3.1. Data Collection

3.1.1. Driving Simulator

The dataset used for system identification was collected from several hundred trials on the Forum8 PC-based driving simulator [210] in the Autonomous and Intelligent

Systems Lab (AISL) at the School of Mechatronic Systems Engineering of Simon Fraser University.

The software is a 3D, virtual reality, and real-time urban visualization and transport modeling software referred to as UC-Win/Road. Users can manipulate a dynamic 3D space, import and edit CAD data, build and texture simple block models, automatically build roads, tunnels, and bridges, view multiple design alternatives in real-time, both offline and online, as well as being able to visualize and edit intelligent traffic in different scenarios. The hardware is a quarter-cab fixed-base structure which consists of a simulator of a car with automatic transmission (see Figure 3.1). The simulator includes a driver seat, a steering wheel, brake and accelerator pedals, and a gearshift. Three 42” monitors, connected to a common platform, allow the virtual reality appear more realistic. An analog dashboard is used to display speedometer and revolution meter. The software development kit (SDK) of this set is in Delphi, and the plugins of the software can be designed by the users. Integration of the simulator hardware and the software provides a real-time interaction of the driver with the virtual environment through visual, auditory, and haptic channels.

Figure 3.1. Driving simulator used for data collection

One of the main challenges to overcome was to interface Matlab/Simulink with the driving simulator. We solved this problem using the user datagram protocol (UDP) network. We wrote a plugin within the UC-Win/Road environment which sends and receives real-time data on ports number 4050 and 5000. This configuration (Figure 3.2) facilitates sending and receiving data to/from Matlab/Simulink.

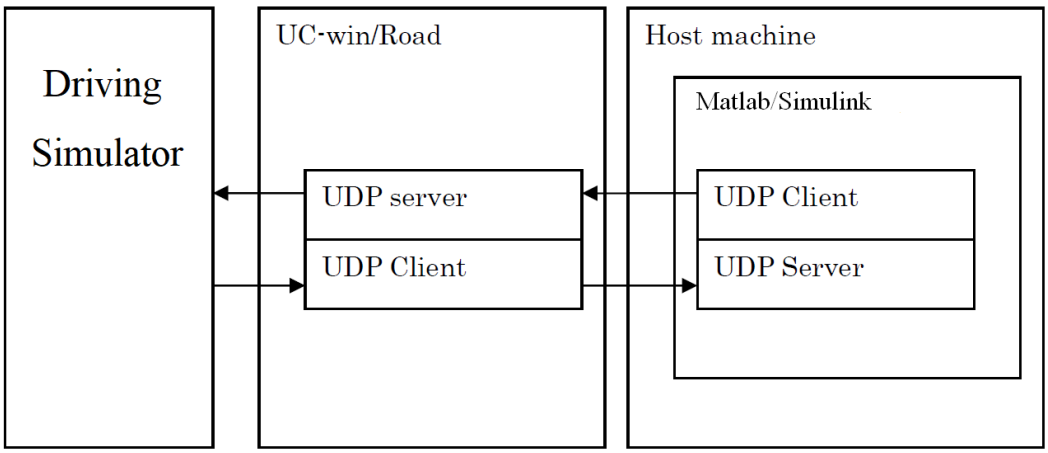

Figure 3.2. UDP connection between Matlab, UC-Win/Road, and the simulator

3.1.2. Experiments

In order to conduct the data collection, we required two sets of data: (i) data from sober drivers, and (ii) data from intoxicated drivers. Regarding the former, we asked ten volunteers who had at least five years of driving experience to participate in the data collection process. All the eight male and two female subjects were in their late twenties or early thirties. We collected the data ensuring that the subjects were sober and alert as drowsiness, drugs, age, fatigue, or emotional states interfered with the driving behavior of the participants. We also made sure that all of the volunteers had sufficient time to get to know the system and feel comfortable with the driving simulator. Data was collected between 9:00 to 10:00 am for all the subjects. There was no distraction in the environment while the subjects were driving and as data was being collected.

Collecting data for the latter group presented us with challenges. We could not have “drunk” participants in the research laboratory for obvious reasons. Therefore, we decided to “simulate” the state of intoxication. We came across Fatal Vision Goggles that is claimed to mimic the state of alcohol intoxication [211, 212]. One of the most famous indices to show the level of alcohol intoxication is Blood Alcohol Concentration (BAC) [213]. The manufacturer of these goggles suggests that the driving behavior of someone wearing a Silver Label Fatal Vision goggles is comparable to a person with a BAC of 0.17 to 0.20 [214]. In addition, a common phenomenon for driving-while-

impaired (DWI) motorists is that they do not pay much attention to objects (other cars, persons, animals, and obstacles) before these objects move from drivers' peripheral vision into their line of central vision [215]. In order to make the simulation studies more realistic, we attached a couple of lenses to the goggles to create the so-called tunnel vision as shown in Figure 3.3.

Figure 3.3. Silver Label Fatal Vision goggles which equal to BAC of 0.17 to 0.20 and tunnel vision lenses attached to them

The U.S. National Highway Traffic Safety Administration (NHTSA) has conducted a comprehensive study on drunk driving [8] which suggests that one of the main characteristics of drunk driving is having problem to maintain proper lane position leading to occasional weaving, swerving, turning with a wide radius, and drifting as depicted in Figure 3.4. These behaviors were observed in all of the volunteers when they wore the goggles.

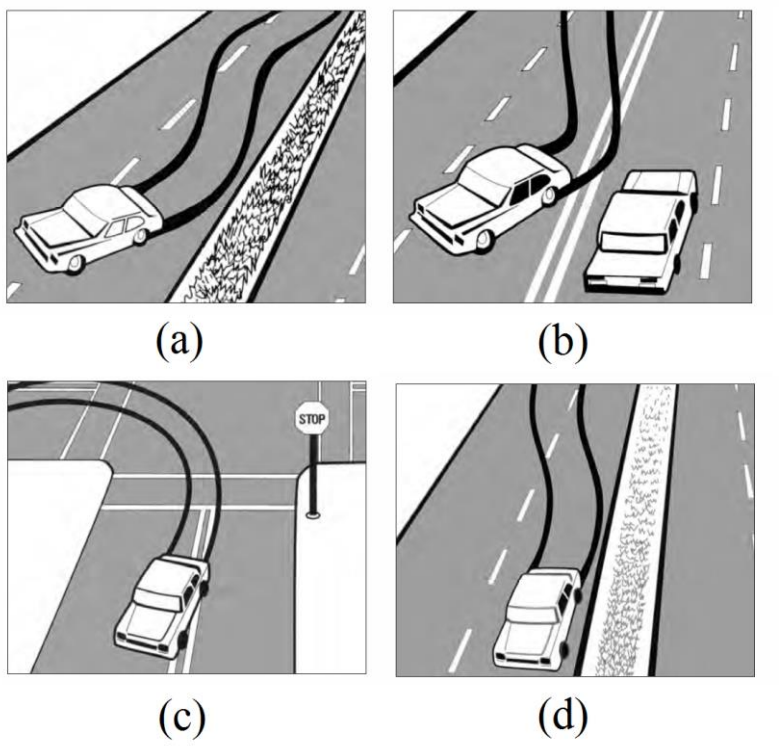

Figure 3.4. DWI driver problems in maintaining proper lane position: (a) weaving, (b) swerving, (c) turning with a wide radius, (d) drifting [8]

We designed four different roads for data collection. The first road was just a simple turn, which was used both as a right turn when driving in it from the beginning to the end, and a left turn when driving from its end to the beginning. The other three roads were short, medium, and long, with the length of 3.5 km, 10 km, and 72 km, respectively. All of them had 5 lanes in each direction and the width of each lane was 2.7 m. The first two roads and the curvatures of the second two roads are shown in Figure 3.5 and Figure 3.6, respectively. They were designed with different curvatures to excite all modes of the driver lateral control behavior and make the data richer. Whereas having a rich data set and ensuring sufficient excitation are very important steps for the purpose of system identification, they have generally been ignored in previous studies of driver modeling [216, 217]. Majority of reported studies have only considered simple straight highways.

(a) (b)

Figure 3.5. (a) Road no. 1, a simple turn (b) Road no. 2, a short road (3.5 *km*)

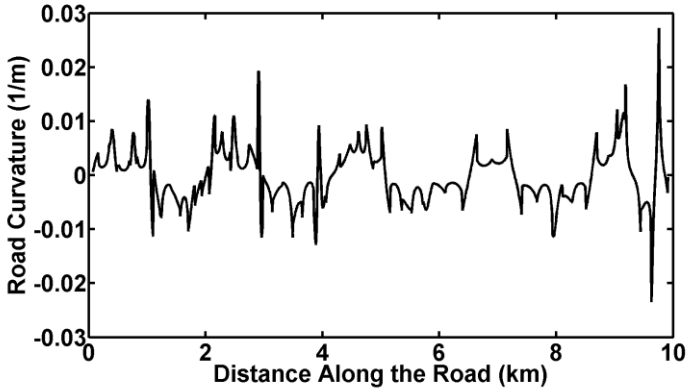

(a)

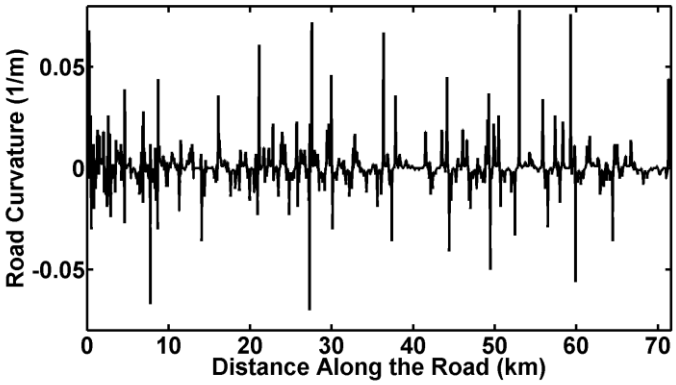

(b)

Figure 3.6. The curvature of (a) road no. 3, medium road (10 *km*) (b) road no. 4, long road (72 *km*)

The volunteers attended five sessions of driving. The first session was designed for their familiarization with the simulator and lasted about two hours for each driver. This practice run involved both rural and urban driving, highway, intersection, traffic, and parking scenarios. The main goal of this session was to provide the volunteers with a

"feel" of the dynamics of the driving simulator and the driving environment. In the second visit, each subject was asked to drive along the road no. 1 twice, once from the beginning and another time from the end. They drove down the roads nos. 2 to 4 once in the same session. The same procedure was repeated in the third visit, but the volunteers were asked to wear the goggles. The fourth and fifth trials were identical to the third and second ones, respectively. The reason to collect data in different sessions was to prevent the fatigue of the drivers. Based on the recommendations in [11] and [216], the numbers of these sessions and drivers are enough in order to establish the desired models. The drivers started all the roads in the third lane and were asked to remain in that lane. They were instructed to strictly adhere to a speed limit of 80 km/h. The experiments were conducted in a low traffic environment whereby occasional motorcycles, sedans, sport utility vehicles (SUVs), and trucks passed by.

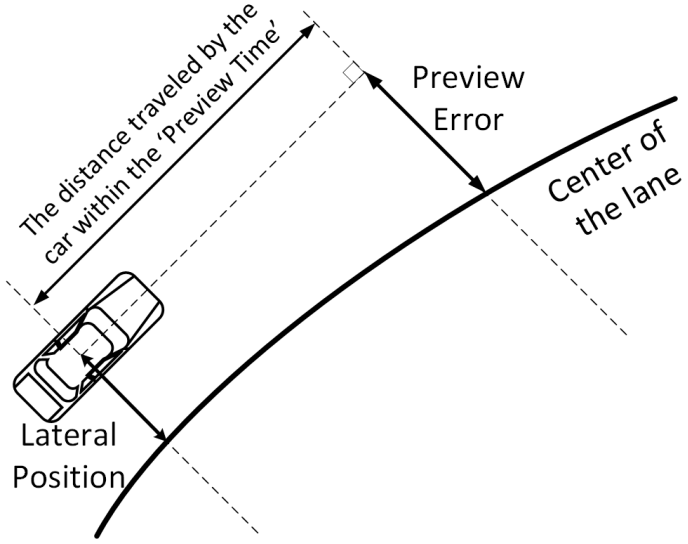

Figure 3.7. The magnitude of the Preview Error (PE) and the Lateral Position are shown. The signs are considered positive if the position is on the right side of the center of the lane. Otherwise, it is considered negative.

Output logs consisting of 60 parameters including xyz positions, the direction of the car, steering wheel angle, pedals values, yaw, pitch, roll, road curvature, and the offset from the lane center were recorded at each instance for each driver. In the next section, we will further discuss that the preview error signal and the steering wheel angle were employed for the identification purpose. While the steering wheel angle is easily

available, the preview error signal should be calculated using the position and the direction measurements of the car and the coordinates of the center of the lane, as depicted in Figure 3.7. Samples of these two signals from one of the subject drivers are shown in Figure 3.8.

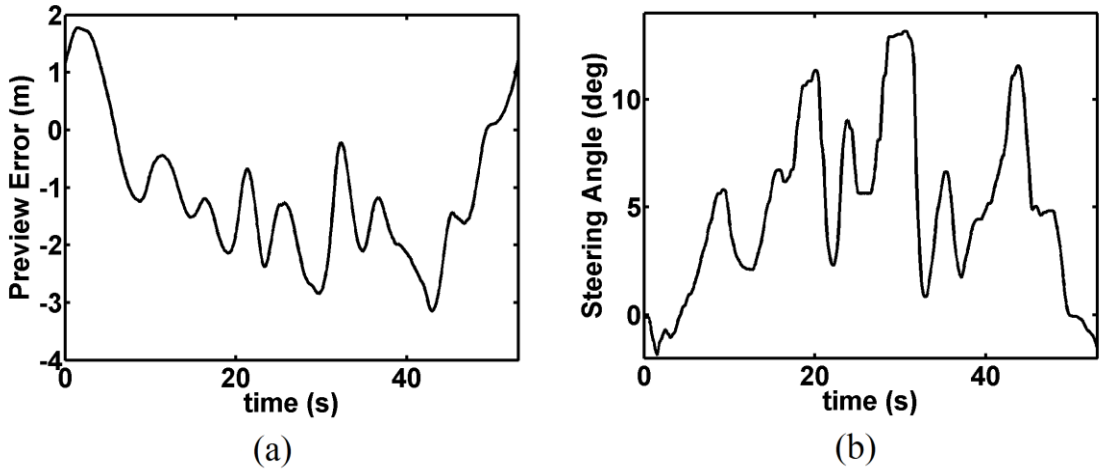

Figure 3.8. Sample (a) preview error and (b) steering wheel angle data collected on road no. 1

3.2. Identification of Sober and Intoxicated Driver Lateral Control Behaviors

We apply system identification techniques on the data sets collected from the driving simulator to estimate two models for drivers while they are sober and intoxicated. These models will be used in the next section to detect drunk drivers. We consider a black-box driver model where the input of the driver is the preview error (pe) and the output is the steering wheel angle (δ). This idea of the lateral control behavior of the driver is shown in Figure 3.9.

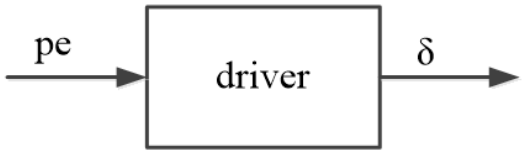

Figure 3.9. Black-box driver model where pe is the preview error and δ is the steering wheel angle

3.2.1. Pre-processing the Data

The periodogram of data is plotted in Figure 3.10. This periodogram is computed by taking the absolute squares of the Fourier transforms of the data, divided by the number of data points, and multiplied by the sampling interval. This data spectrum shows that the two signals we use in our system identification do not have any significant frequency component above 1.7 Hz (10.7 rad/s). Since the rule of thumb is to use a frequency ten times this value as the sampling time, we set the sampling rate to 17 Hz for our signals.

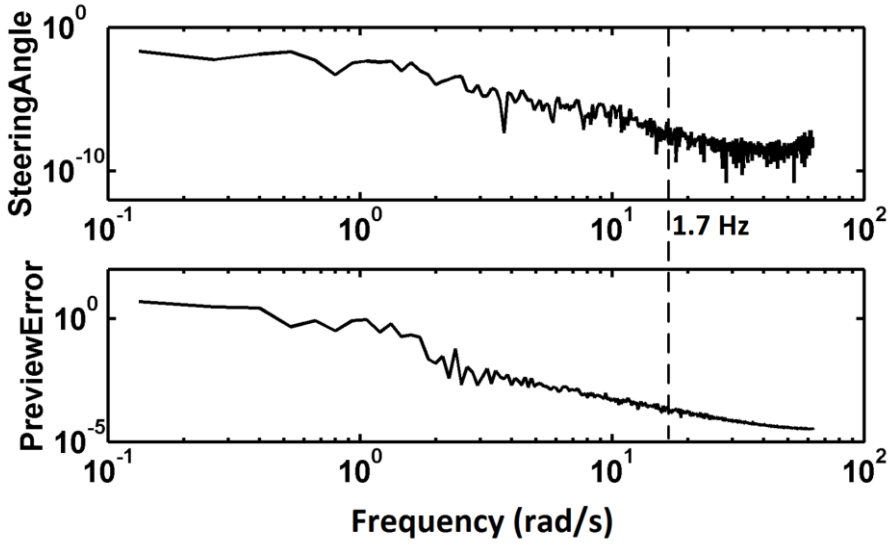

Figure 3.10. Sample signals spectra. The values of components after 1.7 Hz (10.7 rad/s) are very small.

The distance between the center of the lane and the center of gravity of the car was considered as the lateral position, as shown in Figure 3.7. We noticed that most drivers did not drive exactly at the center of the lane, even on straight roads. In fact, this lateral position is rather subjective to each driver. Therefore, it should be measured and subtracted from the data so that the dynamics of driver behavior would not be influenced by this offset. Each driver might tend to drive at the right or left side of the lane center, close to or far from it. Therefore, we measured the mean lateral position error for each of the subject drivers and then removed it from the data, through subtraction from the preview error. For this purpose, we asked each driver to drive in the center of the middle

lane of a 5-lane 10-kilometers straight highway without any traffic. The measured mean lateral positions are 10, 5, 38, 34, 17, 18, -1, -29, -25, and -16 centimeters for our drivers. Negative values imply that these drivers tend to drive on the left side of the center of the lane.

In overall, there were 100 sets of data collected for sober driving and another 100 sets were collected for intoxicated driving. We divided each set into two halves: the first half was used for the identification purpose and also finding parametric uncertainty ranges for the models, and the second half was used to evaluate the obtained models (validation data).

3.2.2. Model Structure

Selecting a model structure is a trade-off between simplicity and accuracy of the model to be identified. The two models obtained for sober and drunk drivers will be used in the next section for online identification and detection of DWI motorists. This constraint imposes some limitations on the model structures, one of which is that they necessitate using parametric models. In this study, we considered six different model structures to describe the driver behavior. The structure which resulted in a better model validation was finally selected.

The general linear time-invariant model structure that we considered was also subject to additive random disturbances [218] given by :

$$\delta(t) = G(q)pe(t) + H(q)e(t) \qquad (3\text{-}1)$$

in discrete-time with

$$G(q) = \sum_{k=1}^{\infty} g(k)q^{-k} \qquad (3\text{-}2)$$

$$H(q) = 1 + \sum_{k=1}^{\infty} h(k)q^{-k} \qquad (3\text{-}3)$$

where δ is the steering wheel angle, pe is the preview error, e is the disturbance which we consider as a sequence of independent random variables with zero mean values, G and

H are the transfer functions from pe and e to δ, respectively, q^{-1} is the backward shift operator, and the sequence $\{g(k)\}_1^\infty$ is the impulse response of the system.

For describing the relation between the preview error and the steering wheel angle signals, the simplest parametric input-output relationship used in our study was the auto-regressive with exogenous input (ARX) structure. Such models are very common in signal-processing applications. In these models, $G(q)$ and $H(q)$ in (3-1) are considered as

$$G(q) = \frac{B(q)}{A(q)} \qquad (3\text{-}4)$$

and

$$H(q) = \frac{1}{A(q)} \qquad (3\text{-}5)$$

where

$$A(q) = 1 + a_1 q^{-1} + \cdots + a_{na} q^{-na} \qquad (3\text{-}6)$$

and

$$B(q) = b_1 q^{-1} + \cdots + b_{nb} q^{-nb} \qquad (3\text{-}7)$$

The simplicity of this ARX model is a remarkable advantage, and it can be selected subject to passing residual analysis (whiteness and independence tests of residuals). However, it fails at describing the disturbance term. This shortcoming can be overcome by considering the disturbance term as a moving average of white noise. By doing this, the structure of $G(q)$ in (3-4) remains the same, but $H(q)$ in (3-5) is replaced by

$$H(q) = \frac{C(q)}{A(q)} \qquad (3\text{-}8)$$

where

$$C(q) = 1 + c_1 q^{-1} + \cdots + c_{nc} q^{-nc} \qquad (3\text{-}9)$$

This model is known as the auto-regressive moving average with exogenous input (ARMAX), and it is a common structure in econometrics and control for both control design and system description. Another version of this structure includes an integrator in noise structure, $e(t)$. In these models the structure of the disturbance is

$$\frac{C(q)}{A(q)\Delta}\, e(t) \qquad (3\text{-}10)$$

where

$$\Delta = 1 - q^{-1} \qquad (3\text{-}11)$$

Putting Δ in the denominator of the noise model indicates that the noise is non-stationary ($e(t)/\Delta$ is known as a random walk) and it forces integration in the controller to be designed later. In this study, we considered the third and the fourth model structures to be used as ARX and ARMAX with the noise integrator Δ, which are referred to as ARIX and ARIMAX models, respectively.

All the four considered models so far in our study had a common factor A in the denominators of the transfer functions G and H in (3-1). Output error (OE) and Box-Jenkins (BJ) model structures are the other two models that we considered for describing the lateral behavior of drivers. These models did not have the common factor A in the transfer function from noise to output. In the output error model structure, the term $e(t)$ was directly added to the output. In other words, we parameterized the dynamics of the driver behavior in this model, but we did not estimate a noise model:

$$\delta(t) = \frac{B(q)}{F(q)} pe(t) + e(t) \qquad (3\text{-}12)$$

Finally, the Box-Jenkins model structure provides completely independent parameterization for the driver dynamics and the noise, using rational polynomial functions. The advantage of this structure is that it provides the highest flexibility for modeling compared to the previous five models. The disadvantage is the higher number of parameters to be estimated. This model structure can be described as

$$\delta(t) = \frac{B(q)}{F(q)} pe(t) + \frac{C(q)}{D(q)} e(t) \qquad (3\text{-}13)$$

The six model structures used in this study are summarized in Table 3.1. After estimating the parameters of each model, the *best* one was employed for online identification and detection of drunk drivers in next section. The *best* model structure is the one that shows better results in these two validations tests: First, we compared the measured outputs and the simulated ones for models obtained in different structures. Second, we tested the residuals for whiteness and independence of past inputs.

Table 3.1. Black-box model structures used here as special cases of $A\delta = B/F\ pe + C/D\ e$

Model Structure	*Polynomials Used*	*Noise Integration*
ARX	A, B	No
ARMAX	A, B, C	No
ARIX	A, B	Yes
ARIMAX	A, B, C	Yes
OE	B, F	No
BJ	B, F, C, D	No

After selecting each model structure, it is important to select the order of the model. The common method is trying several values for the orders and choosing the best. There is a compromise between simplicity and accuracy in this stage as well. In addition, there are some criteria for choosing the model order available in the literature [218]. Akaike information criteria (AIC), final prediction error (FPE), and Rissanen MDL criterion are three of these criteria which are used in our study [219, 220].

3.2.3. Delay Estimation

Regardless of the model structure we choose for identification, there is an inherent delay in the behavior of the driver which should also be identified. One option for determining the value of the delay is simply to use the driver reaction time suggested in the literature (e.g., in [120]). However, the input-output pair and the preview time used here is unique, and it has never been used previously. Therefore, it is not possible to use this method to identify the delay.

Another option for finding the delay of systems is plotting the impulse response of the system. In this case, the delay was obtained by identifying the time when the first variation in response occurred. However, since our data was collected in a closed-loop system, the delay estimated using the impulse response method is not valid [218].

In this study, we consider a fixed ARX model with a range of delays for the input-output channel and then choose the delay which results in the best fit. We repeat this for each driver to find the appropriate delay value for each subject. This delay time, which is the summation of reaction time and neuromuscular delay [120], will be used in all six models identified for each driver.

3.2.4. Closed-loop Identification

An important problem in system identification is the existence of feedback in the data. The techniques used for system identification will be different if the data is collected in a closed-loop system. The setup in which we collect the data in this study is a closed-loop system, i.e., contains output feedback. The simulator is controlled by the steering command given by the driver (δ) and the driver uses the preview error (pe) as his/her input for lateral control of the vehicle. In other words, while it is ideal for system identification techniques that the input of the system to be identified (pe here) be independent of the previous outputs (δ here), they are strongly correlated in a closed-loop configuration (see Figure 3.11).

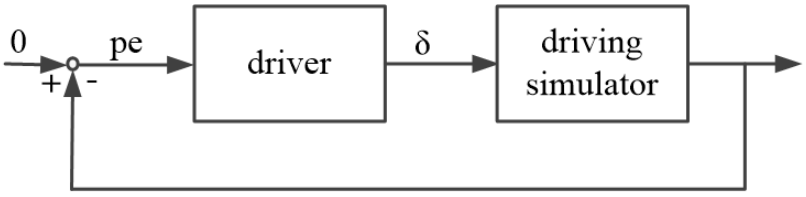

Figure 3.11. Schematic closed-loop system used for identification

The most important problem with the closed-loop data is that it usually has significantly less excitation compared to the data collected in an open-loop system. This problem refers to the concept of persistent excitation [221]. In fact, one of the main goals of introducing feedback in a system is reducing the sensitivity of the closed-loop system

to changes in the open-loop system. This phenomenon has a negative effect on system identification where richness in excitation is crucial.

Since the nature of driving a vehicle involves this closed-loop configuration (it cannot be performed in open-loop), we solved this problem by making the excitation richer by designing roads with a high number of sharp and smooth turns, as shown in Figure 3.6. In addition, we added some small wind disturbance while collecting the data. Finally, we included some unevenness in road pavement in a few parts of the roads. These three elements (curves, winds, and unevenness) significantly increased the richness of data so that it had enough information to be used in the closed-loop identification.

There are three methods available in the literature to identify systems using the closed-loop data: direct, indirect, and joint approaches [218]. The method used here is the direct identification approach where the estimation method is applied straightforwardly: we ignored the feedback and used δ and pe as if they were collected in an open-loop configuration. In addition to data richness problem, which was solved here as explained before, the most significant drawbacks of this approach was the need for good noise models. Since ARMAX, ARIMAX, and BJ structures estimate a noise model, we expected that they could model the driver lateral behavior better than ARX, ARIX, and OE models.

The final problem that should be considered in the closed-loop identification was that many estimation methods that work well and give consistent estimates for the open-loop data would probably fail when used in the direct approach when dealing with the closed-loop data. In fact, even many of the well-known estimation methods cannot be used with the closed-loop data, including instrumental variable method, subspace method, spectral and correlation analysis, and output error methods with the wrong H transfer function (noise model) [218]. Therefore, we applied the prediction error method which produced consistent estimates and optimal accuracy even in the presence of the feedback in data.

3.2.5. Identification Results and Validation

The steering behavior of drivers can be modeled using two different approaches. The first approach is finding a specific model for each driver and the second one is presenting a more general model using the data collected from all the driver subjects. Even though the first approach results in models with smaller uncertainty, it needs two training procedures for each different driver while they are sober and intoxicated. For that reason, we used the second approach in this work and presented two generic models for each case using 200 collected data sets.

The first parameter that should be identified in this method is the preview time. In previous works such as [222], a preview time equal to 1 s was considered for the driver. However, investigating 200 sets of data and testing a range of preview times from 0.1 s to 5 s showed that 1.25 s is the optimal value and results in the best fit for the data, as shown in Figure 3.12.

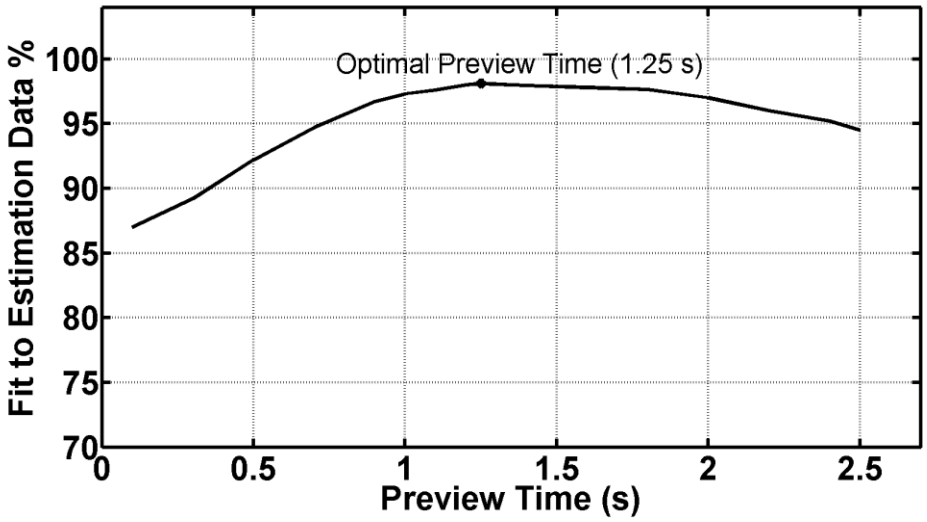

Figure 3.12. The optimal preview time, considering the best fit to estimation, is obtained at $1.25\ s$

The next parameter that should be fixed during the identification procedure was the delay time. Using the method mentioned in section 3.2.3, we identified the average delay time as 1 sample or 0.06 s. This is obtained from an ARX model with $n_a = n_b = 2$

for all the drivers. The delay value (k) that results in the best estimation fit is $k = 1$ which will be used as the delay for all 6 model structures..

Table 3.2. Parameters of six models of steering wheel behavior of sober drivers and an ARIMAX model presented for drunk drivers (last row)

Structure	a_1 / f_1	a_2 / f_2	a_3 / f_3	a_4	a_5	b_1	b_2	c_1	c_2	d_1	d_2
ARX	-1.771	0.126	1.18	-0.527	—	-0.001	—	—	—	—	—
ARIX	-0.767	-0.716	0.726	0.966	-0.216	-0.011	—	—	—	—	—
ARMAX	-1.053	-0.730	0.801	—	—	-0.001	—	0.586	—	—	—
ARIMAX	-0.644	-0.740	0.514	—	—	-0.008	—	0.0142	—	—	—
OE	-3.795	5.472	-3.55	0.874	—	-5e-4	—	—	—	—	—
BJ	-2.833	2.685	-0.852	—	—	-0.001	0.001	-0.040	0.590	-1.782	0.790
ARIMAX (d)	-0.887	-0.760	0.707	—	—	-3.3e-4	—	-0.201	—	—	—

Using a fixed preview time of 1.25 s and a fixed delay time of one sample, the best model structure for sober drivers were found using the residual analysis of the best model (the model that fits data the best) in each structure. Using prediction error estimation techniques, the best parameter values that could describe the lateral control behavior of drivers were found for each of the six structures and shown in Table 3.2.

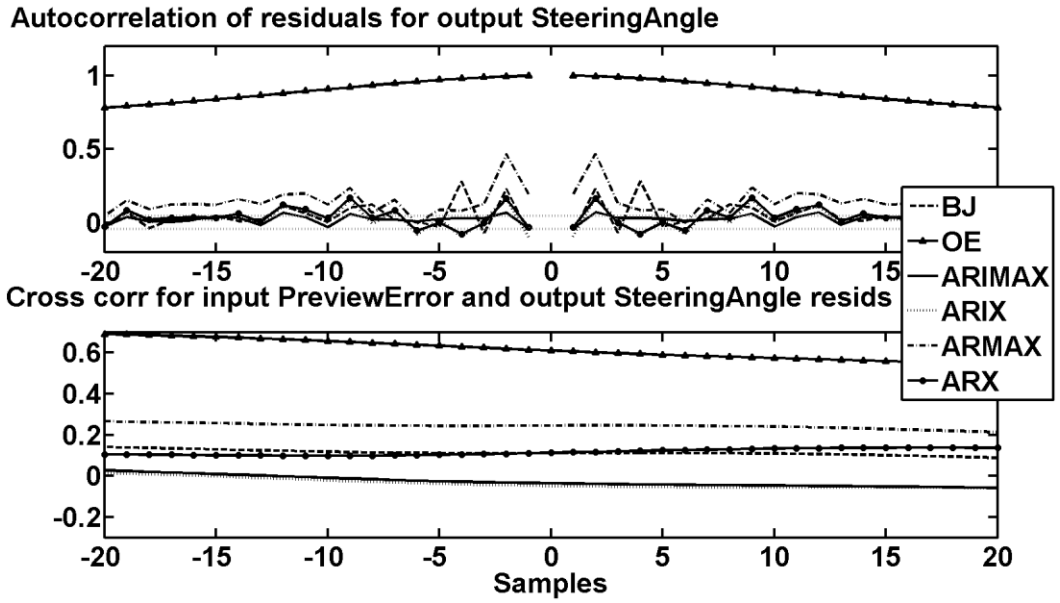

Figure 3.13. Residual analysis of six different models structures. Whiteness test (above) shows that ARIMAX is the only structure that autocorrelation of residuals fit in the 99% confidence interval. Independence test (below) shows the superiority of ARIX and ARIMAX models.

Whiteness test of residuals, shown in Figure 3.13, shows that ARIMAX is the best structure because its auto-correlation plot fits in the 99% confidence interval. Moreover, the independence test (cross-correlation) shows that the selected delay value is appropriate and results in almost zero cross-correlation for the ARIMAX structure. Therefore, this is the model we selected in this study to describe the steering wheel behavior of sober drivers.

One of our objectives of finding a model for sober drivers was to identify a model with a similar structure as intoxicated drivers and to detect them using online system identification. Since the best model we presented for sober drivers is an ARIMAX model, we also found a model with a similar structure for 100 sets of data we have from the drivers who drove the simulator vehicle wearing fatal vision goggles with tunnel vision lenses attached to them (simulated drunk driving). The result is shown in the last row of Table 3.2.

3.3. Online Identification and Drunk Driver Detection

Mathematical models of sober and impaired drivers were presented in the previous section. We would like to use these models to identify alcohol-induced driving. The main idea is to use online identification techniques to update the model of the driver while he/she is driving. The model structure used for online identification should be fixed and the same as the structure we used previously, i.e., ARIMAX structure with $n_a = 3$ and $n_b = n_c = k = 1$.

In order to perform this task, instead of generating one generic model based on the 100 sets of data, 100 different models based on each set of data are generated. Then this procedure was repeated for 100 sets of data collected from impaired drivers. There were five parameters which should be identified for each of these 200 models: a_1, a_2, a_3, b_1, and c_1. The parameter variations of all these 200 models are shown in Figure 3.14. In addition, the mean and the standard deviations of the parameters are displayed in Table 3.3. Since the values of parameters are very close to each other, they cannot be used to detect DWI drivers.

The parameter that can be considered an exception is b_1 which is higher for impaired drivers in most of the models. In the ARIMAX model structure presented here, the parameter b_1 is proportional to the gain of the system (driver). The fact that it is higher for impaired driver is not far from expectation. Human factor scientists have reported previously that alcohol causes aggression in the behavior of the drivers [215]. Higher gain in the driver model is in complete agreement to the aggressive driving style of DWI motorists.

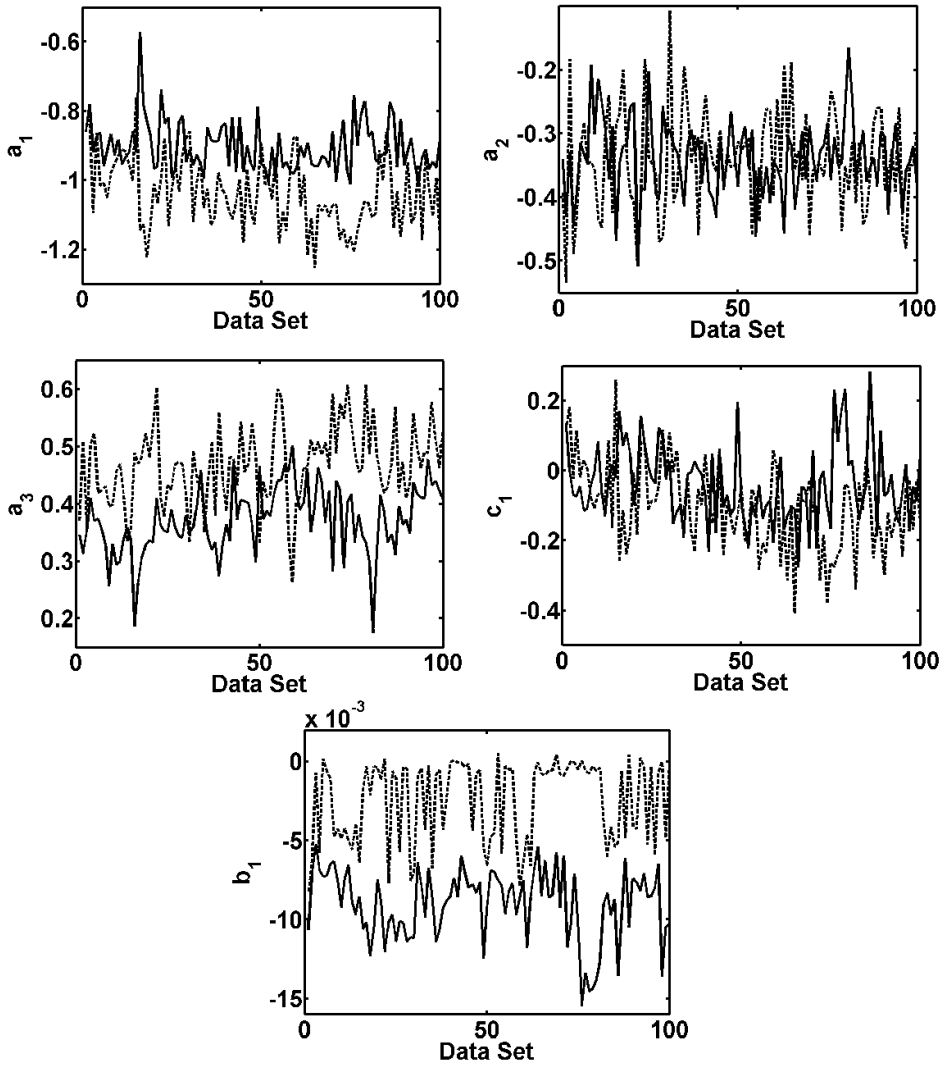

Figure 3.14. The variation of model parameters of sober (solid) and impaired (dashed) drivers

While the values of the parameters of the models related to sober and intoxicated drivers do not show a significant difference, it can be observed that the positions of the

complex conjugate poles of these two models have a meaningful and considerable difference. The model structure used here has three poles in the steering dynamics of the driver. These poles include a real-valued pole between -0.65 and -0.9 and two other poles which are complex conjugate in more than 95% of our data sets, as shown in Figure 3.15.

Table 3.3. Mean and standard deviation of model parameters for sober and impaired drivers

	a_1	a_2	a_3	b_1	c_1
Mean (sober)	-0.9037	-0.3398	0.3706	-0.0091	-0.0383
SD (sober)	0.0729	0.0602	0.0590	0.0022	0.1107
Mean (impaired)	-1.0386	-0.3424	0.4674	-0.0025	-0.1034
SD (impaired)	0.1025	0.0797	0.0686	0.0026	0.1232

The complex conjugate poles associated with each group of the data sets (sober or impaired) are in two regions shown in Figure 3.15. Although these two regions have an overlap, in more than 80% of the models the poles are outside the overlap region. The fact that the poles related to DWI drivers are closer to the point $(1 + j0)$, unit circle, and the instability region, clearly shows that their behavior is more aggressive and confirms all previous results available in the literature.

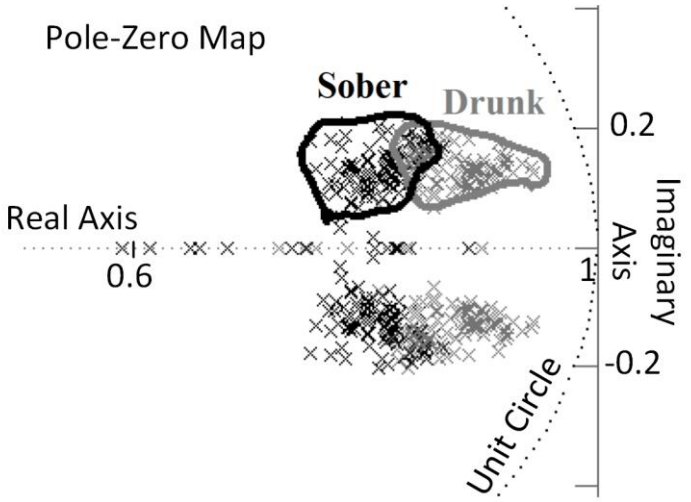

Figure 3.15. Regions of complex conjugate poles of identified models for sober (black) and impaired (gray) drivers (plotted using 200 sets of data)

Although these two regions slightly vary for different car dynamics, for any specific car these two regions can be identified and used to detect alcohol-induced driving. The basic idea is to use recursive system identification techniques and Kalman filter algorithm [218] to update the model of the driver. At each instant, the poles of the driver model are calculated. If for several samples the poles remain in the area associated with intoxicated drivers, one can conclude that the driver is under the influence of alcohol (or drives similarly to someone who is intoxicated).

In order to test the performance of this method, one of the subjects was asked to drive for a few minutes in the simulator. Meanwhile, online identification techniques were performed using the structure and the initial model obtained previously. He was then asked to wear the goggles to simulate the intoxicated driving behavior. This moment is considered to be at $t = 0$. The conjugate pole of the model of the driver, which is inside the region associated with sober drivers, is shown in Figure 3.16 at this moment. Data collection at the sampling rate of 17 Hz is continued and the parameters of the fixed structure model are updated using this data. After about 2 seconds of driving the pole moves out of the sober driver region and after about 10 seconds it enters the region associated with intoxicated drivers. The driver continues driving for about one minute and during this time the poles of updated models remain in the impaired driving region. Hence, the alcohol-induced driving is detected.

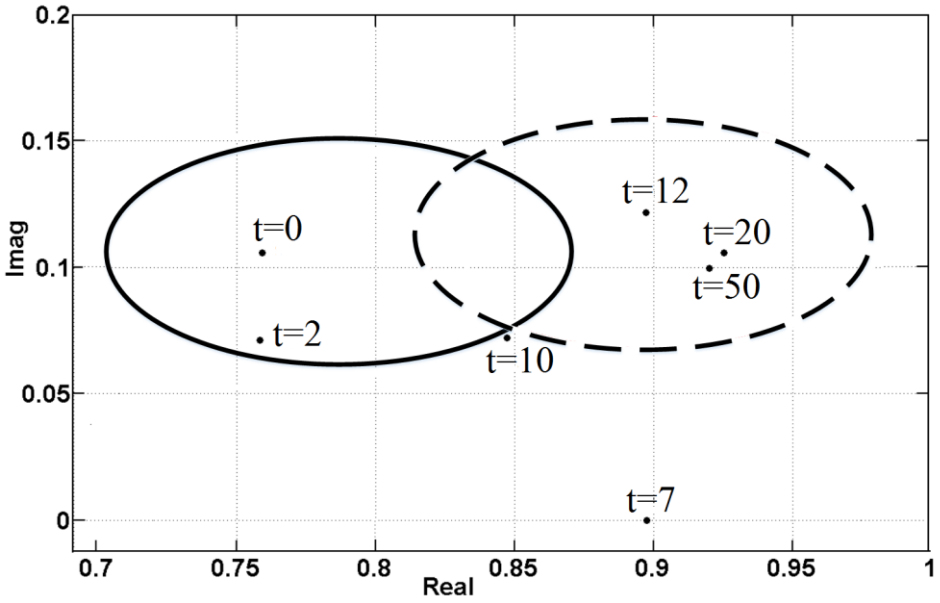

Figure 3.16. Place of complex pole in online identification of intoxicated drivers

In order to test the robustness of the algorithm, this test was repeated 150 times and drivers were asked to drive the car first without the goggles, then wearing the goggles. After 30 *s* the system decided whether they showed the behavior of alcohol-induced drivers or not. In 116 cases (77%) the system successfully detected impaired driving. In 13 cases (9%) the poles remained in the sober region, and they were not detected. In other cases, the poles were outside both of the regions. We also observed a false alarm rate of 8%. These results can be improved by training each driver and finding the regions which are specific to each driver. However, the trend that the complex poles move to the right can be seen in all the cases of intoxicated driving.

3.4. Conclusion

Driver assistance systems and vehicle safety systems are used to improve the driving performance of the driver. One of the important requirements in designing such systems is the driver mathematical model. Although different models of sober drivers are available in the literature, to the best of our knowledge, the steering behavior of intoxicated drivers has not been reported.

In this section, we applied system identification techniques and presented two models to describe the lateral control behavior of sober and drunk drivers. In these models, the preview error at 1.25 s ahead of the vehicle was considered as the input to the driver and the steering wheel angle of the vehicle was treated as the driver's output. Different linear model structures were investigated and the ARIMAX structure was chosen as the best structure to describe the behavior of drivers.

The delay time (reaction time) is a very important parameter to be identified in any system identification problem. The delay we found in our model was about 0.06 s which is less than the usual delay values reported previously for the drivers. This is resulting from the preview error considered as input here. Since the driver output depends on the error if the vehicle goes in the same direction for 1.25 s, the model involves a smaller delay compared to the models that consider instant error as the input of the driver.

The 200 sets of data collected in driving simulator were split into two halves: the first half was used only for identification and the second half for validation of the models. The model validations show that the proposed models can successfully predict the behavior of both types of drivers. Also, the residual analysis was performed, and the validity of the model was confirmed.

In this study, we also introduced a novel method to detect alcohol-induced driving. We showed that if an ARIMAX model is considered for drivers, the positions of two complex conjugate poles of the models will be indicators of the intoxicated driving behavior. We used online identification techniques to identify and update the model of the drivers while they are driving. We demonstrated that this method could facilitate recognition of sober and intoxicated drivers through checking the poles of the model.

This method of identifying DWI drivers not only is useful in detecting alcohol-induced driving but also can be used as a measure to evaluate the performance of the driver. It can also detect any other impairment that might have a similar effect as alcohol on driving behavior. Since the region of specified poles for intoxicated drivers in our model is associated with aggressive behavior of drivers, it can be used to detect any aggressive driving behavior as well.

Detection of driver impairment, especially driver drunkenness, is one of the most important problems in transportation systems and it is very crucial for the safety of all drivers, passengers, and pedestrians. The proposed novel method can be used to develop a warning system for driver impairment as well. However, there is room for further improvement in the future. In this analysis, we used vehicle information (preview error) and vehicle input (steering wheel angle) to detect alcohol impairment. Accelerate and brake signals can also be added to the system to make the detection more accurate. In addition, this information can be used together with the physiological state of the driver to make the DWI detection more precise. Finally, in order to reduce the level of uncertainty, a personalized model of each driver can be used instead of generic models of sober and impaired drivers.

After detection of intoxicated driving, the next step is to modify the steering vehicle signal applied to the vehicle. One solution is removing the driver and performing the steering wheel control autonomously. This solution will be applied in Chapter 5 and Chapter 6. In the next chapter, we investigate the possibility of another solution, which is keeping the driver in the loop and adding serial and parallel controllers to the system to improve the performance.

Chapter 4.

Serial and Parallel Assisting Lateral Controllers

4.1. Introduction

In the previous chapter, we developed and tested two mathematical models to represent intoxicated and sober drivers. After the detection of impaired driving, a semi-autonomous car can be provided with different options including but not limited to switching to autonomous control (overriding the driver), stopping the vehicle, or making a call to the nearest police station. In addition, various advanced driver-assistance systems (ADAS) can be employed to warn the driver or intervene in handling the vehicle.

Although much progress has been made in developing these ADASs, researchers still believe that these systems might distract the driver. For example, the warning systems used in the cars are visual, auditory or haptic [22]. If the driver is looking away, fixed front displays in front of him will not attract his/her attention so it will not be useful. In addition, side screen displays can take the driver's attention off the road and can be dangerous. Auditory or haptic warning systems cannot transmit enough information in a short time. Furthermore, drivers might not like repetitive warning messages when they already have noticed the imminent danger [23].

On the other hand, although the main goal of a driver assistance system is to reduce the physical and mental workload of the driver and therefore to improve safety, the driver would be disengaged from driving if the workload is less than a certain amount.

In this Chapter, we investigate the possibility of two other solutions involving serial and parallel controllers, which can assist the drivers without distracting or disengaging them. The main idea of the serial controller is that the driver control signal (steering signal) is fed to another controller instead of the steering column of the car. The output of this controller is the effective steering signal which acts on the wheels. This control system can be readily implemented using a steer-by-wire system [24] without

requiring additional sensors or actuators (unlike a parallel controller or most similar ADASs). On the other hand, the proposed parallel assisting controller requires additional sensors as it will be explained in section 4.2. The basic idea of this system is to add the driver steering signal to the output of an independent lateral controller. The summation of these two control signals is then fed to the steering column of the vehicle. In this chapter, we investigate whether these two structures can improve the performance of the lateral control of the vehicle.

The organization of the chapter is as follows: Section 4.2 describes the lateral dynamics of the vehicle. The proposed algorithms are described in section 4.3. The simulation results of the serial controller are discussed in section 4.4. The evaluation of this algorithm using human-in-the-loop experiments is presented in the next section. Section 4.6 discusses the simulation and experiment results related to the parallel controller. Finally, section 4.7 concludes this chapter.

4.2. Vehicle Dynamics

A nonlinear six-degree-of-freedom (DOF) vehicle model, which represents the vehicle lateral dynamics as realistically as possible, is developed in [223]. This complex model has sixteen state variables: twelve for the six DOF motions (three translational and three rotational) and four for the tires. A simplified linear two-degree of freedom 'bicycle' model of the vehicle can be obtained from the complex model. Several studies have already established that the simplified model, which we use in this work, is a good approximation of the complex model for all practical purposes [200, 223, 224].

The bicycle model used in this study to describe vehicle lateral dynamics is shown in equation (4-1). The details of this model, its derivation, and its properties will be discussed in Chapter 6 (section 6.1) of this dissertation.

$$\frac{d}{dt}\begin{bmatrix} e_1 \\ \dot{e}_1 \\ e_2 \\ \dot{e}_2 \end{bmatrix} = \begin{bmatrix} 0 & 1 & 0 & 0 \\ 0 & -\frac{2C_{af}+2\,C_{ar}}{mV_x} & \frac{2C_{af}+2\,C_{ar}}{m} & -\frac{2C_{af}l_f-2\,C_{ar}l_r}{mV_x} \\ 0 & 0 & 0 & 1 \\ 0 & -\frac{2C_{af}l_f-2\,C_{ar}l_r}{I_zV_x} & \frac{2C_{af}l_f-2\,C_{ar}l_r}{I_z} & -\frac{2C_{af}{l_f}^2+2\,C_{ar}{l_r}^2}{I_zV_x} \end{bmatrix}\begin{bmatrix} e_1 \\ \dot{e}_1 \\ e_2 \\ \dot{e}_2 \end{bmatrix} +$$

$$\begin{bmatrix} 0 \\ \frac{2C_{af}}{m} \\ 0 \\ \frac{2C_{af}l_f}{I_z} \end{bmatrix}\delta + \begin{bmatrix} 0 \\ -V_x - \frac{2C_{af}l_f-2\,C_{ar}l_r}{mV_x} \\ 0 \\ -\frac{2C_{af}{l_f}^2+2\,C_{ar}{l_r}^2}{I_zV_x} \end{bmatrix}\dot{\psi}_{des} \qquad (4\text{-}1)$$

In the above equation, e_1 is the vehicle displacement error and e_2 is the vehicle orientation error. The longitudinal velocity of the car at its center of gravity is denoted by V_x. The distances of the front and rear tires from the center of gravity and cornering stiffness of each front and rear tire are shown by l_f, l_r, C_{af}, and C_{ar}, respectively. The steering angle is shown by δ and the yaw moment of inertia of the vehicle is I_z. Assuming the radius of the road is R, the rate of change of the desired orientation of the vehicle is defined as $\dot{\psi}_{des} = \frac{V_x}{R}$.

In addition, the output equation of the state-space, the equation that expresses the output as a linear combination of the states, is as follows:

$$y = e_1 + d_s e_2 \qquad (4\text{-}2)$$

where d_s is the look-ahead distance, i.e., the longitudinal distance of the point ahead of the vehicle center of gravity, where the sensor measurements are extracted. The reason why y in equation (4-2) is considered as the output will also be explained in Chapter 6, section 6.1 of this thesis (see page 112). The block diagram of the closed-loop control system is shown in Figure 4.1. In this Figure, $P(s)$ is the vehicle transfer function between the steering angle input for the vehicle and the lateral position measurement output described in equation (4-2). The steering signal (δ) is the output of the controller block, which is the human driver here. The road-determined desired yaw rate $\dot{\psi}_{des}$ affects the system dynamics through a transfer function denoted in Figure 4.1 as $G(s)$

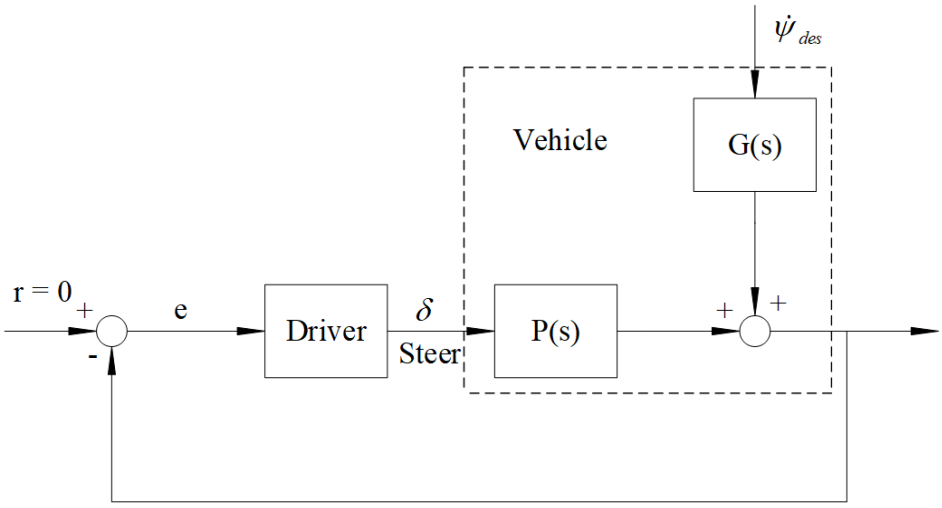

Figure 4.1. Closed-loop driver-vehicle system

4.3. Proposed Algorithms

The conventional driving structure is shown in Figure 4.1. The main controller in this architecture is the human driver. Therefore, if the driver does not drive well (due to fatigue, using cell phones, drunkenness, etc.) the system performs poorly. One solution to this problem is to switch to an autonomous lateral control system, as shown in Figure 4.2. In this system, the driver controls the vehicle in normal conditions and an automatic controller replaces the human driver in other situations. The design of this autonomous lateral controller will be further discussed in Chapters 5 and 6 of this dissertation.

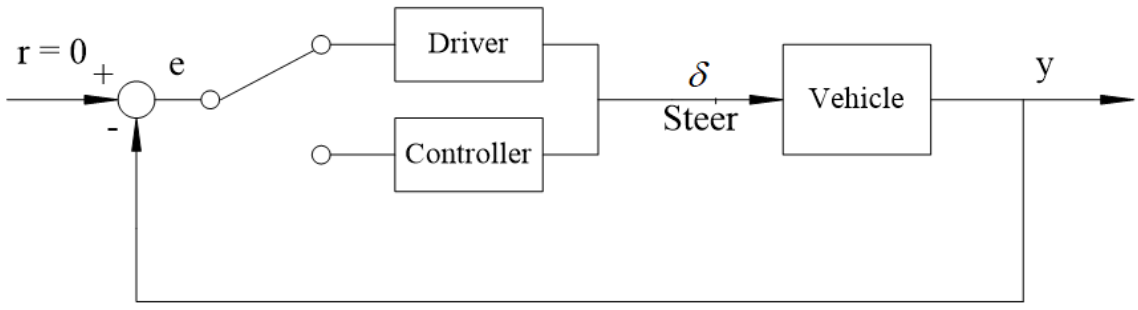

Figure 4.2. Switching to autonomous controller for vehicle lateral control after impaired driver is detected

However, in this chapter, we present two different control structures. The basic idea of the first proposed structure is adding a controller in series with the driver and the

vehicle steering wheel, as shown in Figure 4.3. The main goal is to improve the performance of the whole system while the driver is not driving well due to intoxication or other impairments.

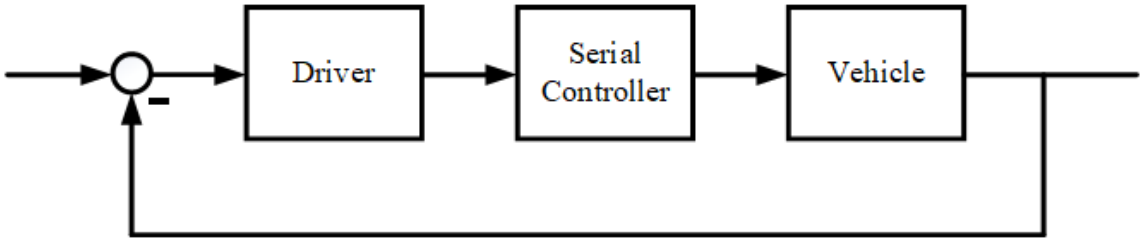

Figure 4.3. Proposed serial assisting lateral controller structure

A parallel controller (as shown in Figure 4.4), instead of this serial controller, has autonomous lateral control ability; however, the price would be extra sensors in the system. The basic idea of this system is to add the driver's steering signal to the output of an independent lateral controller. The summation of these two control signals is then fed to the steering column of the vehicle (see Figure 4.4). Obviously, the parallel control will be less sensitive to driver impairment.

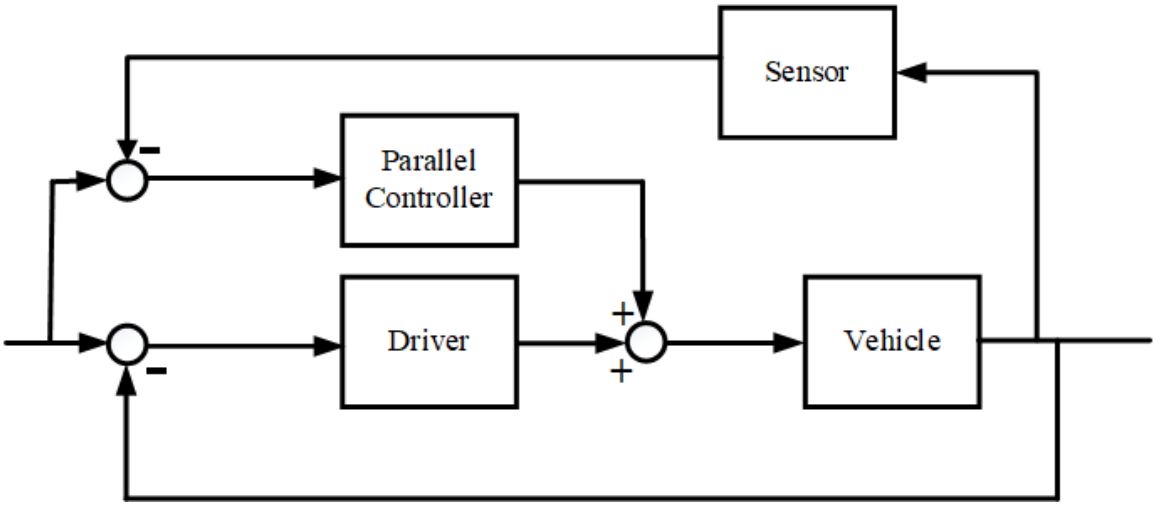

Figure 4.4. Proposed parallel assisting lateral controller structure

In this study, we consider a simple PID controller in standard (non-interacting) configuration [225] for both our serial and parallel controller configurations:

$$C_s(s) = K_{PS}\left(1 + \frac{K_{IS}}{s} + \frac{K_{DS}N_S}{1+\frac{N_S}{s}}\right) \qquad (4\text{-}3)$$

$$C_p(s) = K_{Pp}\left(1 + \frac{K_{Ip}}{s} + \frac{K_{Dp}N_p}{1+\frac{N_p}{s}}\right) \qquad (4\text{-}4)$$

In the next sections, we study the performance of the serial structure through computer simulations and real experiments involving human drivers.

4.4. Simulation Results for Serial Assisting Controller

Considering the structure of the serial assisting lateral controller shown in Figure 4.3 and the model obtained for the intoxicated drivers in Chapter 3, we tuned the PID controller in (4-3). The obtained controller parameters obtained were:

$$K_{Ps} = 0.50,\ \ K_{Is} = 0.02,\ \ K_{Ds} = 5.94,\ \ N_s = 400 \qquad (4\text{-}5)$$

The conventional steering wheel control system (Figure 4.1) and the proposed system including the serial controller (Figure 4.3) were simulated in Matlab. The 'driver' block in both of the systems were the identified intoxicated driver model obtained in Chapter 3. The 'Serial Controller' block in Figure 4.3 is shown in (4-3) and (4-5). The reference (desired) lateral position of the vehicle in this scenario is one meter away from its initial lateral position. The simulation results are shown in Figure 4.5.

The simulation results show that the augmented serial controller can successfully smooth the driving behavior of the driver. Also, the deviation from the reference, which is a common phenomenon among intoxicated drivers, is significantly reduced in the proposed system.

The above results indicate that adding a serial controller can mitigate the weaving driving behavior [8] of impaired drivers. These results are obtained using the fixed model obtained for intoxicated drivers presented in [31]. In the next section, we further investigate the serial assisting lateral control system using our driving simulator setup and actual human drivers.

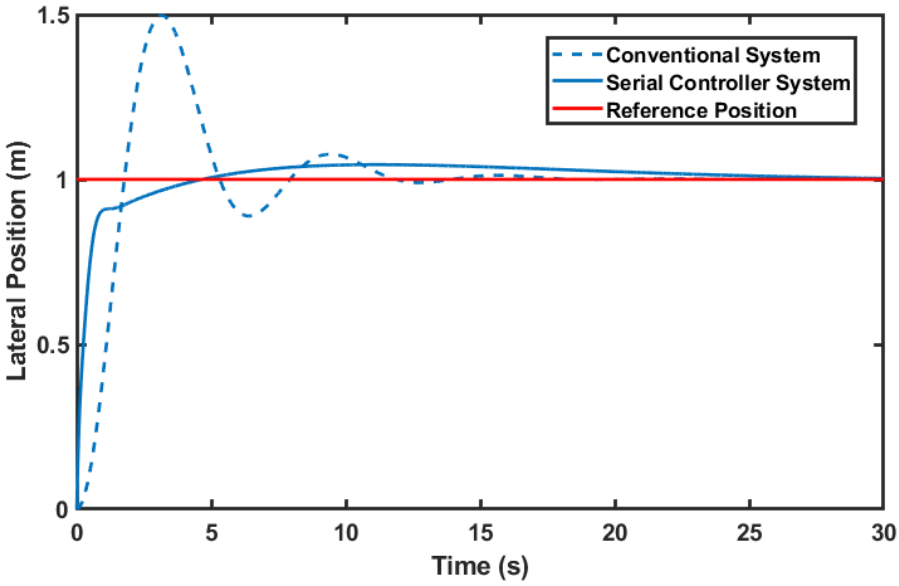

Figure 4.5. Comparison of the performances of conventional steering wheel handling system and suggested serial assisting lateral control (computer simulations)

4.5. Evaluation of Serial Assisting Controller Using Human Drivers

In the previous section, we used computer simulations to show how the proposed serial controller can improve the performance of the steering control system of the vehicle under degrading driver conditions. However, in order to obtain a more realistic assessment of the performance of this controller, we validated the proposed structures in the driving simulator, described in Chapter 3, using actual human drivers. The results from these human-in-the-loop experiments can verify whether the suggested serial controller can improve the performance of the system in keeping the vehicle at the center of the lane.

We asked a human driver wearing the Fatal Vision goggles (to simulate the driving of intoxicated drivers) to drive on a 5-lane straight road twice: first in a normal vehicle, then in a vehicle including the serial controller as shown in Figure 4.3.

The speed of the vehicle was fixed at 70 km/h in this experiment. The vehicle was driven in the third lane initially. At 200 m, there was a sign telling the driver to move

the vehicle to the second lane. At 600 m, there was another sign telling the driver to go to the fourth lane. Finally, there was a sign at 1000 m asking the driver to return to the third lane. This road is shown in Figure 4.6.

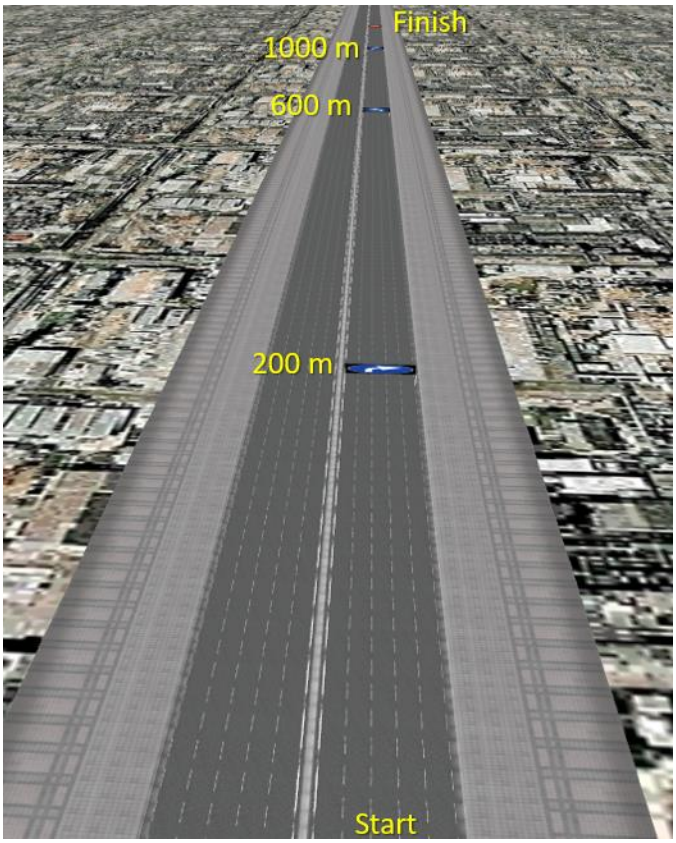

Figure 4.6. The 5-lane straight road

The experiment results are shown in Figure 4.7. In this figure, the vehicle's offset from road center is shown for both cases: (1) when the driver is controlling the vehicle in the conventional configuration shown in Figure 4.1 (blue plot) (2) when the serial controller is added to the system as shown in Figure 4.3 (magenta plot). This figure indicates that whereas the proposed system has improved the performance in some parts, it has had a negative effect in some other parts. In addition, we can see the results obtained from a human driver are significantly different from the results obtained from the computer simulations in Figure 4.5. Therefore, we performed a more systematic study to evaluate the performance of the serial assisting lateral controller.

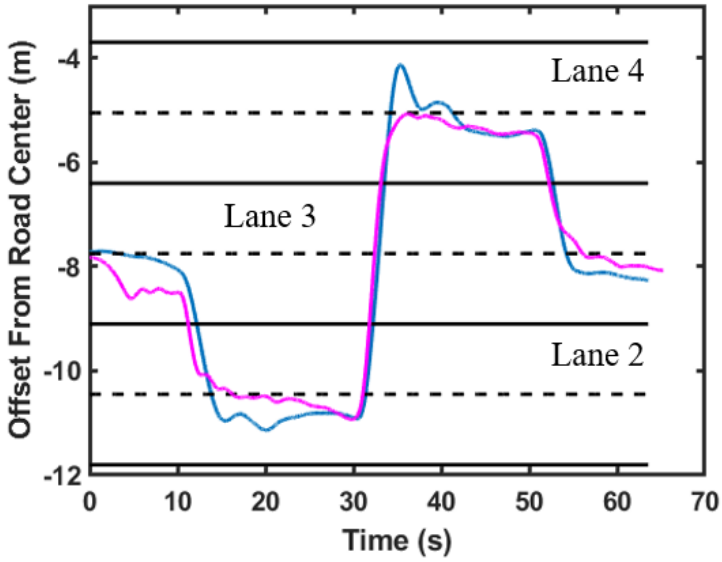

Figure 4.7. Offset from road center of the vehicle in the conventional configuration (blue) and in the configuration including the serial controller (magenta), both driven by the same impaired driver. Dashed lines show the centers of each lane.

In order to evaluate the proposed algorithm properly, we required more human drivers, more datasets obtained from longer driving times, and appropriate evaluation metrics. The next sections of this chapter explain how we addressed these items.

4.5.1. Experiments

The experiments were conducted in the same setup explained in section 3.1. The simulator software was modified so that the serial controller was added to the system. The long road (road no. 4 explained in Chapter 3) was selected for the experiments. Ten drivers volunteered to participate in this experiment. The same Fatal Vision Goggles explained in section 3.1 were used to simulate the driving behaviors of intoxicated drivers. The driving task was about one hour for each. Also, a 10-minute warm-up driving in normal conditions was given to the drivers. The first half of the experiment was conducted in the conventional method (without the serial controller). The serial controller was added to the system in the middle of the experiment. The goal of the drivers was to maintain the vehicle at the center of the lane. The other conditions of driving were the same as explained in Chapter 3 (section 3.1).

4.5.2. Evaluation Metrics

The data from both parts of the experiments, the conventional system (CS) and serial controller system (SCS), are analyzed using two evaluation indices: road departure percentage (RDP) and lateral position standard deviation (LPSD).

In order to define RDP, we defined three variables in Figure 4.8 which shows vehicle location with respect to the lane. Based on this figure, lane departure occurs when $lp \leq \frac{vw}{2}$ or $lp \geq lw - \frac{vw}{2}$. In these two cases, the vehicle enters adjacent lanes. We define RDP as the amount of time when lane departure occurs divided by the whole driving time. This definition follows:

$$RDP = \frac{1}{N}\sum_{n=1}^{N} f\big(lp(n)\big)$$

where N is the total number of data points and

$$f\big(lp(n)\big) = \begin{cases} 1, & \text{if } lp(n) \leq \frac{vw}{2} \text{ or } lp(n) \geq lw - \frac{vw}{2} \\ 0, & \text{if } \frac{vw}{2} < lp(n) < lw - \frac{vw}{2} \end{cases} \quad (4\text{-}6)$$

The goal of defining this evaluation metrics is to test whether the serial controller can maintain lane departures at a lower level or not.

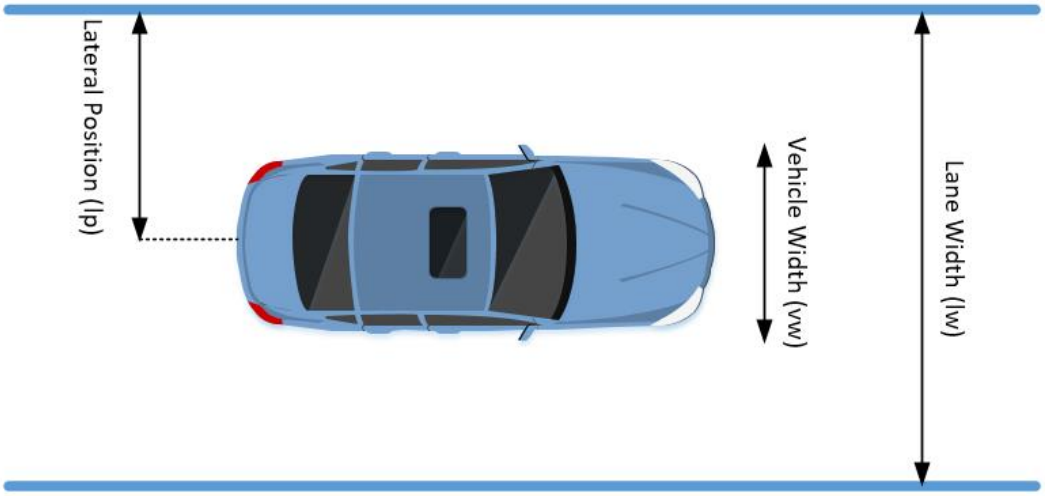

Figure 4.8. Vehicle location with respect to the lane

Lateral position standard deviation (LPSD) is a standard lateral control performance index which is defined as:

$$LPSD(lp) = \sqrt{\frac{1}{N-1}\sum_{n=1}^{N}\left(lp(n) - \frac{1}{N}\sum_{n=1}^{N} lp(n)\right)^2}$$

The goal of defining this evaluation metrics is to test whether the serial controller can reduce the standard deviation of lateral position error.

4.5.3. Results and Discussions

All the volunteer drivers mentioned that they sensed the effect of the serial controller on the steering characteristics of the driving simulator, as soon as the controller was added to the system. They mentioned that the steering response felt more sensitive at first, which caused the lateral control of the vehicle even more difficult. However, they stated that they got used to the new steering behavior shortly after and could control the vehicle.

Driver Adaptation

One of the most important behaviors observed both in the data and in the descriptions of drivers from their experience was the human adaptation phenomenon. Human's ability to adapt to the new system is a very important issue that needs to be considered further. The adaptation related to driver-vehicle interaction was previously investigated for anti-lock braking systems (ABS) in [226] and adaptive cruise control systems (ACC) in [227]. The performance of any advanced driver-assistance system that works together with the driver is affected by the adaptation behavior of the human brain.

The adaptation behavior of drivers is explained mathematically using crossover principle [228]. The crossover principle states that the open-loop transfer function of the combined system of human operator and system (s)he is manually controlling is

$$\frac{\omega_c}{s} e^{-\tau_r s} \qquad (4\text{-}7)$$

around the crossover frequency ω_c . In other words, the frequency response of any manually controlled system, which is vehicle in our case, has a $-20dB/sec$ magnitude slope in the vicinity of the crossover frequency. Therefore, no matter what the characteristics of the vehicle are, the drivers adjust their behaviour so that the overall system has the mentioned frequency response. The implication is that the driver considers the serial connection of the vehicle and our controller as a vehicle with new dynamics. Then the drivers adapt their steering wheel control behavior to satisfy the crossover principle. A similar effect in driving simulators was observed, investigated, and verified by Mitschke in [125]. While only vehicle parameters were changed in that study, the obtained results and observations were similar to what we achieved here (where the serial controller is added).

Comparison of Evaluation Metrics

The average values of RDP and LPSD for both configurations (with and without serial controller) are shown in Figure 4.9 and Figure 4.10, respectively. The difference between evaluation metrics in the conventional system and the system with the serial

controller in these figures are not conclusive. The performance indices have improved only for half of the drivers.

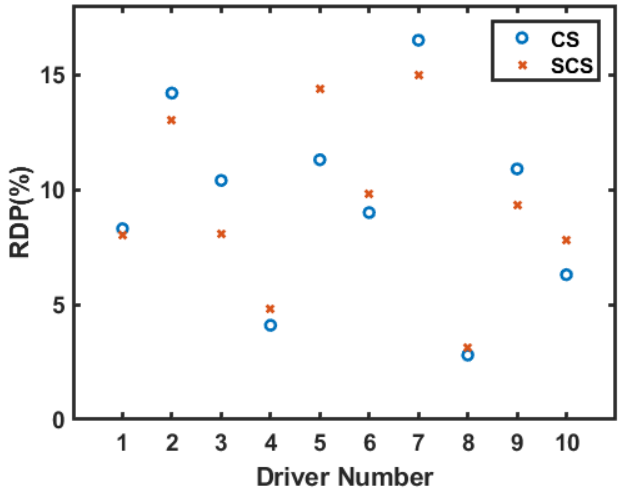

Figure 4.9. Average RDP(%) of different drivers driving in the simulator using conventional system (CS) and serial controller system (SCS)

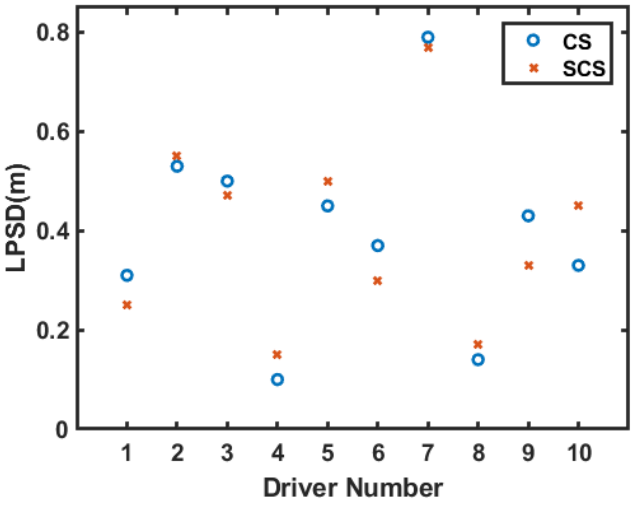

Figure 4.10. Average LPSD of different drivers driving in the simulator using conventional system (CS) and serial controller system (SCS)

The main cause of ineffectiveness of the added serial controller in the case of intoxicated driving is the human adaptation behavior, which was explained earlier. In a nutshell, the drivers adapt to the controller and consider the new system as a vehicle with new handling characteristics.

Another possible explanation for the observed results is Risk Homeostasis Theory (RHT) [229, 230]. This theory explains that the modifications made to the intrinsic risk of environments are nullified in three ways: behavioral adjustments, physical risk avoidance, and mode migration [231]. The results obtained here after adding the serial controller can be considered as an example of behavior adjustment, i.e., the drivers adjust their driving behavior after adding the serial controller so that they achieve a risk level similar to the previous condition. Therefore, changing the characteristics of the vehicle by adding a controller did not improve RDP and LPSD significantly.

Another observation that should be noted is that the different drivers adapted to the controller in different ways. For example, some drove more conservatively to avoid large lateral control error while adapting, whereas some others used more predictive steering action (like turning the steering wheel earlier while approaching a curve). The drivers with more driving practice with the simulator demonstrated a more consistent adaptation behavior. All these different personal adaptation behaviors can be reasons for variation in the results.

The results with our driving simulator supported human driver's adaptation ability, which is a well-known fact. Although this adaptation ability reduces the effectiveness of the serial controller in improving the performance of the vehicles being driven by intoxicated drivers, the added controller can have other benefits such as passengers comfort, investigating of which is not in the scope of this study.

4.6. Simulation Results for Parallel Assisting Controller

Considering the structure of the parallel assisting lateral controller shown in Figure 4.4 and the model obtained for intoxicated driver in Chapter 3, we manually tuned the PID controller in (4-4). The obtained controller parameters obtained are:

$$K_{Pp} = 0.002,\ \ K_{Ip} = 0.067,\ \ K_{Dp} = 3.667,\ \ N_p = 150 \qquad (4\text{-}8)$$

The conventional steering wheel control system (Figure 4.1), the proposed serial assisting control system (Figure 4.3), and the proposed parallel assisting controller

(Figure 4.4) were simulated. The 'driver' block in all three systems are the identified intoxicated driver model obtained in Chapter 3. The 'Serial Controller' block in Figure 4.3 is described in (4-3) and (4-5). The 'Parallel Controller' block in Figure 4.4 is presented in (4-4) and (4-8). In order to make the simulations more realistic, measurement noise is added to the system. In addition, a pulse disturbance (equivalent to a sudden movement of the steering wheel) was added to the control signal in all systems between $t = 10s$ and $t = 11s$. The simulation results are shown in Figure 4.11.

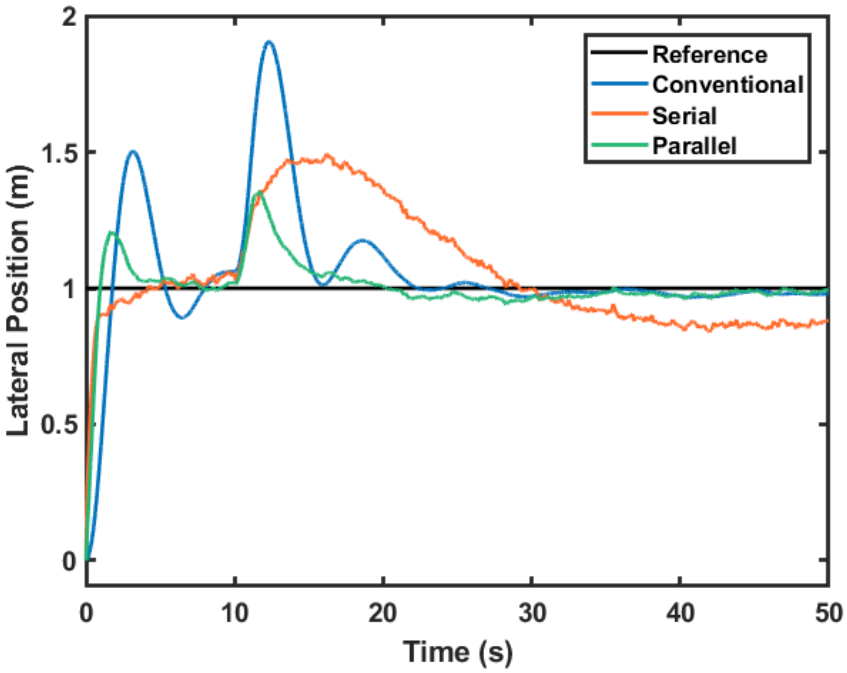

Figure 4.11. Comparison of the performances of conventional, serial assisting, and parallel assisting lateral control systems (computer simulations)

These results show how the proposed parallel assisting controller can keep the vehicle close to the center of the lane in spite of a sudden improper movement of the steering wheel, which is simulated here as a disturbance occurring at $t = 10s$.

In the next step, we performed human-in-the-loop experiments using the driver simulator. We asked a human driver wearing the Fatal Vision goggles (to simulate the driving of intoxicated drivers) to drive on a 5-lane straight road (see Figure 4.6) twice: first in a normal vehicle, then in a vehicle including the parallel controller as shown in Figure 4.4.

At the beginning of each experiment, the speed of the vehicle was fixed at 70 km/h, the vehicle was in the third lane, and the steering wheel angle was zero. After four seconds of driving, the steering wheel was turned left and then turned back to zero in half a second. Then the driver was asked to move the vehicle back to the center of the third lane. The experiment results and the steering wheel angle applied to the vehicle in both cases (conventional system and system with parallel assisting controller) are shown in Figure 4.12 and Figure 4.13, respectively.

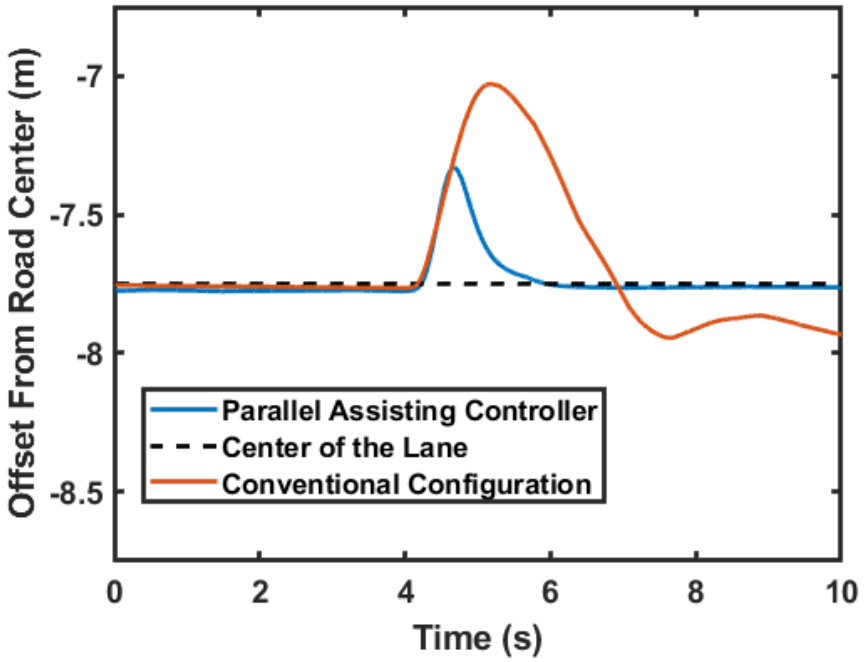

Figure 4.12. Result of the human-in-the-loop experiment with and without the parallel assisting controller

These results confirm the simulation results presented in Figure 4.11, and show that although the disturbance given to the vehicle is significantly higher in the case with the parallel assisting controller (see Figure 4.13), the performance is better in this case. In addition, the parallel controller moves the vehicle back exactly to the center of the lane whereas there is an offset error in the system without the parallel controller.

Based on the obtained results, the suggested structure can improve the driving performance of the drivers. Since a common problem of impaired drivers is maintaining

the vehicle at the center of the lane, the suggested parallel controller can be effective in increasing the road safety especially when the driver is impaired.

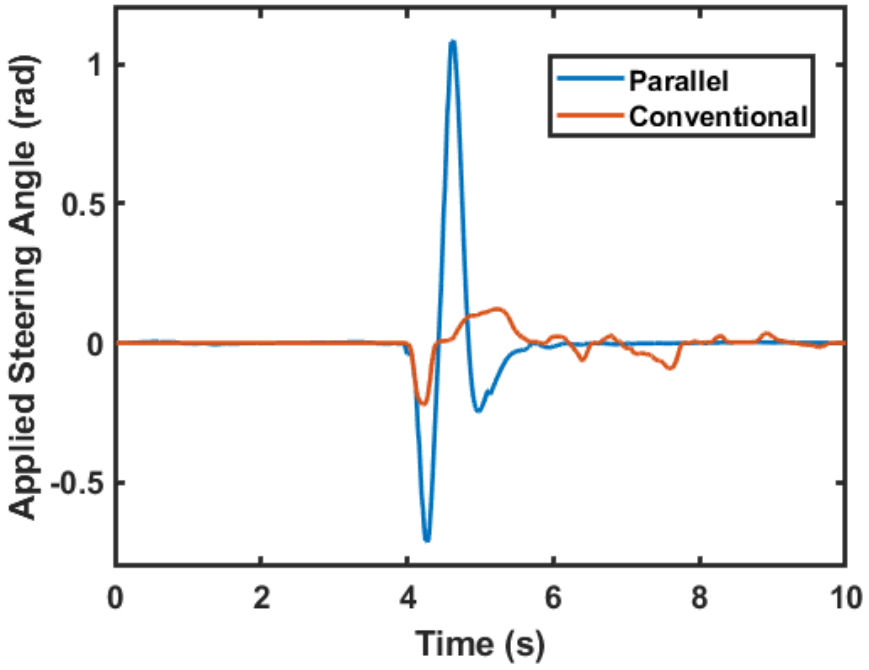

Figure 4.13. Steering wheel signal applied to the vehicle with and without the parallel assisting controller

4.7. Conclusion

In this chapter, the idea of improving the steering action of the driver by serial and parallel controllers was presented. In the first proposed algorithm, the steering signal coming from the steering wheel is fed to a serial controller. The output of the controller becomes the actual steering of the car. In the second suggested algorithm, the output of an independent lateral controller is added to the control signal generated by the human driver.

First, the serial controller was programmed in the driving simulator, and its performance was tested using actual drivers wearing Fatal Vision Goggles. The study of road departure percentage and lateral position standard deviation evaluation indices showed that the improvement caused by the added serial controller is insignificant. The observations agree with driver's adaptation ability and risk homeostasis theory (RHT).

These two phenomena have significant effects on the driver-controller-vehicle system and need more investigations and extensive research.

The added controller modifies the steering command from the driver before it is fed to the steering wheel. As a result, the driver experiences a new *equivalent vehicle*. Because of human driver's adaptation ability, the drivers adjust their behavior so that the overall system follows the crossover principle. Future work continuing this research may consider methods to overcome this problem.

In spite of what mentioned, the serial controller might have other benefits such as ease of driving, passenger comfort, reducing emissions, and less fuel consumption, which need to be further studied. Another advantage of this system is that, unlike many other driver assistance systems, it does not distract or disengage the driver, which improves safety.

In the second part of this chapter, the parallel controller was programmed in Matlab and the driving simulator. In both sets of simulation studies and human-in-the-loop experiment results, we demonstrated that the suggested parallel controller structure is effective in improving the lane keeping task when an impaired driver is controlling the vehicle. Therefore, this additional parallel controller can be added to the vehicle when an impaired driver is detected using the algorithm presented in Chapter 3.

In the next chapter, we consider the case that the driver is completely removed from the loop and the controller should perform the lateral control task independently.

Chapter 5.

Vehicle Lateral Control

In the previous chapter, we investigated the idea of having controllers in series and parallel with the driver to compensate the poor performance of impaired drivers. In the case of the serial controller, because of the adaptation ability of the human brain, the drivers consider the added controller as a part of vehicle dynamics and adapt their driving behavior to the new vehicle behavior after a short driving period. As a result, this brain adaptation ability reduces the benefits of adding a controller. Another possible option is to remove the driver from the loop and replace her/him with a lateral controller after the algorithm introduced in Chapter 3 detects intoxicated driving behaviors.

Vehicle lateral control is an integral part of autonomous and intelligent vehicle control systems. The primary goal of the lateral control, also referred to as steering control, is to navigate a car along a desired path (lane keeping/following). In addition, performing lane change maneuvers, avoiding obstacles and collisions in emergency situations are also related to vehicle lateral control.

In this chapter, we present a comparative study of lateral controllers including state-feedback and output feedback methods, design, and implement them on the driving simulator introduced in Chapter 3 to replace the intoxicated drivers. We also introduce a novel neural-network-based controller developed by our research group. This controller is optimized using genetic algorithms. In section 5.4, we use this new method to design the controller parameters for the vehicle lateral control problem.

5.1. Vehicle Model

A nonlinear six-degree-of-freedom (DOF) vehicle model, which represents the vehicle lateral dynamics as realistically as possible, is developed in [223]. This complex model has sixteen state variables: twelve for the six DOF motions (three translational and three rotational) and four for the tires. However, several studies [200, 223, 224]

demonstrate that using this complex nonlinear sixteen-state-variable model is not necessary to study the lateral behavior of vehicles. We derive and consider two simpler kinematic and dynamic bicycle models in this dissertation which would suffice to describe the lateral vehicle motions and dynamics.

5.1.1. Kinematic Model of the Vehicle

A kinematic model of the lateral movement of the car describes vehicle lateral motion mathematically without considering the forces affecting the motion. In the bicycle model of the vehicle shown in Figure 5.1, the vehicle is assumed to have two wheels. In this model, both front wheels are represented at point A. Similarly, rear wheels are both placed at point B. Independent steering angles are assumed for front and rear wheels which are represented by δ_f and δ_r. In practice, we usually have $\delta_r = 0$. Point C is the center of the gravity of the car. The distances of center of gravity from front and rear wheels are shown by l_f and l_r, respectively.

In order to describe the movement of the vehicle, three coordinates $X, Y,$ and ψ are required. X and Y represent the position of the center of the gravity of the vehicle and ψ represents its orientation. The velocity of the center of gravity of the car (V) can have a different angle than the longitudinal axis of the car. This angle difference is 'slip angle' of the car, and it, is shown by β. The course angle (γ) is defined as the summation of the heading angle (ψ) and the slip angle (β): $\gamma = \psi + \beta$.

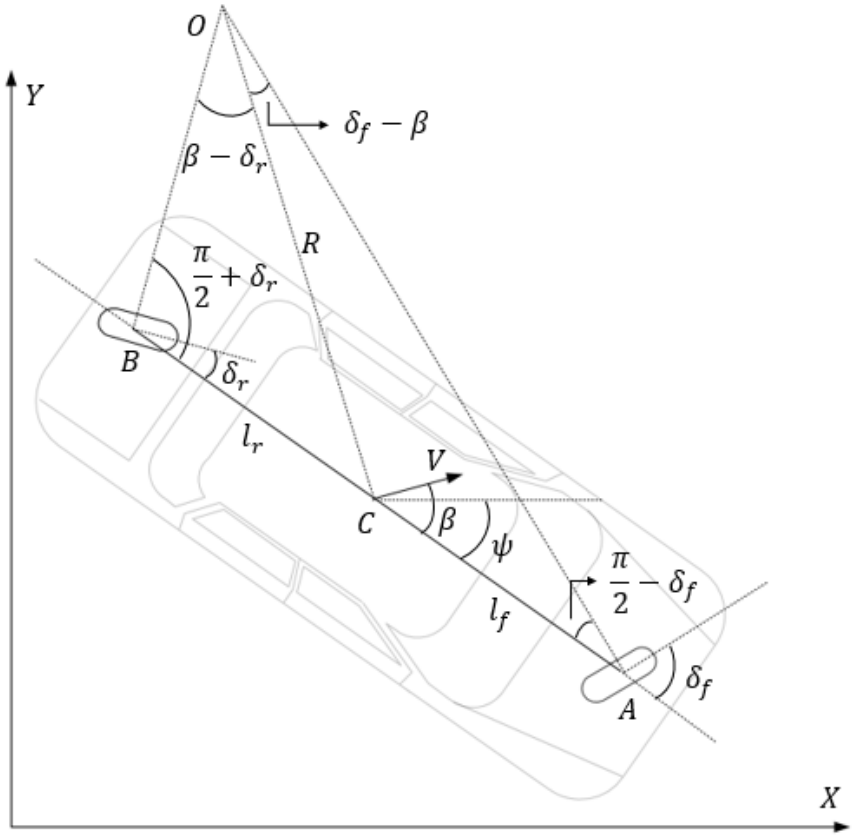

Figure 5.1. Kinematic model of vehicle

The intersection of the two perpendicular lines to the direction of wheels is shown at point O and is called instantaneous rolling center of the vehicle. Connecting this point to the center of gravity gives the line OC. The length of this line defines the radius of the path R.

In triangle OCA we have

$$\frac{\sin(\delta_f - \beta)}{l_f} = \frac{\sin\left(\frac{\pi}{2} - \delta_f\right)}{\mathrm{R}} \qquad (5\text{-}1)$$

Similarly, in triangle OCB we can write

$$\frac{\sin(\beta - \delta_r)}{l_r} = \frac{\sin\left(\frac{\pi}{2} + \delta_r\right)}{\mathrm{R}} \qquad (5\text{-}2)$$

Equation (5-1) yields

$$\frac{\sin(\delta_f)\cos(\beta)-\sin(\beta)\cos(\delta_f)}{l_f} = \frac{\cos(\delta_f)}{R} \qquad (5\text{-}3)$$

Similarly, equation (5-2) results in

$$\frac{\cos(\delta_r)\sin(\beta)-\cos(\beta)\sin(\delta_r)}{l_r} = \frac{\cos(\delta_r)}{R} \qquad (5\text{-}4)$$

Multiplying equations (5-3) and (5-4) by $\frac{l_f}{\cos(\delta_f)}$ and $\frac{l_r}{\cos(\delta_r)}$, respectively, we get

$$\tan(\delta_f)\cos(\beta) - \sin(\beta) = \frac{l_f}{R} \qquad (5\text{-}5)$$

$$\sin(\beta) - \tan(\delta_r)\cos(\beta) = \frac{l_r}{R} \qquad (5\text{-}6)$$

Adding (5-5) and (5-6) results in

$$\big(\tan(\delta_f) - \tan(\delta_r)\big)\cos(\beta) = \frac{l_f+l_r}{R} \qquad (5\text{-}7)$$

The angular velocity of the vehicle is $\frac{V}{R}$. Assuming that the path radius changes slowly, the rate of change of heading angle of the vehicle ($\dot{\psi}$) is equal to the angular velocity (see (6-2)). Combining equations (6-2) and (5-7) results in

$$\dot{\psi} = \frac{V\big(\tan(\delta_f)-\tan(\delta_r)\big)\cos(\beta)}{l_f+l_r} \qquad (5\text{-}8)$$

Considering three inputs δ_f, δ_r, and V, the overall kinematic model of lateral vehicle motion can be written as equations (5-8)(5-40), (5-9), and (5-10).

$$\dot{X} = V\cos(\psi+\beta) \qquad (5\text{-}9)$$

$$\dot{Y} = V\sin(\psi+\beta) \qquad (5\text{-}10)$$

The parameter V is the speed of the vehicle and the methods to calculate and control it will be obtained from the longitudinal model of the vehicle which will be explained in Chapter 7.

Multiplying equation (5-5) by l_r and subtracting it from equation (5-6) multiplied by l_f gives the following equation which can be used to calculate the slip angle:

$$\beta = \tan^{-1}\left(\frac{l_f \tan\delta_r + l_r \tan\delta_f}{l_f + l_r}\right) \qquad (5\text{-}11)$$

The main assumption made in developing the above kinematic model is that the direction of the front and rear wheels are the same as velocity vectors at points A and B (in Figure 5.1), respectively. In other words, slip angles at both wheels are assumed to be zero. This assumption is valid only at low speed movement of the vehicle. Considering the conditions that our final system is going to be used in, wheel slip angles might sometimes be nonzero. Therefore, in the next section we also consider a dynamic model, which is valid at high speeds, for the lateral control problem.

5.1.2. Dynamic Model of Vehicle

As mentioned in the previous section, the kinematic model developed in equations (5-8), (5-9), and (5-10) is not valid at higher speeds of the vehicle. A simplified linear two-degree of freedom 'bicycle' model of the vehicle can be obtained from the complex sixteen-state-variable model. Several studies have already established that the simplified model, which we use in this work, is a good approximation of the complex model for all practical purposes [200, 223, 224].

The bicycle model used in this study to describe vehicle lateral dynamics is shown in equation (5-12). The details of this equation, how we derived it, and why we use it are explained in section 6.1 of this dissertation.

$$\frac{d}{dt}\begin{bmatrix} e_1 \\ \dot{e}_1 \\ e_2 \\ \dot{e}_2 \end{bmatrix} = \begin{bmatrix} 0 & 1 & 0 & 0 \\ 0 & -\frac{2C_{af} + 2\,C_{ar}}{mV_x} & \frac{2C_{af} + 2\,C_{ar}}{m} & -\frac{2C_{af}l_f - 2\,C_{ar}l_r}{mV_x} \\ 0 & 0 & 0 & 1 \\ 0 & -\frac{2C_{af}l_f - 2\,C_{ar}l_r}{I_z V_x} & \frac{2C_{af}l_f - 2\,C_{ar}l_r}{I_z} & -\frac{2C_{af}{l_f}^2 + 2\,C_{ar}{l_r}^2}{I_z V_x} \end{bmatrix} \begin{bmatrix} e_1 \\ \dot{e}_1 \\ e_2 \\ \dot{e}_2 \end{bmatrix} +$$

$$\begin{bmatrix} 0 \\ \frac{2C_{af}}{m} \\ 0 \\ \frac{2C_{af}l_f}{I_z} \end{bmatrix}\delta + \begin{bmatrix} 0 \\ -V_x - \frac{2C_{af}l_f - 2\,C_{ar}l_r}{mV_x} \\ 0 \\ -\frac{2C_{af}{l_f}^2 + 2\,C_{ar}{l_r}^2}{I_z V_x} \end{bmatrix}\dot{\psi}_{des} \qquad (5\text{-}12)$$

In the above equation, e_1 is the vehicle displacement error and e_2 is the vehicle orientation error. The longitudinal velocity of the car at its center of gravity is denoted by V_x. The distances of the front and rear tires from the center of gravity and cornering stiffness of each front and rear tire are shown by l_f, l_r, C_{af}, and C_{ar}, respectively. The steering angle is shown by δ and the yaw moment of inertia of the vehicle is I_z. Assuming the radius of the road is R, the rate of change of the desired orientation of the vehicle is defined as $\dot{\psi}_{des} = \frac{V_x}{R}$.

The bicycle model described above is used for both controller design and simulation studies. This model is a modified version of the original bicycle model. The ultimate goal of this study is designing a lateral control (steering control) for the lane keeping in autonomous vehicles. Therefore, we converted the original state-space representation of lateral dynamics to a model where the state variables are the position and orientation errors with respect to the center of the lane.

The lateral position of the vehicle with respect to the road is usually measured at a location ahead of the vehicle (look-ahead strategy). The output equation of the state-space, the equation that expresses the output as a linear combination of the states, is as follows:

$$y = e_1 + d_s e_2 \qquad (5\text{-}13)$$

where d_s is the look-ahead distance, which is the longitudinal distance of the point ahead of the vehicle center of gravity, where we make the sensor measurements.

Considering equations (5-12) and (5-13), we can represent the conventional output feedback system as shown in Figure 5.2. In this Figure, $P(s)$ is the plant transfer function between the steering angle input for the vehicle and the lateral position

measurement output described in equation (5-12). The steering signal (δ) is the output of the controller block in autonomous vehicles. In conventional driving, this signal is controlled by the driver, as shown in Figure 5.2. The road-determined desired yaw rate $\dot{\psi}_{des}$ affects the system dynamics through a transfer function denoted in Figure 5.2 as $G(s)$.

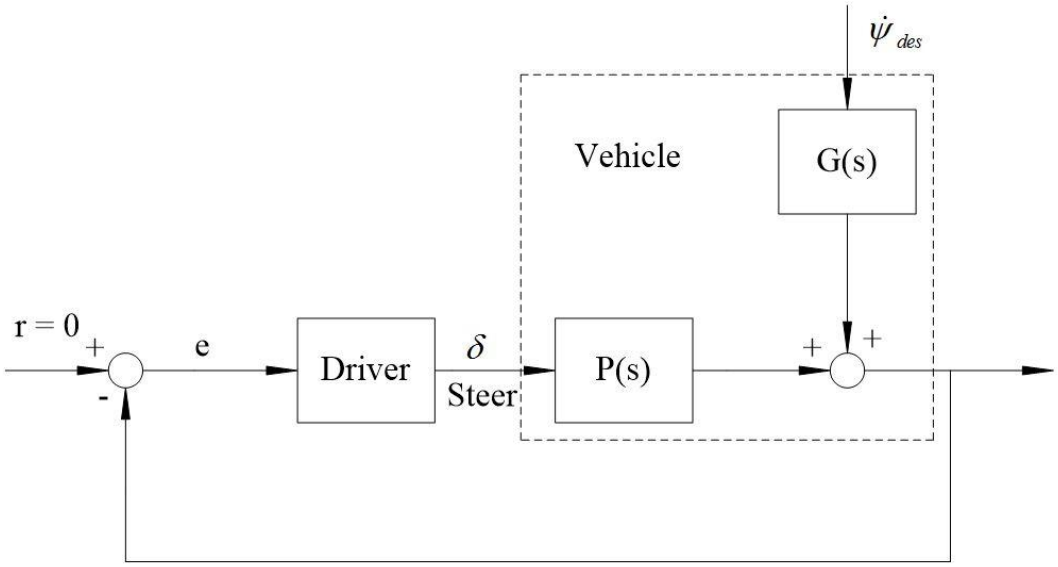

Figure 5.2. Closed-loop driver-vehicle system

The above model of vehicle lateral dynamics is based on fixed coordinates. Since the controllers use errors with respect to body fixed coordinates, this is appropriate for lateral controller design. However, a global picture of vehicle trajectory should also be obtained. The global position of the vehicle can be written as

$$X = X_{des} - e_1 \sin\psi \qquad (5\text{-}14)$$

$$Y = Y_{des} + e_1 \cos\psi \qquad (5\text{-}15)$$

where X_{des} and Y_{des} are the global coordinates of the road.

Using $X_{des} = \int_0^t V \cos\psi_{des}\, dt$, $Y_{des} = \int_0^t V \sin\psi_{des}\, dt$, and $\psi = e_2 + \psi_{des}$ in equations (5-14) and (5-15), the global coordinates of the car can be written as the following equations:

$$X = \int_0^t V \cos\psi_{des}\, dt \;\; - e_1 \sin(e_2 + \psi_{des}) \qquad (5\text{-}16)$$

$$Y = \int_0^t V \sin\psi_{des}\, dt \;\; + e_1 \cos(e_2 + \psi_{des}) \qquad (5\text{-}17)$$

Having the kinematic and dynamic models of vehicle lateral motion explained in this section, we design several controllers to be implemented on our system in the next sections. The controllers designed in this chapter include a novel fused neural network controller introduced by our group, which will be described in Section 5.4.

5.2. State-feedback Controller

As explained in the previous section, the bicycle model assumption results in a state-space representation (equation (5-12)) of vehicle which can be summarized as

$$\dot{x} = Ax + B_1\delta + B_2\dot{\psi}_{des} \qquad (5\text{-}18)$$

with

$$x = \begin{bmatrix} e_1 \\ \dot{e_1} \\ e_2 \\ \dot{e_2} \end{bmatrix} \qquad (5\text{-}19)$$

where e_1 is the distance of the center of the gravity of the vehicle from the center line of the lane and e_2 is the orientation error of the vehicle with respect to the road. The numerical value of the parameters in (5-18) are given below:

$$C_{af} = 80000, \qquad C_{ar} = 80000, \qquad l_f = 1.1, \qquad l_r = 1.58,$$

$$I_z = 2873, \qquad m = 1573 \qquad (5\text{-}20)$$

No matter what the values of parameters in (5-20) are, the matrix A in (5-18) has 4 eigenvalues, two of which are at the origin. Therefore, the open-loop system is unstable. However, since the pair (A, B_1) is controllable, we can use the following control law such that the closed-loop system $(A + B_1K)$ has arbitrary eigenvalues.

$$\delta = Kx = k_1 e_1 + k_2 \dot{e_1} + k_3 e_2 + k_4 \dot{e_2} \qquad (5\text{-}21)$$

Using the pole-placement techniques explained in [232], in order to place the eigenvalues at $[-7+2j \quad -7-2j \quad -9 \quad -11]^T$, the designed controller would be

$$K = [0.3456 \quad 0.0356 \quad 1.3365 \quad 0.0499] \qquad (5\text{-}22)$$

Since the data coming from the actual vehicle sensors will include noise, a normally (Gaussian) distributed random signal with zero mean and standard deviation equal to 0.02 is added to all the state measurements. The results for a straight road are shown in Figure 5.3 and Figure 5.4. These figures show that the designed state-feedback controller can satisfactorily stabilize and control the lateral dynamics of the system. However, these results were obtained on a straight road, where the term $B_2\dot{\psi}_{des}$ in (5-41) is zero.

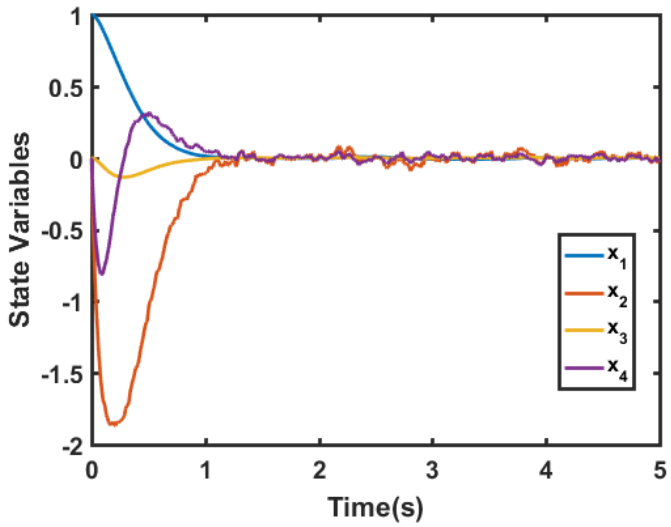

Figure 5.3. States of vehicle's lateral dynamics controlled by state-feedback on a straight road

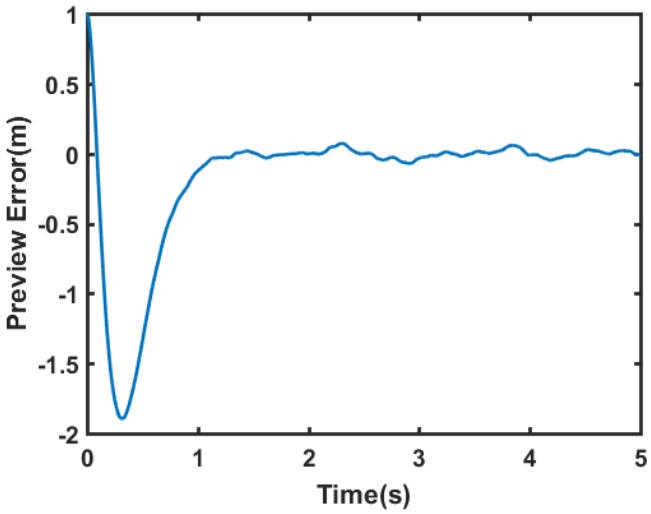

Figure 5.4. Preview error (output) of vehicle's lateral dynamics controlled by state-feedback on a straight road

On the roads where the curvature is not zero ($B_2\dot{\psi}_{des} \neq 0$), although the closed-loop system would be asymptotically stable (the term $(A + B_1K)$ would have negative eigenvalues) if the state-feedback controller in (5-21) is properly designed, but the tracking error will not converge to zero. This error can be compensated by a feedforward term (δ_{ff}):

$$\delta = Kx + \delta_{ff} \qquad (5\text{-}23)$$

If we use the steering wheel angle given by (5-23) instead (5-21), the closed-loop system becomes

$$\dot{x}(t) = (A + B_1K)x + B_1\delta_{ff} + B_2\dot{\psi}_{des} \qquad (5\text{-}24)$$

Laplace transform of (5-24) and some simplifications result in

$$X(s) = \big(sI - (A + B_1K)\big)^{-1}\Big(B_1L\big(\delta_{ff}\big) + B_2L\big(\dot{\psi}_{des}\big)\Big) \qquad (5\text{-}25)$$

with $L\big(\delta_{ff}\big)$ and $L\big(\dot{\psi}_{des}\big)$ being the Laplace transforms of δ_{ff} and $\dot{\psi}_{des}$, respectively. Considering $\dot{\psi}_{des} = \frac{V_x}{R}$, assuming δ_{ff} is constant (therefore its Laplace transform is $\frac{\delta_{ff}}{s}$), and using final value theorem [233], we can write the steady-state value of error as

$$x_{ss} = \lim_{t\to\infty} x(t) = \lim_{s\to 0} sX(s) = -(A + B_1K)^{-1}\left(B_1\delta_{ff} + B_2\frac{V_x}{R}\right) \quad (5\text{-}26)$$

Replacing A, B_1, and B_2 from (5-12), and K from (5-23), and simplifying the result yields in

$$x_{ss} = \begin{bmatrix} -\frac{\delta_{ff}}{k_1} \\ 0 \\ 0 \\ 0 \end{bmatrix} + \begin{bmatrix} \frac{1}{k_1}\frac{mV_x^2}{R(l_f+l_r)}\left(\frac{l_r}{2C_{af}} - \frac{l_f}{2C_{ar}} - \frac{l_f}{2C_{ar}}k_3\right) + \frac{1}{k_1R}\left(l_f + l_r + l_rk_3\right) \\ 0 \\ \frac{1}{2RC_{ar}(l_f+l_r)}\left(-2C_{ar}l_fl_r - 2C_{ar}l_r^2 + l_fmV_x^2\right) \\ 0 \end{bmatrix} \quad (5\text{-}27)$$

Equation (5-27) shows that a proper choice of feedforward controller (δ_{ff}) can make the lateral error zero. This proper value of δ_{ff} is

$$\delta_{ff} = \frac{mV_x^2}{R(l_f+l_r)}\left(\frac{l_r}{2C_{af}} - \frac{l_f}{2C_{ar}} - \frac{l_f}{2C_{ar}}k_3\right) + \frac{l_f+l_r+l_rk_3}{R} \quad (5\text{-}28)$$

However, the yaw angle error ($x_3 = e_2$) is independent of the feedforward term and has the following steady-state value:

$$x_{3ss} = e_{2ss} = \frac{1}{2RC_{ar}(l_f+l_r)}\left(-2C_{ar}l_fl_r - 2C_{ar}l_r^2 + l_fmV_x^2\right) \quad (5\text{-}29)$$

If we simplify (5-29) we can see that the steady-state error of e_2 would be zero only if

$$2C_{ar}l_r\left(l_f + l_r\right) = l_fmV_x^2 \quad (5\text{-}30)$$

The condition in (5-30) is met at a certain speed which is independent of the road curvature. For the vehicle whose parameters are mentioned in (5-20), this specific speed is $V_x = 71km/h$.

In order to see the effect of the feedforward controller, the previous experiment is repeated on a curved road. Figure 5.5 shows how x_1 (lateral error, e_1) does not approach to zero when the road is not straight. In addition, this figure shows how adding the

feedforward controller fixes that problem. We can also see that, as explained above in (5-29), adding δ_{ff} cannot make x_3 (yaw angle error, e_2) zero.

The preview error (output of the vehicle, defined in (5-13)) and the control signal (steering wheel angle) are shown in Figure 5.6 and Figure 5.7, respectively. These figures show the improvement caused by adding the feedforward term. The fact that the preview error does not reach zero in curves is the non-zero steady-state value of x_3 shown in (5-29). However, the error is very small and can be neglected.

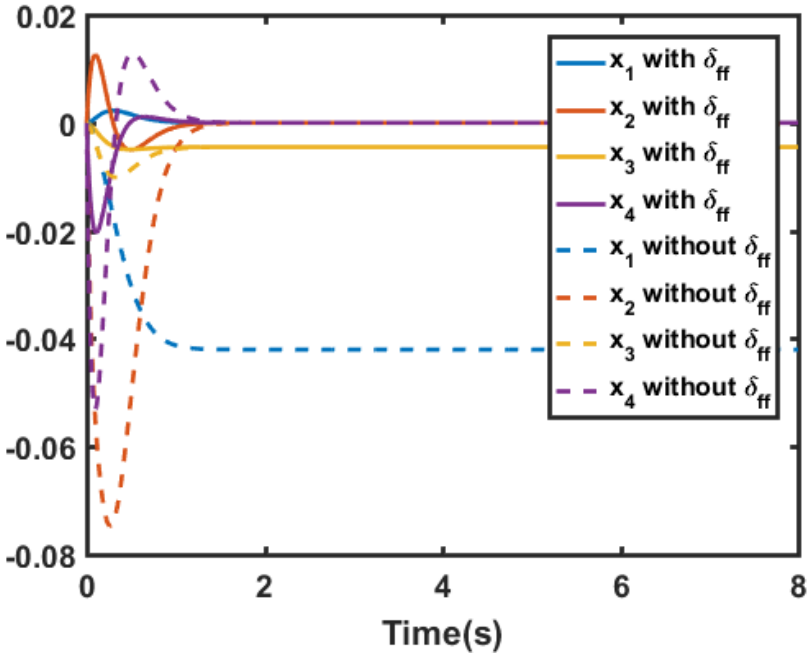

Figure 5.5. Vehicle states on a curved road with and without the feedforward controller

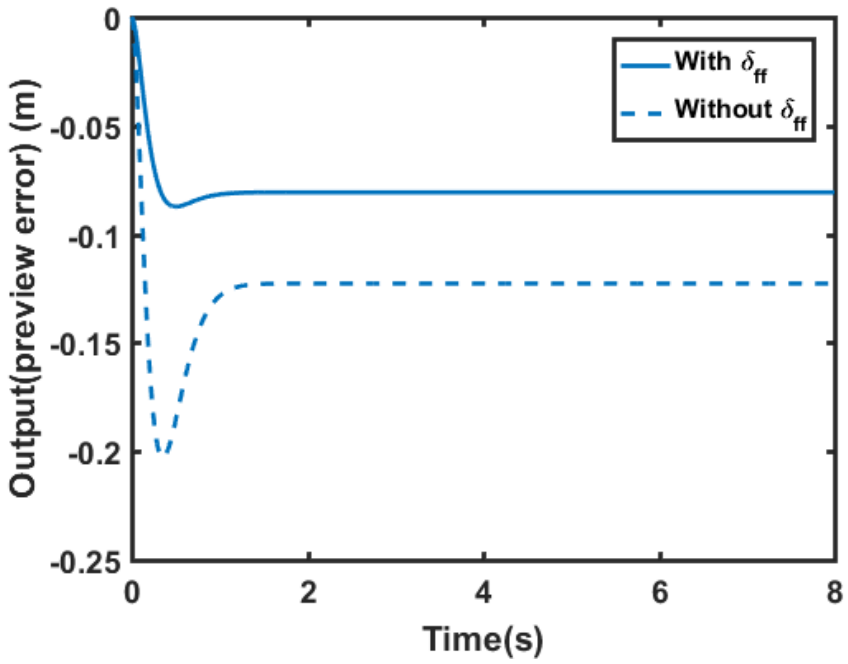

Figure 5.6. Vehicle preview error on a curved road with and without the feedforward controller

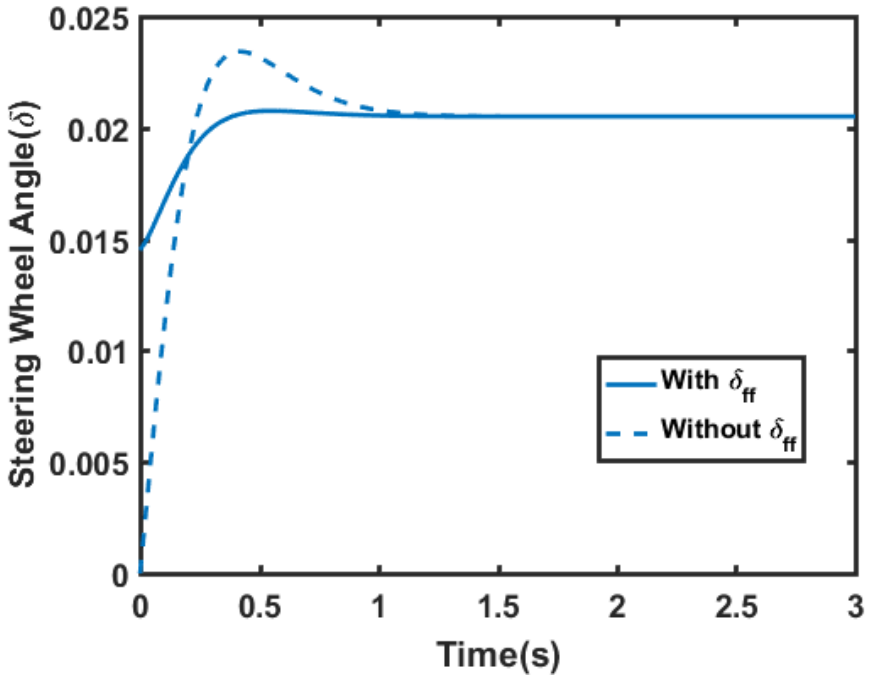

Figure 5.7. Steering wheel angle of the vehicle on a curved road with and without feedforward controller

5.3. Output Feedback

The vehicle's lateral error can be measured at somewhere ahead of the vehicle. The sensors that can measure this error include differential global positioning systems [184], cameras [185, 186], and magnetometers [168]. The block diagram of the closed-loop system that uses preview error in an output feedback configuration is shown in Figure 5.2. In this Figure, $P(s)$ is the vehicle transfer function between the steering angle input for the vehicle and the lateral position measurement output described in equation (5-13). The steering signal (δ) is the output of the controller block in autonomous vehicles.

Using the vehicle parameters mentioned in (5-20) we have

$$P(s) = \frac{285.5s^2+1986.6s+15181.3}{s^4+11.71s^3+59.94s^2} \qquad (5\text{-}31)$$

The poles and zeros of (5-31) are shown in Figure 5.8. This figure shows that $P(s)$ has a pair of complex conjugate poles and two poles at the origin which makes it unstable. In addition, the system has a pair of complex conjugate zeros. Increasing the value of d_s would decrease the imaginary part of these zeros, which would result in better damping of the system.

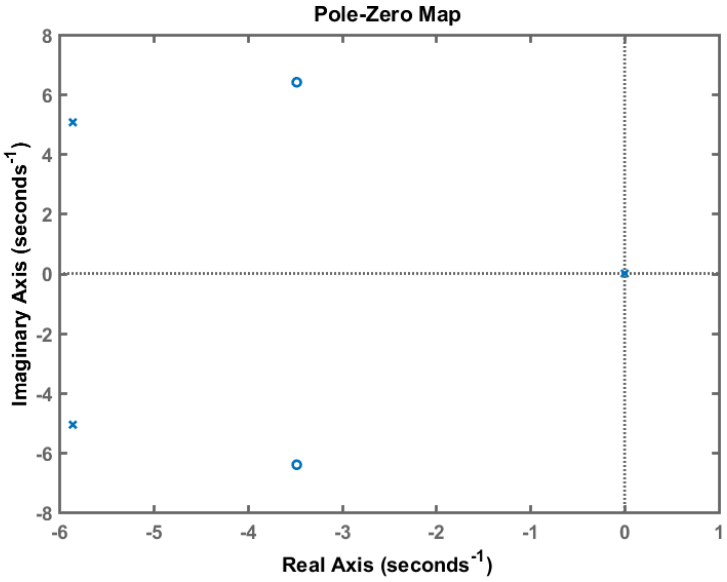

Figure 5.8. Pole-zero map of $P(s)$

First, we consider a simple proportional controller to analyze the behavior of this system:

$$C_p(s) = K_p \qquad (5\text{-}32)$$

where K_p is the proportional gain of the controller.

The root locus of the system considering varying values of K_p in (5-32) is shown in Figure 5.9. This figure shows that for a small value of K_p the system would be unstable. Therefore, a large enough value of proportional gain is required to stabilize the system. For the parameters mentioned in this analysis, the minimum required value for K_p to make the system stable is 0.25.

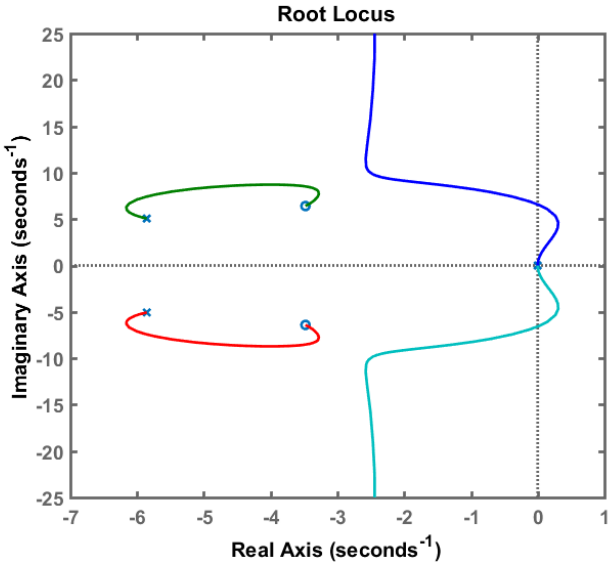

Figure 5.9. Root locus of the system with proportional controller

An important point that we should note is the fact that although larger values of proportional gain would stabilize the system, the system will still have poor stability margins and might become unstable in the presence of uncertainties. These poor stability margins are shown in the Bode plot of the system using a unity gain proportional controller in Figure 5.10. Using $K_p = 1$, a phase margin of 15.2 degrees is obtained as demonstrated in Figure 5.10. Considering a proportional gain of $K_p = 0.2$ results in an unstable overall system. On the other hand, increasing the proportional gain to K_p to 10 will result in a phase margin of only 5. This is should not be surprising considering Figure 5.10. This figure shows that using $K_p = 1$, the phase margin is close to the best possible, because the gain-crossover frequency ($15.5\ rad/s$) is close to the frequency where the phase is at the maximum.

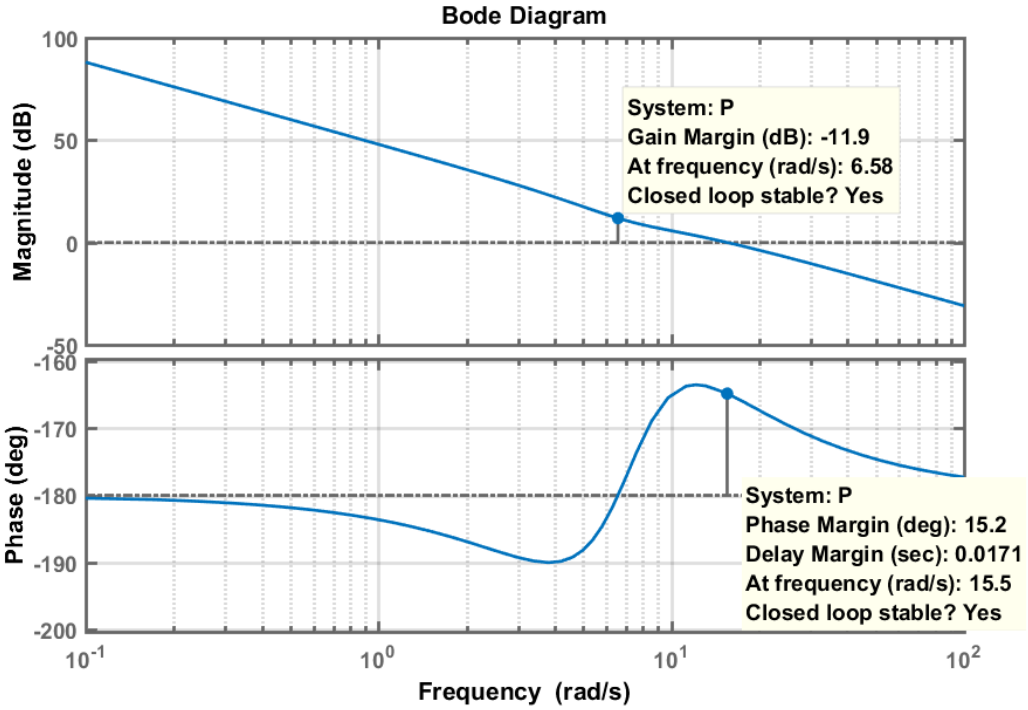

Figure 5.10. Stability margins of the system with proportional controller $K_p = 1$

In order to increase the stability margins of the system, hence its robustness, we can add phase to the system in the gain-crossover range. A lead compensator can do this task. We consider the following transfer function for the compensator (controller)

$$C_{Lead}(s) = \frac{a\tau s+1}{\tau s+1} \qquad (5\text{-}33)$$

with $a > 1$. The reader should note that the zero-frequency gain does not change if we use this structure of lead compensator. If the parameters a and τ are designed properly, the compensator in (5-33) can increase the phase of the system at gain-crossover frequency, which results in higher phase-margin and better robustness of the system. The maximum phase added by (5-33) is

$$\phi_{max} = \sin\left(\frac{a-1}{a+1}\right) \qquad (5\text{-}34)$$

which is added to the system at the following frequency

$$\omega_m = \frac{1}{\tau\sqrt{a}} \qquad (5\text{-}35)$$

In order to determine the design parameters in (5-33), we consider a desired added phase of $\phi_{max} = 45°$. Using (5-34), we get $a = 6.82$. Since we would like this phase be added to the system at the gain-crossover frequency, which is $15.5\frac{rad}{s}$ (see Figure 5.10), using (5-35) and considering $a = 6.82$ and $\omega_m = 15.5$, we get $\tau = 0.0247$. Therefore, the final controller can be considered as

$$C_{Lead}(s) = \frac{0.1685s+1}{0.0247s+1} \qquad (5\text{-}36)$$

The Bode plot for the system controlled by (5-36) is shown in Figure 5.11. This figure shows that the designed lead controller increases the phase margin of the system to 46.8°. Although the phase margin has significantly increased, it is a little less than what we used in the design procedure ($\phi_{max} = 45°$). The reason is the fact that adding the lead compensator changes the gain-crossover frequency of the system too, which can be seen in Figure 5.11. This figure shows that the gain-crossover frequency is different from the frequency at which the peak of the phase diagram occurs.

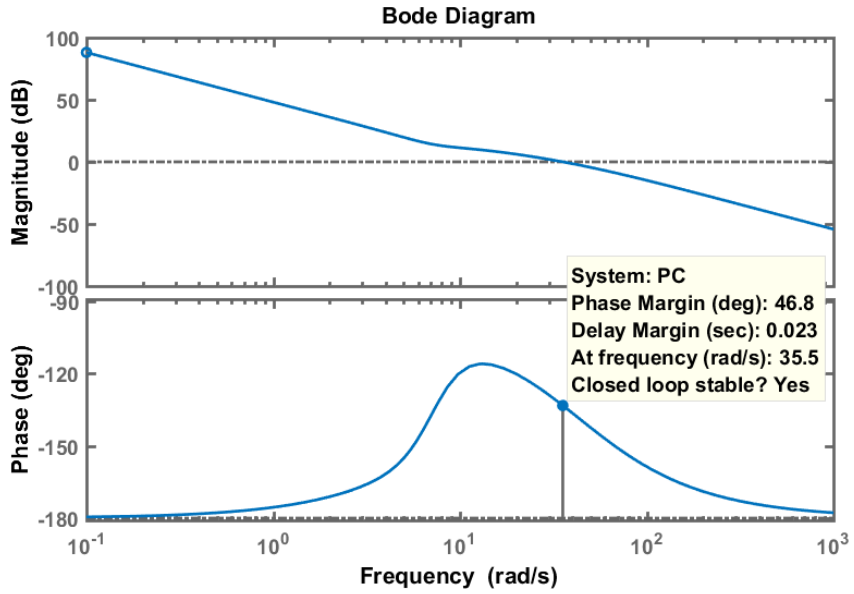

Figure 5.11. Bode plot of the system controlled by lead compensator and $K_p = 1$

The robustness of the system can be further improved by changing the gain-crossover frequency of the system. This task can be done by changing the proportional gain of the system from $K_p = 1$ to $K_p = 0.3163$. The result is shown in Figure 5.12. The

phase margin of the system shown in this figure is 64° which is significantly more than the original system. The final output feedback controller (C_{fof}) used to obtain the more robust system shown in Figure 5.12 is

$$C_{fof}(s) = K_p C_{Lead}(s) = 0.3163 \frac{0.1685s+1}{0.0247s+1} \qquad (5\text{-}37)$$

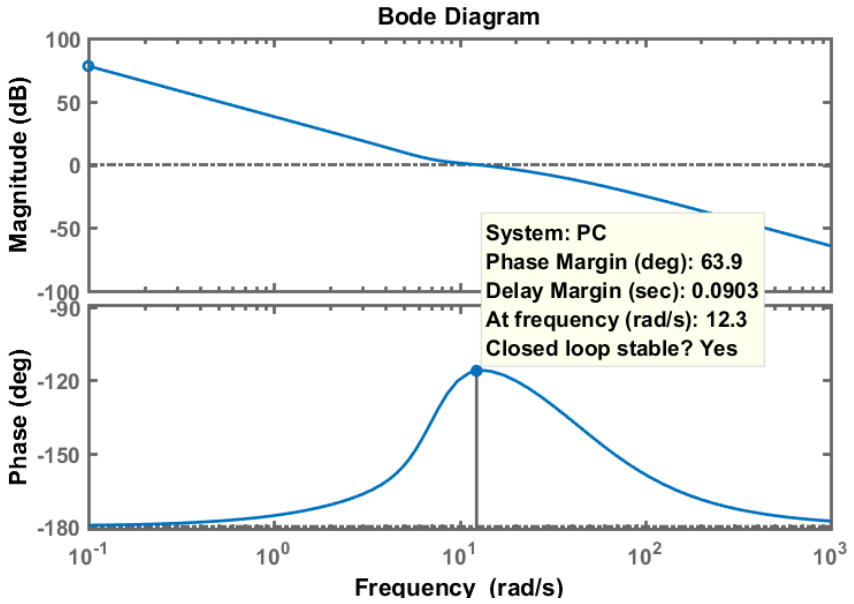

Figure 5.12. Bode plot of the system controlled by lead compensator and $K_p = 0.3163$

It should be noted that increasing the value of look-ahead distance would result in better damping in the closed-loop output feedback system shown in Figure 5.12. If a vision system (for example camera) is used for measuring the lateral error, the measurements would be look-ahead. However, if differential GPS or magnetometers are used, the measurements would be look-down ($d_s = 0$). In this case, the look-ahead error can be obtained using yaw angle measrements and combining it with the look-down measurements as described in (5-13). In other words, instead of directly measuring $y = e_1 + d_s e_2$ (look-ahead error) by camera, we can measure e_1 (look-down error) and e_2 (yaw angle error), and then artificially increase d_s.

5.4. A Novel Simple Controller for Vehicle Lateral Control

Multilayer neural network controllers have been extensively applied to control nonlinear systems with different network structure and different connection weights [234]. The reason is the nonlinear mapping characteristic of these powerful processing networks. The mapping nonlinearity directly relates to the number of neurons in the network. Nevertheless, the choice of the neural network structure and the number of neurons and layers are application dependent.

A decomposition design method is proposed to simplify the design process of the neural network controller for known physical structure systems. The concept of decomposition is an attractive tool to tackle systems that require two input parameters – say displacement and orientation– as their control variables [235]. For vehicle lateral control, the controller has to keep the vehicle position within the lane while maintaining the vehicle orientation parallel to a reference lane. In this system, while the controller maintains the displacement, the angle changes simultaneously.

The neural network designed by task decomposition would reduce the number of connection weights and hence reduce the network complexity, compared to the conventional neural network controllers available for vehicle lateral control problem. In this section, the neural network controller simplification process is described for vehicle lateral control system. The task decomposition technique starts with identifying control objectives from the statement of the problem and assigns the appropriate parameters to individual subtasks. When the subtasks are identified, we can obtain the intuitive control laws for each subtask based on the understanding of the control system. From an intuitive control law, control variables related to the control subtasks can be obtained. For the network architecture, independent sub-networks should be created for individual subtasks and by using the related control variables as network inputs. Finally, the outputs of the independent sub-network are fused together as the controller output.

The neural network simplification process based on task decomposition can be summarized in the following steps:

1. Decompose the control objective into subtasks.
2. Set up intuitive control law for the subtasks.
3. Identify control variables for the subtasks from the intuitive control law obtained in step 2.
4. Create independent sub-networks for the subtasks and using the corresponding control variables obtained in step 3 as sub-network inputs.
5. Fuse the sub-networks output together as the controller output.

Let us demonstrate the first three steps by considering the lateral control problem as outlined in Table 5.1.

Table 5.1. Controller design process for the lateral control problem

Step 1	Subtask 1	Maintain zero lateral position error
	Subtask 2	Maintain zero orientation error
Step 2	Control law 1	Change the steering wheel angle when the lateral position error deviates from zero
	Control law 2	Change the steering wheel angle when the orientation error deviates from zero
Step 3	Control variables 1	Lateral position error and its rate
	Control variables 2	Orientation error and its rate

The network structure is shown in Figure 5.13. The network, in general form, has four inputs $(\theta, \dot{\theta}, d, \dot{d})$ and one control output (u). In the lateral control problem, for example, we have $d = e_1 = x_1$, $\dot{d} = \dot{e}_1 = x_2$, $\theta = e_2 = x_3$, and $\dot{\theta} = \dot{e}_2 = x_4$. The control output in this case is the steering wheel angle $u = \delta$. There are two main sub-networks in the network and each sub-network targets on one sub-task of the systems. The first sub-network deals with the angle and aims to maintain it at zero. The second network deals with the displacement of the control system. Finally, the sub-networks outputs are fused together by a simple summation to form the final controller output.

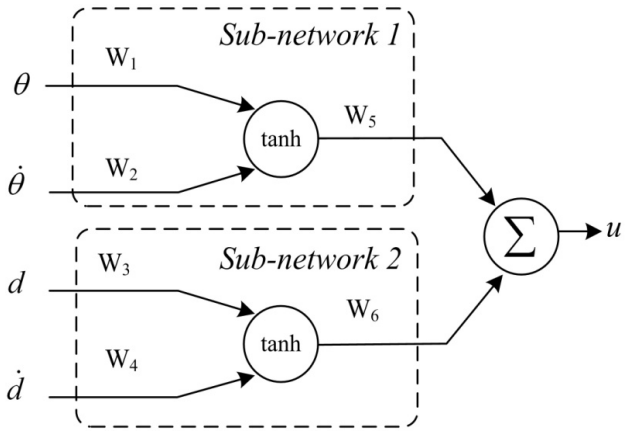

Figure 5.13. The structure of the neural network controller

This network structure design divides variables into groups and sets them into different sub-networks. Since each sub-network handles a different task, the number of connection weights is reduced. Equations (5-38) to (5-40) show the characteristic of the network.

$$Z_1 = \tanh\left(\theta . W_1 + \dot{\theta} . W_2\right) \qquad (5\text{-}38)$$

$$Z_2 = \tanh\left(d . W_3 + \dot{d} . W_4\right) \qquad (5\text{-}39)$$

$$u = Z_1 W_5 + Z_2 W_6 \qquad (5\text{-}40)$$

where Z_1 and Z_2 are the outputs from the sub-networks 1 and 2, respectively. W_1 to W_6 are the connection weights shown in Figure 5.13.

5.4.1. Neural network optimization via genetic algorithms

As noted before, the proposed controller architecture is simple, flexible and can be optimized by different methods. We suggest using Genetic Algorithms (GA) [236, 237] for this optimization, as shown in Figure 5.14. In the initial stage, GA starts with a randomly generated population. The initial population is decoded into the connection weights of the network controller for fitness evaluation. GA then selects parent chromosomes from the initial population according to the evaluated fitness. The reproduction module produces a set of offspring based on the selected parent chromosomes. The offspring generation then undergoes both decoding and evaluation

processes to obtain the fitness of the children generation. The chromosomes fitness of both children and old (the initial population) generations are compared to formulate a new generation. The parent chromosomes will be selected from the new generation for offspring reproduction and thus forms an optimization cycle. The above optimization cycle is repeated until either the maximum number of generation is reached, or predefined optimal solution is obtained.

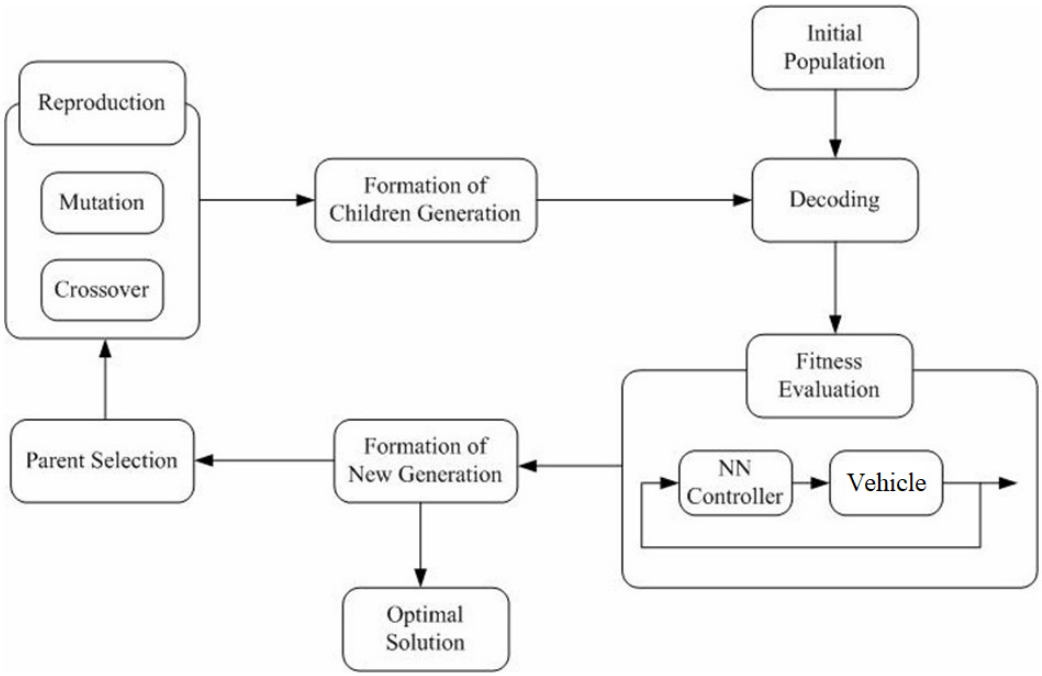

Figure 5.14. Genetic algorithm optimization flow

The above-described cycle consists of three main modules namely evaluation, parent selection, and reproduction modules. In the evaluation module, the chromosomes are decoded into the connection weights of the network controller and the controller is tested with simulation. Then the system states are used to evaluate the chromosomes fitness. The details of the fitness function will be discussed in section 5.4.3.

In the parent selection module, parent chromosomes are selected based on roulette wheel selection [238] for offspring reproduction. The parent and children chromosome are compared, the chromosome with higher fitness are selected for the next generation.

The population performance will be continuously improved due to the fact that parents are replaced by fitter children in each generation.

In the reproduction module, GA applies genetic operators, i.e., crossover and mutation, on selected parent chromosomes to generate a new set of connection weight, i.e., children. The children will be tested and evaluated in the evaluation module.

5.4.2. Coding of connection weights into chromosomes

Since the activation function and structure are fixed and predefined, the chromosomes define the network solely by its connection weights. Figure 5.15 shows the coding of connection weight into the chromosome. The six connection weights are coded into six real value genes instead of binary coding because the real value does not lose precision due to binary quantization.

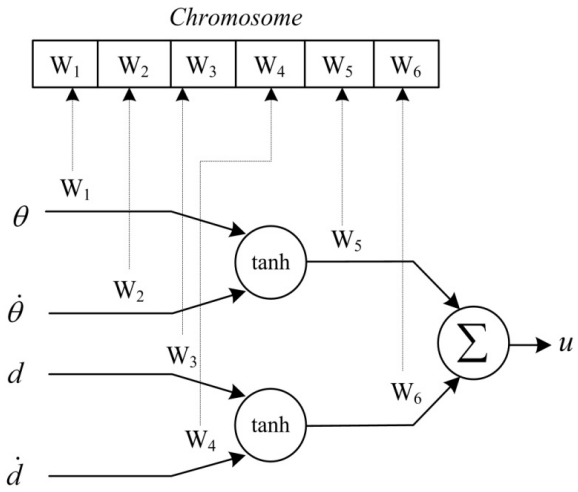

Figure 5.15. Coding of network weights into chromosome

5.4.3. Fitness evaluation

Using the equations describing the dynamics of the system, and equations (5-38) to (5-40) which give the control input, the error can be obtained. We use the sum of the performance index *integral time-weighted absolute error (ITAE)* of displacement and orientation errors. The fitness function is defined based on this sum, as follows:

$$fitness = \frac{1}{1+\int(|e_1|+|e_2|)tdt} \qquad (5\text{-}41)$$

where e_1 and e_2 are displacement and orientation errors, respectively. ITAE is a performance index known for a balanced response with a reasonable rise time and overshoot, compared to *integral squared error (ISE)* performance index.

5.4.4. Computation procedure for the neural network optimization

The procedure for optimizing the neural network controller can be described as follows:

1) Fix the searching range of individual genes in the chromosomes.

2) Initialize n chromosomes randomly to form an initial population.

3) Decode chromosomes into neural network controller and test its performance in simulation. Then, calculate the fitness value from (5-41) and assign chromosome fitness.

4) Select parent chromosomes from the population to reproduce children chromosomes. The selection is based on roulette wheel selection.

5) Reproduce children chromosomes by crossover and mutation. One-point crossover is used to recombine the genetic material in two parent chromosomes to make two children. Mutation is used to introduce innovative materials to the population.

6) Decode children chromosome into neural network controller to evaluate fitness.

7) Select 50 best-fit chromosomes from children and parent chromosome to form a new generation.

8) Repeat Steps 3 to 7 until either maximum number of generations is reached or the desired fitness value is evaluated.

We should note that the roulette wheel selection may lead to premature convergence and binary tournament selection is preferred. However, as the search space is small in our problem, the roulette wheel selection is acceptable.

5.4.5. Simulation Results

In this section, the proposed controller is designed for the lateral control problem, and the simulation results are presented.

The parameter settings of GA are listed in Table 5.2. There are 50 chromosomes in each generation. The maximum number of generation is 400. A new generation is reproduced by mutation and crossover with rates of 0.2 and 0.8, respectively. Fitness function for fitness evaluation is based on the integral time of the absolute error.

Table 5.2. Genetic algorithm parameters

Population size	50
Maximum generation	400
Crossover rate	0.8
Mutation rate	0.2
Fitness function	1/(1+ITAE)

The vehicle model parameters are the mentioned in (6-33). The connection weight search spaces of W_1, W_2, W_3, and W_4 are [-40, 40], and they are [-30, 30] for W_5 and W_6. The optimized connection weights obtained after GA optimization are shown in Table 5.3.

Table 5.3. Optimized connection weights

Vehicle lateral dynamics	W_1	13.3270	W_4	11.0144
	W_2	30.8529	W_5	11.2883
	W_3	34.2793	W_6	-23.7703

In order to compare the performance of the proposed controller, we designed a standard linear state feedback controller (LC) for the linearized models of the system [232]. Since the linearized model of the system is state-controllable, the poles can be assigned arbitrarily. The feedback gain matrix determination is done using Ackermann's formula [232]. The state feedback controller gains for the vehicle (K_v) are shown in Table 5.4. In addition, the associated closed-loop system poles are also mentioned in this Table.

Table 5.4. Linear state-feedback controller gains

System	Closed-loop poles		K_1	K_2	K_3	K_4
Vehicle lateral dynamics	$-1.2 \pm 0.9j, -10, -10$	K_v	11.1	-2.7	-11.1	-0.3

The lateral control performance of the proposed controller on a straight road scenario is shown in Figure 5.16 and Figure 5.17. The road curvature was set to zero throughout the simulation as a straight road condition was assumed. The initial state of the vehicle was located at $10cm$ away from the reference lane and parallel to it; i.e. zero orientation error. The distance set-point from the reference lane was $20cm$.

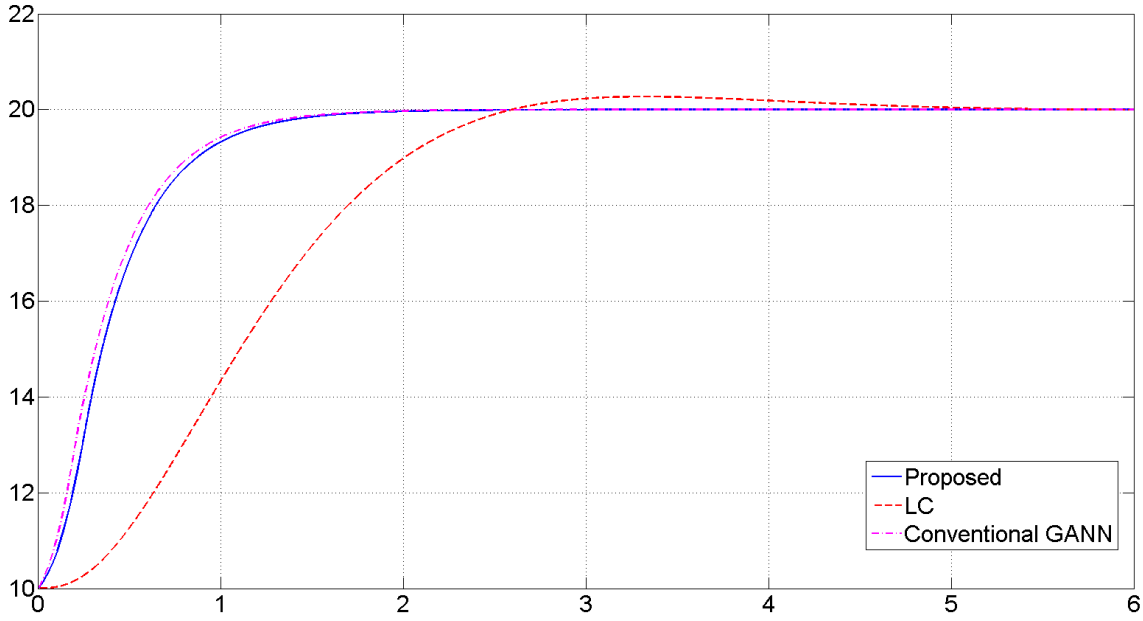

Figure 5.16. Lateral control simulation result of lateral displacement

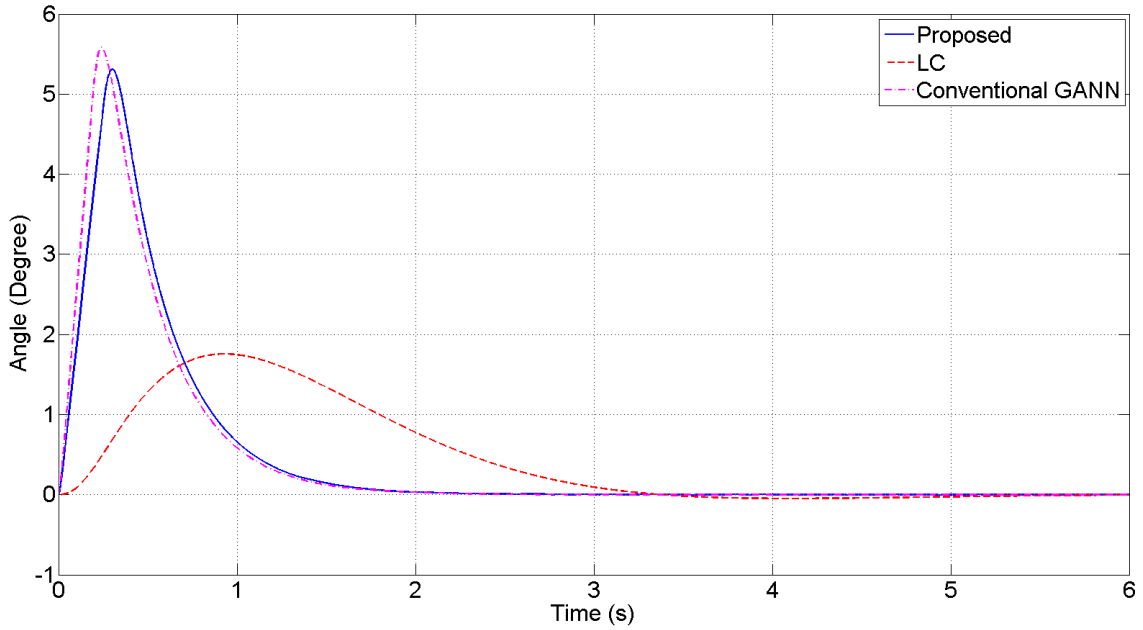

Figure 5.17. Lateral control simulation result of vehicle orientation

In Figure 5.16, the vehicle lateral position maneuvers to set-point after $2s$, whereas this time was more than $5s$ for the linear controller. In Figure 5.17, the angle between vehicle center line and the road was calculated by the difference between front and tail displacements. The maximum angle was about $5°$ and it resumes to 0 after $2s$.

In addition to comparison with linear state feedback controller, the performance of the proposed controller is compared with a conventional neural network controller [239]. The neural network controller used in this paper for comparison is a feed-forward network with a hidden layer of size four with symmetric sigmoid functions (see Figure 5.18). This topology consists of 20 weights to be determined. These weights are optimized using Genetic Algorithm. The values of the weights obtained for lateral control problem are:

$$a = \begin{bmatrix} 22.1691 & 6.8327 & 28.8852 & 14.2108 \\ 6.1040 & -17.1301 & 4.2256 & -24.2986 \\ -6.6490 & -17.5206 & 13.8430 & -3.8738 \\ 19.8577 & 0.1882 & -8.8330 & -0.7479 \end{bmatrix} \quad (5\text{-}42)$$

and

$$b = \begin{bmatrix} -12.8255 \\ -5.6457 \\ -4.7671 \\ -24.2987 \end{bmatrix} \quad (5\text{-}43)$$

where a_{ij} is the weight between input i and sigmoid function j, and b consists of the weights between the hidden layer and the output.

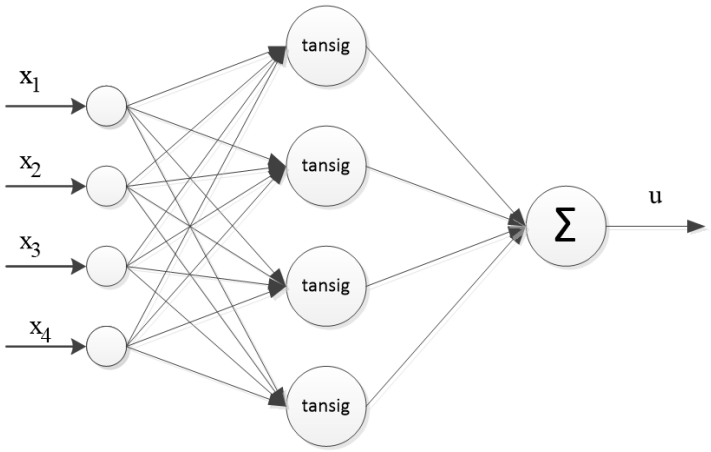

Figure 5.18. Genetic algorithm neural network architecture used for comparison

Although performance results obtained using this GA NN is almost the same as the results achieved by the proposed controller, the numbers of function evaluations were 6500 and 1650 for the conventional and the proposed controller, respectively. These numbers of function evaluation demonstrate a significant reduction in execution time and computational complexity. In other words, although the idea of using GA to update NN is not new, the simplicity and speed of the proposed structure make it superior to conventional GA NN controllers.

The evolution of the genetic algorithm, considering the fitness value, is shown in Figure 5.19. Since some members of some of the generations cause instability of the system, hence too large fitness values, only the best individual of each generation is shown in this figure.

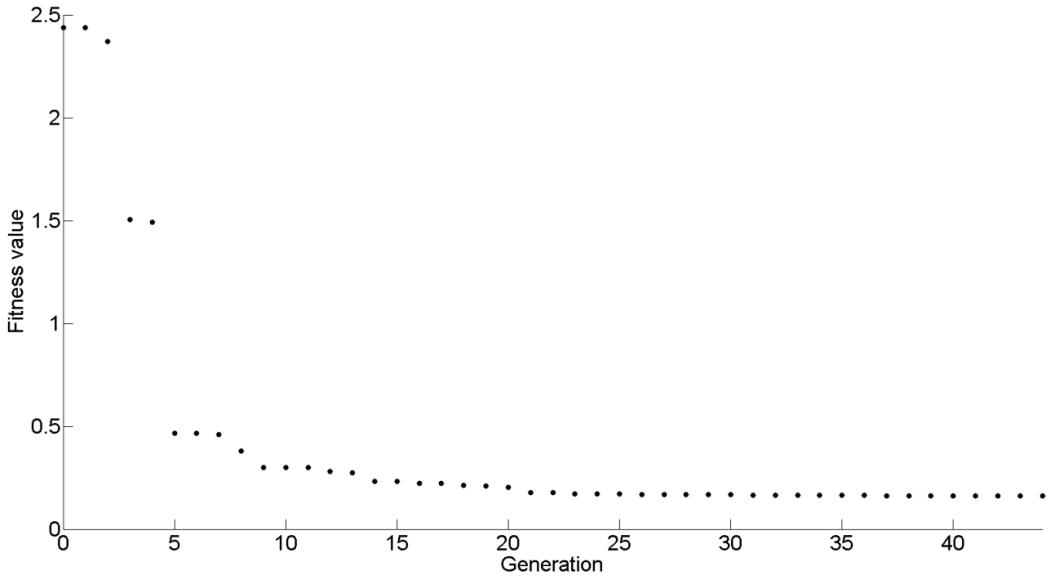

Figure 5.19. The best individual of each generation

In order to check the performance of the proposed controller under different initial conditions, the lateral control system was simulated with different initial states $e_1, \dot{e}_1, e_2,$ and $\dot{e}_2$. The results are shown in Figure 5.20 and Figure 5.21. These figures show that the proposed controller has good performance regardless of the choice of the initial conditions (displacement and orientation of the vehicle).

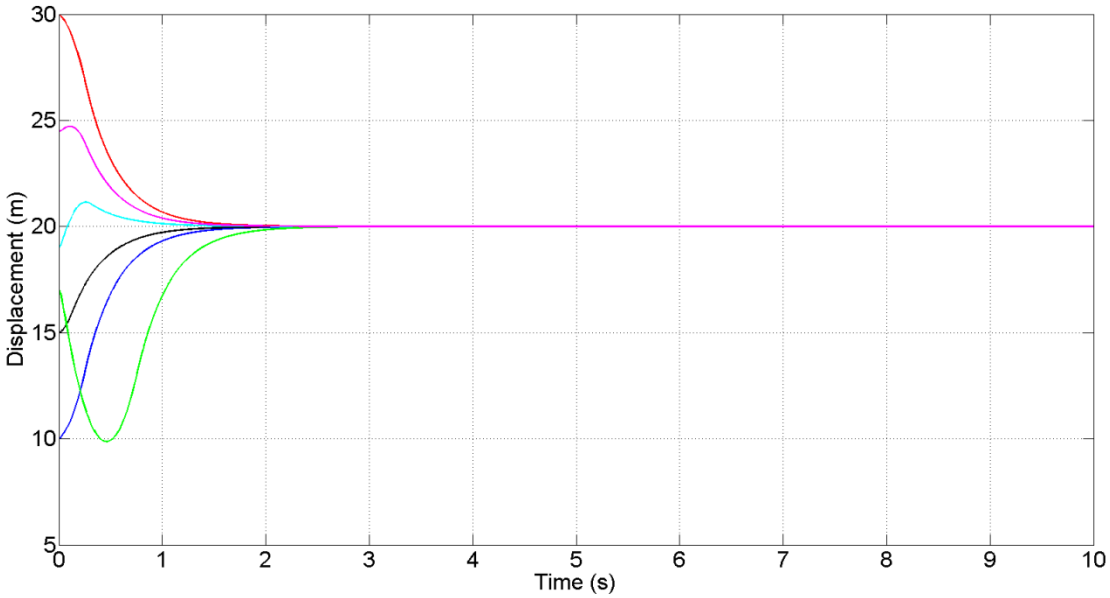

Figure 5.20. Lateral control simulation result of lateral displacement with different initial conditions

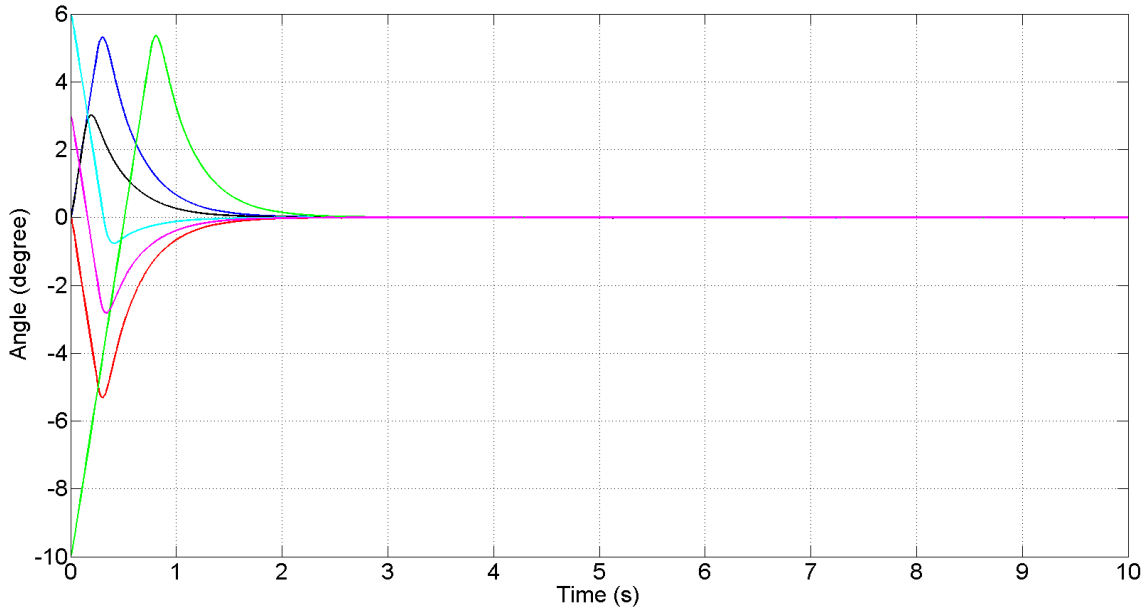

Figure 5.21. Lateral control simulation result of vehicle orientation with different initial conditions

5.4.6. Robustness Analysis

In this section, we investigate the controller robustness using Monte-Carlo evaluation method [240]. The neural network controller optimized by the genetic algorithm was based on a linearized bicycle model which inevitably included incomplete vehicle dynamic information. Furthermore, the parameters change due to the change in vehicle speed, mass, road friction and tire cornering stiffness were not reflected in the model. Therefore, it is important to show that the controller is robust to parameter variation.

10,000 Monte-Carlo evaluations are performed to illustrate the effect of parameter variation on the step response of the neural network controller. A single model parameter was randomly selected and varied $\pm 25\%$ using uniform uncertainty in each evaluation. Figure 5.22 shows 10,000 step responses of the bicycle model with $\pm 25\%$ parameter uncertainties using the proposed controller.

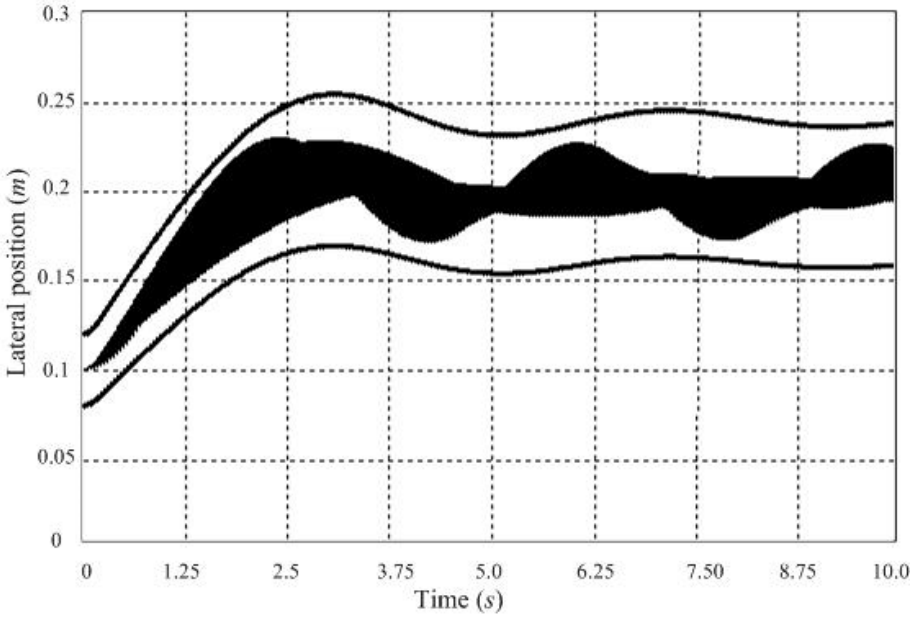

Figure 5.22. Monte-Carlo evaluation with $\pm$ 25% parameters uncertainty

Envelopes shown in Figure 5.22 are constructed based on the nominal step responses of the vehicle controlled by the neural network controller. The step response is multiplied by factors 1.2 and 0.8 to define $\pm$ 20% deviation limits. The purpose of defining the envelope is to estimate the probability of step response violating the envelope. That is the probability of a step response to falling out of the envelope if system parameters have $\pm$25% variation.

Figure 5.22 demonstrates that all the 10,000 Monte-Carlo evaluation results are within the defined $\pm$20% deviation envelopes. Based on the Monte-Carlo evaluation result, we conclude that the proposed neural network controller is robust to $\pm$25% parameters uncertainty and it is stable within this range of operation.

5.5. Conclusion

In this chapter, we described and analyzed the kinematic and dynamic models of vehicle lateral motions. By re-writing the original bicycle model equations using the re-defined variables, the lateral model was converted to a state-space representation where the state variables are the position and orientation errors, and their derivatives, with

respect to the center of the lane. This modification facilitates controller design in this chapter and the remainder of this dissertation.

Based on the vehicle model, a state feedback controller was designed to keep the vehicle at the center of the lane using pole-placement techniques. Also, the effects of adding a feed-forward controller to the designed state feedback controller were studied. Based on this analysis, the appropriate feed-forward controller was designed to improve the performance of the system, especially in the curved sections of the road.

We considered the output of the system as the preview error at a distance ahead of the vehicle and designed several output feedback controllers for the system. We applied the root locus technique to find the minimum required proportional gain to stabilize the system. Using the Bode plots of the closed-loop system, we designed a lead compensator to increase the stability margins.

Finally, a novel, simple neural-network controller, which was recently introduced by our group, was used to design a lateral controller. Unlike the other controllers designed in this chapter, the new controller was not model-based. In other words, the mathematical model of the vehicle was not necessary to find the controller parameters in this algorithm. The performance of this designed controller was comparable to conventional neural network controllers. However, the complexity of the proposed method is much less which results in a simpler design procedure and fewer function evaluations for GA optimization of the neural network weights. We also considered 25% variation in model parameters and demonstrated the robustness of the algorithm using Monte-Carlo analysis.

Although these lateral controllers were designed in a way to be robust to some parameter variations, the disturbances and model uncertainties in real life scenarios might be more severe. Wind gusts, icy roads, road banking angles, drastic changes in vehicle cornering stiffness because of the road conditions, and other parameter variations might happen while driving. In addition, some of these conditions might occur at the same time, which makes the problem even more difficult. As explained in Chapter 2, these

complexities are less considered in the literature. In the next chapter, we apply a recently introduced robust adaptive controller to solve this problem.

Chapter 6.

$\mathcal{L}_1$ Adaptive Steering Control

In the previous chapter, we designed several lateral controllers. We also showed the significance and importance of lateral control in autonomous vehicles through the literature review in Chapter 2. However, the problem presents additional challenges when external disturbances, uncertainties, and parameter variations are considered. These complexities are less considered in the literature. Therefore, it is envisaged that robust adaptive control is an excellent candidate to address these problems successfully.

Less than a decade ago, $\mathcal{L}_1$ adaptive control was introduced by Hovakimyan and Cao [27-29]. The following properties of this controller make it a suitable choice for the vehicle lateral control problem. The key features of this control architecture are guaranteed robustness and fast adaptation. These ensure that the control system is robust to variations in the uncertainty and parameters of the system as well as demonstrating an acceptable performance. The $\mathcal{L}_1$ control algorithm also ensures uniformly bounded transient response and steady-state tracking. This goal is achieved by proper formulation of the control objective in a way that the uncertainties of the system can be compensated for within the bandwidth of the control channel [27]. In this algorithm, the decoupling of adaptation and robustness is made possible by building the robustness specifications in the problem formulation. This method increases the speed of adaptation which will be restricted only by hardware limitations. In other words, employing $\mathcal{L}_1$ adaptive control addresses fast adaptation which is beneficial for both robustness and performance. One of the crucial steps in this algorithm is selecting the underlying filter structure, which can be addressed using classical and robust control techniques.

Within the above context, the contribution of this communication is two folds: (i) The algorithm will guarantee stability and performance in trajectory (lane center) tracking in the presence of model uncertainties, wind disturbance, road banking angle, and icy roads, assuming there is no sensor failure. (ii) The proposed controller will rapidly adapt to variations in the parameters of the system model and compensate the

effects of unknown disturbances. Also, since this method is adaptive, it is a suitable choice for vehicle lateral control problem in the presence of parameter variations. Lastly, because of its guaranteed robustness, $\mathcal{L}_1$ adaptive controller is an appropriate controller for handling vehicle lateral model uncertainties and disturbances such as the wind, slippery roads, and road banking angles.

In this chapter, we implement $\mathcal{L}_1$ adaptive control on the vehicle lateral control problem. The main objective is to design a controller that ensures the vehicle follows the reference trajectory (center of the lane) with robustness to uncertain parameters of the vehicle lateral dynamics. The designed $\mathcal{L}_1$ adaptive control signal compensates the uncertainties and variations in model parameters in the presence of disturbances. As with the previous chapters, a bicycle model for the vehicle lateral dynamics is considered. We will demonstrate the desirable performance of the proposed adaptive controller at steady-state as well as the transient response. The simulation results confirm that the controller significantly improves the transient response of the vehicle lateral controller in the presence of wind gusts, road bank angle, icy or slippery road conditions, measurement noise, and other parameter uncertainties and unknown disturbances.

6.1. Vehicle Lateral Dynamics

6.1.1. Nominal Model

A nonlinear six-degree-of-freedom (DOF) vehicle model, which represents the vehicle lateral dynamics as realistically as possible, is developed in [223]. This complex model has sixteen state variables: twelve for the six DOF motions (three translational and three rotational) and four for the tires. A simplified linear two-degrees of freedom 'bicycle' model of the vehicle can be obtained from the complex model. Several studies have already established that the simplified model, which we will use in this work, is a good approximation of the complex model for all practical purposes [200, 223, 224]. In this model, the vehicle yaw angle ψ and lateral position y are considered as the two degrees of freedom of the car, as shown in Figure 6.1. We consider O as the center of the rotation of the vehicle. The lateral position of the car can be measured along the y axis to

the point O. The yaw angle is considered as the angle between horizontal axis of the car (x) and the global horizontal axis (X). This is demonstrated in Figure 6.1.

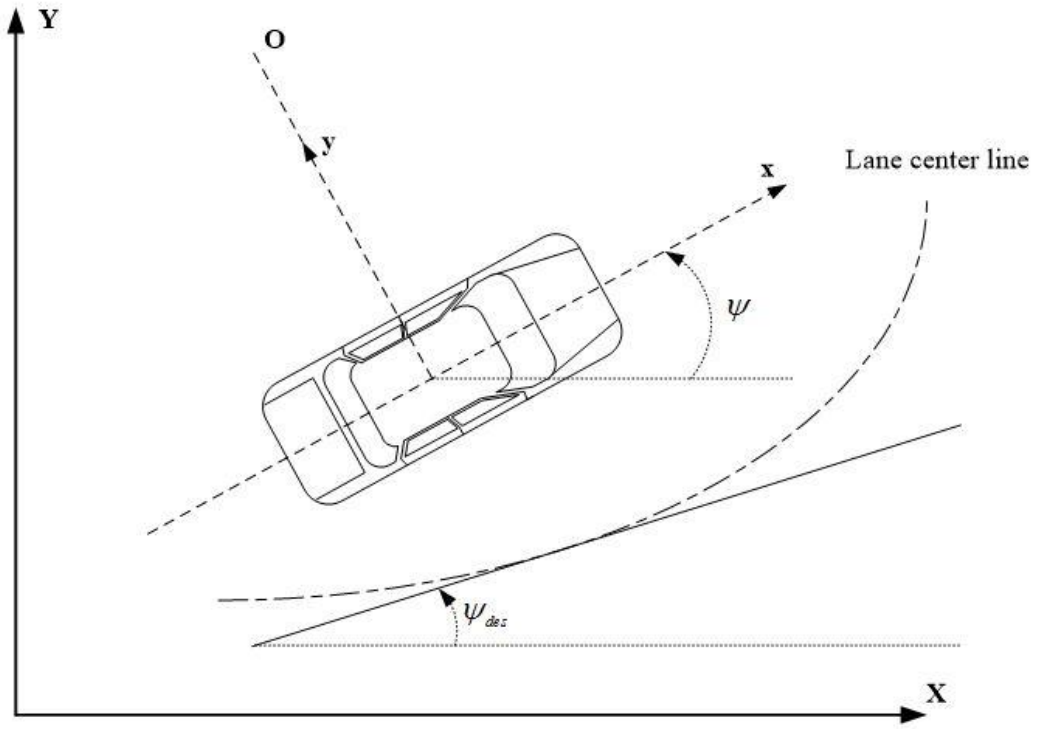

Figure 6.1. Vehicle lateral dynamics

The longitudinal velocity of the car at its center of gravity is denoted by V_x. The distances of the front and rear tires from the center of gravity and cornering stiffness of each front and rear tire are shown by l_f, l_r, C_{af}, and C_{ar}, respectively. The steering angle is shown by δ and the yaw moment of inertia of the vehicle is I_z. Considering lateral position, yaw angle, and their derivatives as the state variables, and using Newton's second law for motion along the y-axis, the state-space model of lateral vehicle dynamics can be shown by the following equation [224]:

$$\frac{d}{dt}\begin{bmatrix} y \\ \dot{y} \\ \psi \\ \dot{\psi} \end{bmatrix} = \begin{bmatrix} 0 & 1 & 0 & 0 \\ 0 & -\frac{2C_{af}+2\,C_{ar}}{mV_x} & 0 & -V_x - \frac{2C_{af}l_f - 2\,C_{ar}l_r}{mV_x} \\ 0 & 0 & 0 & 1 \\ 0 & -\frac{2C_{af}l_f - 2\,C_{ar}l_r}{I_z V_x} & 0 & -\frac{2C_{af}{l_f}^2 + 2\,C_{ar}{l_r}^2}{I_z V_x} \end{bmatrix} \begin{bmatrix} y \\ \dot{y} \\ \psi \\ \dot{\psi} \end{bmatrix} + \begin{bmatrix} 0 \\ \frac{2C_{af}}{m} \\ 0 \\ \frac{2C_{af}l_f}{I_z} \end{bmatrix} \delta \qquad (6\text{-}1)$$

The ultimate goal of this study is designing a lateral control (steering control) for the lane keeping in autonomous vehicles. Therefore, we prefer to convert the above state-space representation of lateral dynamics to a model where the state variables are the position and orientation errors with respect to the center of the lane. Therefore, the above lateral model can be re-defined in terms of two error variables: e_1 which is the distance of the center of the gravity of the vehicle from the center line of the lane and e_2 which is the orientation error of the vehicle with respect to the road.

Assuming the radius of the road is R, the rate of change of the desired orientation of the vehicle can be defined as

$$\dot{\psi}_{des} = \frac{V_x}{R} \qquad (6\text{-}2)$$

Based on the above state variables, the tracking objective of the lateral control problem can be expressed as a problem of stabilizing the following dynamics at the origin:

$$\frac{d}{dt}\begin{bmatrix} e_1 \\ \dot{e}_1 \\ e_2 \\ \dot{e}_2 \end{bmatrix} = \begin{bmatrix} 0 & 1 & 0 & 0 \\ 0 & -\frac{2C_{af}+2\,C_{ar}}{mV_x} & \frac{2C_{af}+2\,C_{ar}}{m} & -\frac{2C_{af}l_f-2\,C_{ar}l_r}{mV_x} \\ 0 & 0 & 0 & 1 \\ 0 & -\frac{2C_{af}l_f-2\,C_{ar}l_r}{I_zV_x} & \frac{2C_{af}l_f-2\,C_{ar}l_r}{I_z} & -\frac{2C_{af}{l_f}^2+2\,C_{ar}{l_r}^2}{I_zV_x} \end{bmatrix}\begin{bmatrix} e_1 \\ \dot{e}_1 \\ e_2 \\ \dot{e}_2 \end{bmatrix} +$$

$$\begin{bmatrix} 0 \\ \frac{2C_{af}}{m} \\ 0 \\ \frac{2C_{af}l_f}{I_z} \end{bmatrix}\delta + \begin{bmatrix} 0 \\ -V_x - \frac{2C_{af}l_f-2\,C_{ar}l_r}{mV_x} \\ 0 \\ -\frac{2C_{af}{l_f}^2+2\,C_{ar}{l_r}^2}{I_zV_x} \end{bmatrix}\dot{\psi}_{des} \qquad (6\text{-}3)$$

The lateral position of the vehicle with respect to the road is usually measured at a location ahead of the vehicle, as shown in Figure 6.2. Various sensors have been used by researchers to measure this lateral preview error [186].

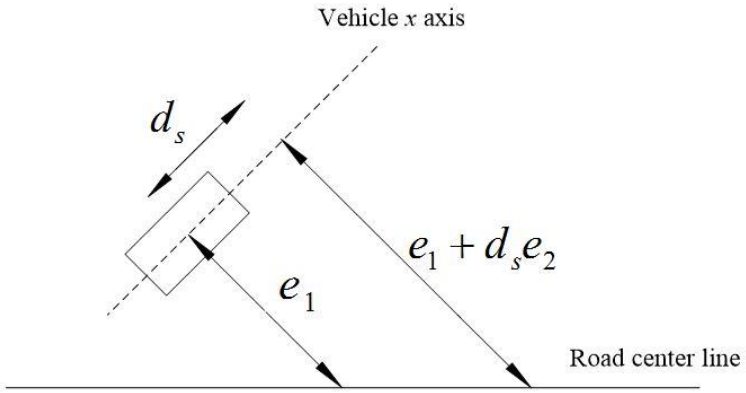

Figure 6.2. Measurement of preview error

Assuming that e_2 is small, we can approximate the chord length by the arc length. Therefore, the output equation of the state-space, the equation that expresses the output as a linear combination of the states, is as follows:

$$y = e_1 + d_s e_2 \qquad (6\text{-}4)$$

where d_s is the look-ahead distance, which is the longitudinal distance of the point ahead of the vehicle center of gravity, where we make the sensor measurements.

6.1.2. Road Bank Angle

The bank angle is the angle at which the vehicle is inclined about its longitudinal axis with respect to the horizontal line. Road bank angle has a direct influence on the vehicle dynamics. Whereas quantities like speed or lateral error can be obtained by direct measurement, bank angle cannot be measured as easily. Although some methods for estimating this value have been reported [241], the decoupling of parametric uncertainties (such as variations of cornering stiffness of tires and vehicle mass) from the road bank angle still needs to be addressed.

Compensating the road bank angle is neglected in many of the lateral control algorithms, including those algorithms discussed in the previous chapters. In this study, we treat this variable as a disturbance or an unknown input to the vehicle and include it in all closed-loop simulations. We expect the control algorithm to compensate its effect without having any measurement of its value. The effect of the road bank angle is

considered in the dynamic model of the vehicle by adding the following term to the right-hand side of (6-3):

$$\begin{bmatrix} 0 \\ g \\ 0 \\ 0 \end{bmatrix} \sin(\phi) \qquad (6\text{-}5)$$

where g is the gravitational acceleration and ϕ is road bank angle.

6.1.3. Parametric Uncertainties

Variations of the parameters in (6-3) affect the vehicle dynamics. Whereas the parameters l_f, l_r and d_s are fixed and known, mass (m), moment of inertia (I_z), longitudinal speed (V_x), and cornering stiffness (C_{af} and C_{ar}) might deviate from their nominal values.

Peng and Tomizuka showed in [223] that the most significant variations of vehicle dynamics are caused by the uncertainties in the value of cornering stiffness. The values of C_{af} and C_{ar} are affected by many factors: tire slip ratio, tire slip angle, tire pressure, load, velocity, temperature, and, most importantly, the road condition. Not only these values vary in a wide range, but also, they change the behavior of the vehicle drastically. The nominal and range of variations of the parameters are adopted from [223] and tabulated in

Table 6.1. Parameters of the vehicle model

Parameter	Symbol	Unit	Nominal	Min (relative)	Max (relative)
Mass	m	kg	1573	0.85	1.15
Moment of Inertia	I_z	$kg.m^2$	2873	0.85	1.15
Cornering Stiffness	C_{af}, C_{ar}	N/rad	80000	0.2	2

Here, we assume all the above parametric uncertainties exist concurrently. Specifically, we assume one section of the road is icy, and the cornering stiffness drops to its minimum value, as it will be explained in section 6.3.

6.1.4. Wind Gust

The vehicle lateral control system should be able to maintain the car in the center of the lane when there is wind gust disturbance. The effect of the wind on vehicle lateral dynamics is derived in [223]. As per recommendation in [241], we add the following term to the right-hand side of (6-3):

$$\begin{bmatrix} 0 \\ F_w/m \\ 0 \\ T_w/I_z \end{bmatrix} \qquad (6\text{-}6)$$

where F_w and T_w are wind force and torque acting on vehicle in lateral direction

6.2. $\mathcal{L}_1$ Adaptive Control

In this section, we present an overview of the $\mathcal{L}_1$ adaptive controller which was first reported by Cao and Hovakimyan [28, 29]. One of the main advantages of $\mathcal{L}_1$ controller over other adaptive control strategies is decoupling of the adaptation rate and the robustness. This goal is achieved by selecting an appropriate low-pass filter on the control signals. In all control algorithms, there is the issue of the trade-off between performance and robustness. The mentioned decoupling results in an easier solution for this trade-off problem. Although a compromise between the robustness and the adaptation rate exists in this algorithm too, the techniques used in this method facilitates handling the trade-off problem.

Many variations of $\mathcal{L}_1$ adaptive controller have been reported after it was first introduced [27]. We employ a particular architecture of this controller that suitably addresses the lateral vehicle control with uncertainties on the parameters of the vehicle dynamics. This version of the controller employs output feedback in the presence of

unknown time-varying nonlinearities [242]. The main reason for the selection of this algorithm is that it does not require explicit measurement of the states of the systems as sensors that measure such states may not be available.

This algorithm guarantees that the transient response for system's both signals, input and output, are uniformly bounded as compared to similar signals of a reference system. The bounds for the error signals between the controlled system and the reference system can be reduced by increasing the adaptation gain [27]. The details of these bounds and their relationships with the adaptation gain are given in [28] and [27].

6.2.1. Problem Formulation

In this methodology, the following structure is considered for the system

$$Y(s) = A(s)\big(U(s) + D(s)\big) \qquad (6\text{-}7)$$

where $Y(s)$ is the Laplace transform of system's output $y(t)$, $U(s)$ is the Laplace transform of $u(t)$ which is the system's input, $A(s)$ is the unknown transfer function of the system, and $D(s)$ is the Laplace transform of the nonlinear time-varying disturbances and uncertainties, represented by $d(t) = f(t, y(t))$. Two assumptions are made for the unknown f:

Assumption 1 (Lipschitz continuity): Arbitrary large constants $L > 0$ and $L_0 > 0$ exist such that the following inequalities hold uniformly:

$$\begin{cases} |f(t, y_1) - f(t, y_2)| \le L|y_1 - y_2| \\ |f(t, y)| \le L|y| + L_0 \end{cases} \qquad (6\text{-}8)$$

Assumption 2: The rate of variation of uncertainties is uniformly bounded. In other words, there exist arbitrarily large constants $L_1 > 0$, $L_2 > 0$, and $L_3 > 0$ such that

$$\left|\dot{d}(t)\right| \le L_1|\dot{y}(t)| + L_2|y(t)| + L_3 \qquad (6\text{-}9)$$

The control objective is to design an adaptive controller such that $y(t)$ tracks the reference $r(t)$ as a desired reference model $M(s)$:

$$M(s) = \frac{m}{s+m},\ m > 0 \qquad (6\text{-}10)$$

6.2.2. $\mathcal{L}_1$ Adaptive Control Structure

Based on (6-7) and (6-10), the system can be written in terms of the reference system:

$$Y(s) = M(s)\big(U(s) + \sigma(s)\big) \qquad (6\text{-}11)$$

where

$$\sigma(s) = \frac{\big(A(s)-M(s)\big)U(s)+A(s)D(s)}{M(s)} \qquad (6\text{-}12)$$

The design of $\mathcal{L}_1$ adaptive controller involves designing a strictly proper filter $C(s)$ with $C(0) = 1$ which results in stable $H(s)$ where

$$H(s) = \frac{A(s)M(s)}{C(s)A(s)+\big(1-C(s)\big)M(s)} \qquad (6\text{-}13)$$

and the following norm condition is satisfied

$$\|G(s)\|_{\mathcal{L}_1} L < 1 \qquad (6\text{-}14)$$

where

$$G(s) = H(s)\big(1 - C(s)\big) \qquad (6\text{-}15)$$

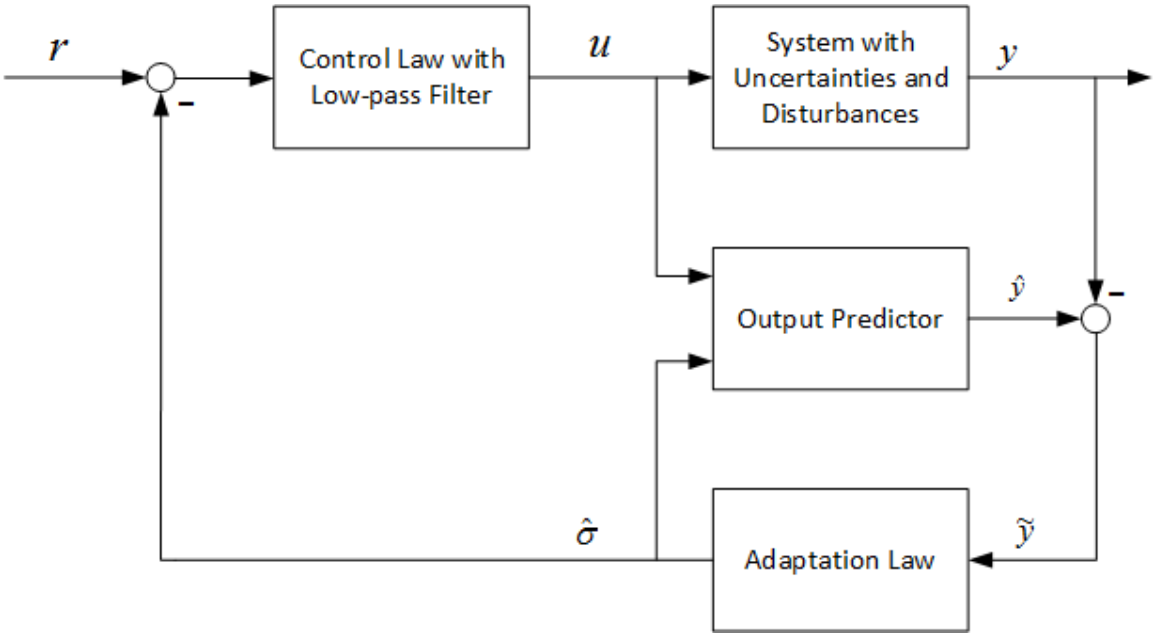

Figure 6.3. Closed-loop system with $\mathcal{L}_1$ output feedback adaptive controller

The general structure of a closed-loop output feedback $\mathcal{L}_1$ adaptive controller is illustrated in Figure 6.3. In addition to the control law, this algorithm consists of an output predictor and an adaptation law.

1) Output Predictor

The following output predictor is used here

$$\dot{\hat{y}} = -m\hat{y}(t) + m\big(u(t) + \hat{\sigma}(t)\big),\ \hat{y}(0) = 0 \qquad (6\text{-}16)$$

where $\hat{\sigma}(t)$ is the adaptive estimate obtained by the adaptation law block.

2) Adaptation Law

The adaptive estimate $\hat{\sigma}(t)$ is obtained by

$$\dot{\hat{\sigma}}(t) = \Gamma\mathrm{Proj}\big(\hat{\sigma}(t), -\tilde{y}(t)\big),\ \hat{\sigma}(0) = 0 \qquad (6\text{-}17)$$

where Proj is the projection function defined in Appendix A, $\tilde{y}(t) = \hat{y}(t) - y(t)$ is the error between the predictor in (6-16) and the output of the system in (6-11), and $\Gamma \in \mathbb{R}^+$ is the adaptation gain. Projection is used to ensure the bounds for parameter estimation.

3) Control Law with Low-pass Filter

The following control signal is generated by this algorithm to compensate the uncertainties within the desired bandwidth:

$$U(s) = C(s)\big(R(s) - \hat{\sigma}(s)\big) \qquad (6\text{-}18)$$

where $C(s)$ is a strictly proper low-pass filter with $C(0) = 1$. The unity dc gain of the filter ensures tracking [27]. In this work, a first-order low-pass filter is considered:

$$C(s) = \frac{\omega}{s+\omega} \qquad (6\text{-}19)$$

6.2.3. Closed-loop Reference system

Supposing that the adaptive variable $\hat{\sigma}(t)$ is exactly estimated, $\hat{\sigma}(t) = \sigma(t)$, if we define the control signal $U(s)$ to be equal to $R(s) - \sigma(s)$, the output signal $Y(s)$ would exactly match $M(s)R(s)$. However, in the $\mathcal{L}_1$ adaptive control algorithm, since we need to approximate the uncertain $\sigma(s)$ signal, the system's ideal input signal $R(s) - \sigma(s)$ is filtered with a low-pass filter $C(s)$. The main reason is to remove the high-frequency chattering phenomenon which is common in adaptive control algorithms [243]. As a result, the expected closed-loop reference response is altered.

Assuming the uncertainties are entirely known (non-adaptive version of the adaptive controller), the closed-loop reference system would be given by

$$Y_{ref}(s) = M(s)\left(U_{ref}(s) + \sigma_{ref}(s)\right) \qquad (6\text{-}20)$$

$$U_{ref}(s) = C(s)(R(s) - \sigma_{ref}(\mathrm{s})) \qquad (6\text{-}21)$$

$$\sigma_{ref}(s) = \frac{\big(A(s)-M(s)\big)U_{ref}(s)+A(s)D_{ref}(s)}{M(s)} \qquad (6\text{-}22)$$

where $D_{ref}(s)$ is the Laplace transform of $d_{ref}(t) = f(t, y_{ref}(t))$. Substituting (6-22) in (6-21) and cancellation of $M(s)$ from both numerator and denominator, which requires a stable non-minimum phase reference model $M(s)$ to ensure stability, results in

$$U_{ref}(s) = \frac{C(s)M(s)R(s) - C(s)A(s)D(s)}{C(s)A(s) + \big(1 - C(s)\big)M(s)} \qquad (6\text{-}23)$$

Substituting the closed-loop reference command (6-23) into (6-20), we get

$$Y_{ref}(s) = H(s)\Big(C(s)R(s) + \big(1 - C(s)\big)D_{ref}(s)\Big) \qquad (6\text{-}24)$$

where $H(s)$ is given by (6-13). Therefore, $M(s)$ and $C(s)$ should be selected to ensure the stability of $H(s)$. In addition, the condition in (6-14) should be met so that the small-gain theorem can be applied [27].

As mentioned before, the ideal control signal would lead to the desired system response $M(s)R(s)$ by exactly cancelling all the uncertainties. Obviously, the response in the reference system in (6-20) and (6-21) is different from the ideal one. In fact, the control signal in (6-21) cancels only the uncertainties which are in the bandwidth of the low-pass filter $C(s)$. The parameter ω in (6-19) can be selected such that the bandwidth of the filter is compatible with the control channel specifications. This is exactly what one hopes to obtain in any feedback control problem in the presence of uncertainties and disturbances.

The adaptive system in this algorithm tries to approximate the parameter $\sigma_{ref}(t)$ with the estimate $\hat{\sigma}(t)$ obtained from (6-17). However, we should examine the conditions that result in stability of the signal that $\hat{\sigma}(t)$ is attempting to estimate, which is $\sigma_{ref}(t)$. Pay attention that $u_{ref}(t)$ and $\sigma_{ref}(t)$ are never explicitly calculated. Actually, the reason that we need to estimate them is the fact that we cannot calculate them. However, we can and should investigate the stability of $\sigma_{ref}(t)$.

Substituting $U_{ref}(s)$ from (6-21) in (6-22) we get

$$\sigma_{ref}(s) = \frac{\big(A(s) - M(s)\big)U_{ref}(s) + A(s)D_{ref}(s)}{M(s)}$$

$$= \frac{\big(A(s) - M(s)\big)C(s)\Big(R(s) - \sigma_{ref}(s)\Big)A(s)D_{ref}(s)}{M(s)}$$

$$= \frac{C(s)\left(A(s)-M(s)\right)}{M(s)} R(s) - \frac{C(s)\left(A(s)-M(s)\right)}{M(s)} \sigma_{ref}(s) + \frac{A(s)}{M(s)} D_{ref}(s) \qquad (6\text{-}25)$$

Figure 6.4 shows the block diagram of $\sigma_{ref}(s)$ obtained in (6-25). We can get the closed-loop equation for $\sigma_{ref}(s)$ of by solving (6-25) for $\sigma_{ref}(s)$:

$$\sigma_{ref}(s) = \frac{C(s)\left(A(s)-M(s)\right)R(s)+A(s)D_{ref}(s)}{C(s)A(s)+\left(1-C(s)\right)M(s)} \qquad (6\text{-}26)$$

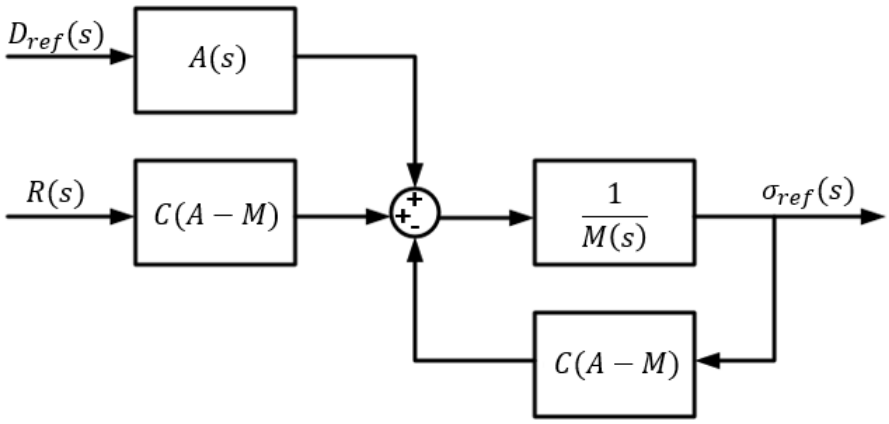

Figure 6.4. Block diagram of $\sigma_{ref}(s)$

Letting

$$A(s) = \frac{A_n(s)}{A_d(s)}$$

$$C(s) = \frac{C_n(s)}{C_d(s)} \qquad (6\text{-}27)$$

$$M(s) = \frac{M_n(s)}{M_d(s)}$$

we can write the polynomial format of $\sigma_{ref}(s)$ as

$$\sigma_{ref}(s) = \frac{C_n(s)\left(A_n(s)M_d(s)-A_d(s)M_n(s)\right)R(s)+C_d(s)A_n(s)M_d(s)D_{ref}(s)}{C_n(s)A_n(s)M_d(s)+\left(C_d(s)-C_n(s)\right)A_d(s)M_n(s)} \qquad (6\text{-}28)$$

Replacing (6-27) in (6-13), we get

$$H(s) = \frac{C_d(s)A_n(s)M_n(s)}{C_n(s)A_n(s)M_d(s)+\big(C_d(s)-C_n(s)\big)A_d(s)M_n(s)} \qquad (6\text{-}29)$$

Comparing (6-28) and (6-29) we note that $\sigma_{ref}(s)$ and $H(s)$ have the same polynomial in their denominators. Therefore, $\sigma_{ref}(s)$ is stable if $H(s)$ is stable.

6.2.4. Designing the Controller Parameters

To design an adaptive $\mathcal{L}_1$ adaptive controller for the vehicle lateral control problem, a first-order reference model, as shown in (6-10), is selected. The reason is that the first-order dynamics behavior is expected from the vehicle when it is adjusting itself in the center of the lane. The parameter m in (6-10) should be tuned. The other parameters that need to be designed are the bandwidth (ω) of the low-pass filter in (6-19), and the adaptation gain (Γ) in (6-17).

At frequencies well below the bandwidth of the filter (way smaller than ω), the filter $C(s)$ acts similar to an all-pass filter ($C(s) \approx 1$) and from (6-13) we have:

$$H(s) \approx M(s) \qquad (6\text{-}30)$$

In this case, the reference output of the system can be written using (6-24):

$$Y_{ref}(s) \approx M(s)R(s) \qquad (6\text{-}31)$$

Similarly, at frequencies well above the bandwidth of the low pass filter (above ω), the filter $C(s)$ acts similar to a no-pass filter ($C(s) \approx 0$), and from (6-13) we have:

$$H(s) \approx A(s) \qquad (6\text{-}32)$$

Obviously, a higher cut-off frequency (ω) in $C(s)$ results in a closed-loop reference system that acts more similarly to the desired model. However, it increases the chattering problem and reduces the stability of the system. The requirement of stability of $H(s)$ limits the range of m and ω that can be considered for designing the controller. As

mentioned, a higher ω would result in a $Y_{ref}(s)$ (response of $H(s)C(s)$) which is close to $Y_{ideal}(s)$ (response of $M(s)$). Even if these two values are close to each other, the actual closed-loop output of the system, $Y(s)$, would be different from these values if adaptation of $\sigma(s)$ is not done fast enough. In other words, the adaptation gain Γ should be selected large enough so that the output of the system follows the reference closed-loop output closely.

In summary, the control process, shown in Figure 6.3, can be described as follows. The output of the unknown system, including disturbances and uncertainties, is compared to the output of the predictor in (6-16), which has the dynamics of the desired reference model. The adaptation law in (6-17) uses the mentioned comparison and generates the adaptive estimate $\hat{\sigma}(t)$. This adaptation estimate, in addition to the reference signal, are given to the control law with a low-pass filter in (6-18) to generate the control signal. The parameters which need to be tuned are m in (6-16), Γ in (6-17), and ω in (6-18). Pay attention that the higher Γ is, the more similar $Y(s)$ (the actual response of the system) and $Y_{ref}(s)$ (the response to $H(s)C(s)$) are. In addition, the higher ω is, the more similar $Y_{ref}(s)$ and $Y_{ideal}(s)$ (the response to $M(s)$) are. Also, the bigger m is, the faster the response of $Y_{ideal}(s)$ is.

The steps of the algorithm applied in this work can be summarized as follows:

1. The parameters m and ω are selected such that the condition in (6-13) is met. In addition, m determines the behavior of the ideal system, and ω should be large enough so that the behavior of the reference system be similar to the one of the ideal system.

2. The adaptation gain Γ is selected as large as possible such that the actual response of the system is close to the reference system. Especially, the value of Γ should not be less than the value that makes $\hat{\sigma}(t)$ unstable.

3. The prediction of the output signal ($\hat{y}(t)$) is given by (6-16).

4. The adaptive estimate of the uncertainties ($\hat{\sigma}(t)$) is given by (6-17).

5. The adaptive control signal ($u(t)$) is given by (6-18).

6.3. Simulations and Results

The dynamics of the vehicle are considered as explained in section 6.1 and parameters of this model, in the nominal case, are considered as follows [224]:

$$C_{af} = 80000, \qquad C_{ar} = 80000, \qquad l_f = 1.1, \qquad l_r = 1.58,$$

$$I_z = 2873, \qquad m = 1573 \qquad (6\text{-}33)$$

The road banking angle in (6-5) and the wind gusts in (6-6) are considered as disturbances to the system. The model parametric uncertainties in Table 6.1 and the neglected dynamics in the bicycle model are considered as the uncertainties. The look-ahead distance, where the sensor measurements are made as shown in (6-4), is considered $d_s = 18\, m$.

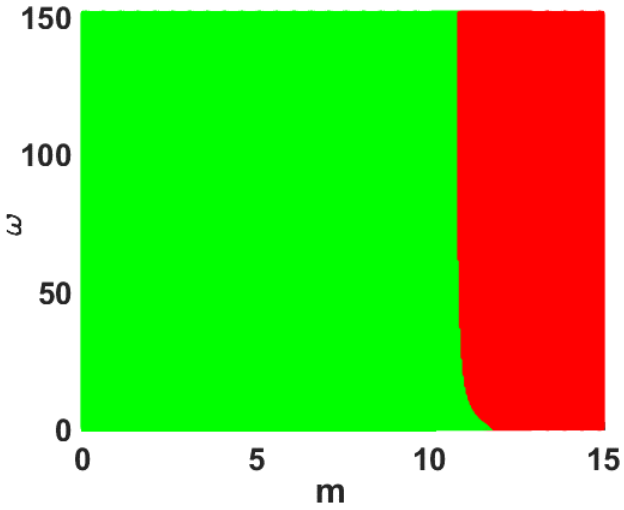

Figure 6.5. Region of pair (m, ω) for stable $H(s)$ (left region)

The range of acceptable values of m and ω for stability of $H(s)$ in (6-13) is shown in Figure 6.5. This result shows that if the reference model is selected slower than a certain speed, the cut-off frequency of the low-pass filter can be chosen arbitrarily for meeting the condition in (6-13).

In this algorithm, the adaptive system attempts to estimate the parameter $\sigma_{ref}(t)$ by updating the parameter $\hat{\sigma}(t)$ using (6-17). We proved in section 6.2.3 that $\sigma_{ref}(t)$ is

stable if $H(s)$ is stable. However, the controller parameters should be designed such that the signal $\hat{\sigma}(t)$ is stable too. In order to investigate the stability of this signal, we use the following equation obtained in [244]:

$$\hat{\sigma}(s) = \frac{C(s)\big(A(s)-M(s)\big)R(s)+A(s)D(s)}{\frac{1}{\Gamma}s+C(s)A(s)+\big(1-C(s)\big)M(s)} \qquad (6\text{-}34)$$

As we expect, when $\Gamma \to \infty$, the estimate $\hat{\sigma}(s) \to \sigma_{ref}(s)$. One useful method to investigate the stability of this system, based on the variations of the adaptive gain Γ, is to use the root locus method. In order to use this method, we write the denominator of (6-34) as

$$1 + \Gamma T(s) \qquad (6\text{-}35)$$

where

$$T(s) = \frac{C(s)A(s)+\big(1-C(s)\big)M(s)}{s} \qquad (6\text{-}36)$$

Comparing (6-13) and (6-36), we can see that the zeros of $T(s)$ match the poles of $H(s)$. Obviously if the parameters m and ω are selected in the green area in Figure 6.5, the open-loop zeros of $T(s)$, which are equal to closed-loop poles of (6-34) or (6-35) for large values of Γ, are stable. . However, the poles of $T(s)$, in addition to the trivial pole at $s = 0$, match the poles $C(s)$, $M(s)$, and $A(s)$. In the vehicle lateral dynamics system, the poles of $A(s)$ are unstable even for the nominal case without uncertainties. As the adaptation gain Γ increases from 0, to ∞, the poles of $\hat{\sigma}(s)$ move from the unstable poles of $T(s)$ to the stable zeros of $T(s)$. However, the unmatched poles go to ∞ following some asymptotes. Since these asymptotes might lead to unstable right half plane, we should be specifically careful about these unmatched poles. In addition, the adaptation gain should be chosen large enough to make sure that the matched poles are stable.

We studied the effect of changing the acceptable (see Figure 6.5) parameters of $C(s)$ and $M(s)$, i.e. ω and m, on the poles of $H(s)$ for the vehicle lateral dynamics (6-3) using nominal values mentioned in (6-33). If these two parameters are selected from the green region shown in Figure 6.5, the dominant real pole of $H(s)$ does not move

significantly, and it is always around -0.8. However, the dominant imaginary poles strongly depend on the pair (m, ω). They would be farther from $j\omega$ axis in complex plane when m is smaller. This results in a trade-off because a smaller m is equivalent to slower response in the reference model. The root locus of (6-35) for the vehicle lateral dynamics for a fixed m and ω is shown in Figure 6.6. The higher the parameter ω is, the higher adaptation gain Γ is required to stabilize $H(s)$. In this system, any $\Gamma > 2770$ stabilizes $\hat{\sigma}(s)$.

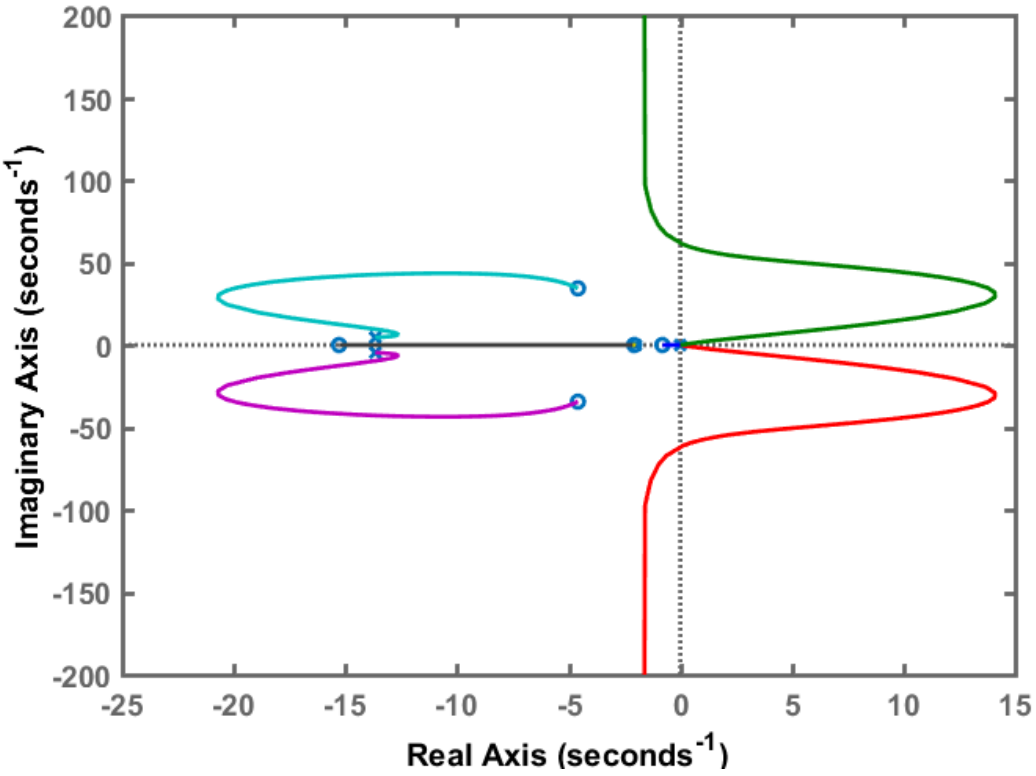

Figure 6.6. Root locus for $\Gamma > 0$ for $\hat{\sigma}(s)$ using nominal parameters of vehicle dynamics

In all the simulations, an initial offset of 1 meter is considered for the vehicle. The wind uncertainty starts at $t = 9s$ and reaches its maximum $t = 11s$ with a force of $F_w = -500$ Newtons and moment of $T_w = -200$ Newton-meters in the lateral direction and affects the vehicle as explained in (6-6). The road bank angle starts at the same time as the wind, and it affects the lateral dynamics of the vehicle in the same direction as the wind, as shown in (6-5). This angle reaches its maximum of 6° at $t = 11s$. The variations of both the wind and road bank angle disturbances are shown in Figure 6.7. In this figure,

the value of one at $11 \leq t \leq 13$ shows the maximum value of wind force (-500N) and the maximum value of road bank angle (6°). The other values at other times are scaled accordingly between 0 and 1. The reader may note that the variations of these disturbances are matched so that the behavior of the system can be studied in the worst case where the peak of both disturbances happen at the same time $(11 \leq t \leq 13)$.

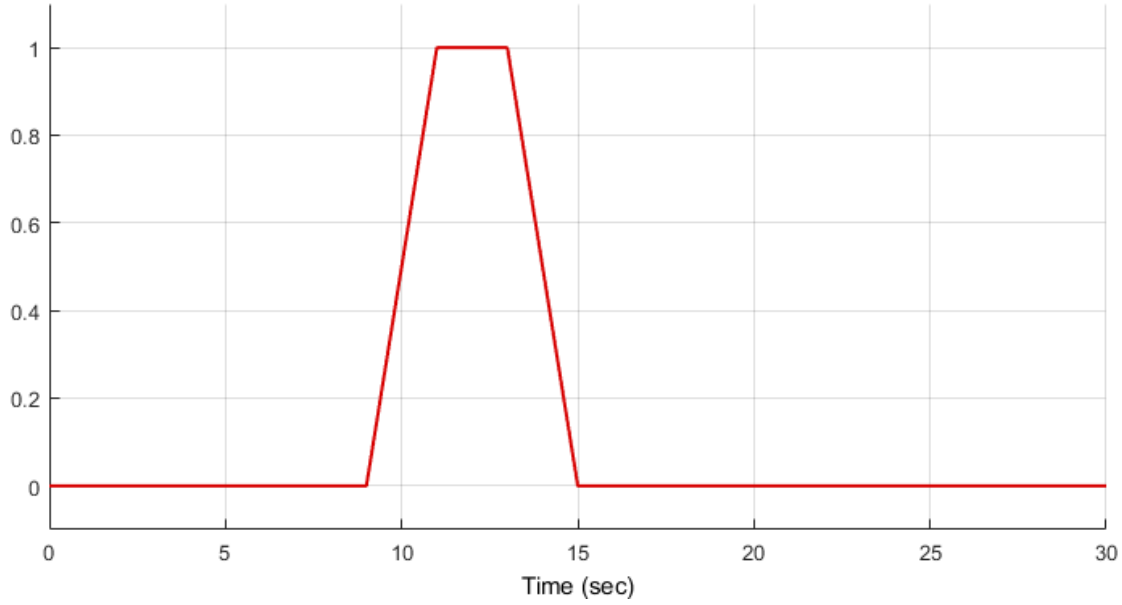

Figure 6.7. Scaled variation of wind and road banking angle disturbances

The road condition is assumed to suddenly change at $t = 11s$ to an icy section where C_{af} and C_{ar} change to 0.2 times their nominal value, as shown in Table 6.1. The road remains icy until the end of simulations at $t = 30s$.

The performance of the $\mathcal{L}_1$ adaptive controller in steering the vehicle in the desired path, in the presence of the above uncertainties and disturbances, is compared with three other controllers. First, a conventional state feedback controller is designed to compare the performances of the controllers in the same scenario for disturbances and uncertainties. A state feedback controller that is designed for the nominal case would fail to stabilize the system in the extreme condition assumed in this scenario. Therefore, we designed the controller considering that the cornering stiffness parameters of the vehicle were at 60% of the nominal value, exactly in the middle of the nominal value and the extreme case of 20% used in the simulations. Second, a lead compensator was designed

for the system. Adding phase in the gain crossover range (low-frequency range) increases the gain margin and phase margin, as explained in details in Chapter 5. This results in a more robust control system in the presence of uncertainties and disturbances. Finally, a PID controller, which is known to have good disturbance rejection, is designed. The controller parameters used for all controllers in the simulations are mentioned in Table 6.2.

Table 6.2. The controller parameters used for the simulations

Controller	Control Signal	Parameters
State-feedback	$u = k_1x_1 + k_2x_2 + k_3x_3 + k_4x_4$	$k_1 = 0.0137,\ k_2 = 0.0024$ $k_3 = 0.2023,\ k_4 = -0.0412$
Lead Controller	$C_L(s) = k\dfrac{T_n s + 1}{T_d s + 1}$	$T_n = 0.5, \quad T_d = 0.1,$ $k = 0.08$
PID Controller	$C_{PID}(s) = K_P + \dfrac{K_I}{s} + \dfrac{K_D N}{1 + \dfrac{N}{s}}$	$K_P = 0.06, \quad K_I = 0.03$ $K_D = 0.01, \quad N = 100$
$\mathcal{L}_1$ adaptive	Equations (6-16) to (6-18)	$m = 2,\ \omega = 2,$ $\Gamma = 50000$

The performance of these controllers in maintaining the vehicle at the center of the lane in the presence of the above-mentioned wind gusts, road bank angle, and icy section of road is shown in Figure 6.8 and Figure 6.9. The outputs of the vehicle lateral system controlled by these four controllers, which equals the preview error explained in (6-4), are compared in Figure 6.8. This figure shows that despite the sudden change in road and weather conditions, the $\mathcal{L}_1$ adaptive controller designed here can satisfactorily keep the preview error close to zero during the whole simulation time. The position of vehicle compared to the center of the lane is also shown for all controllers in Figure 6.9 for $d_s = 18$.

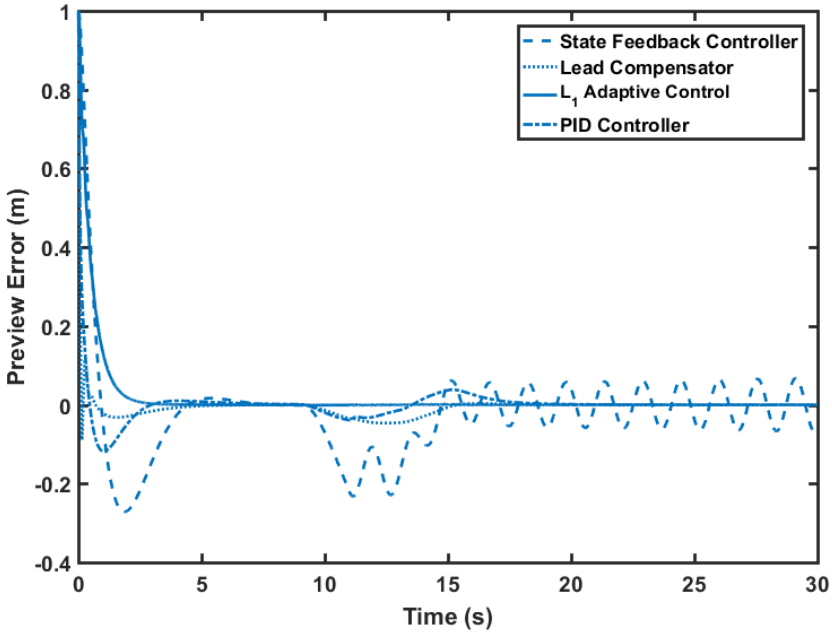

Figure 6.8. Comparison of preview error of vehicle controlled with four different controllers

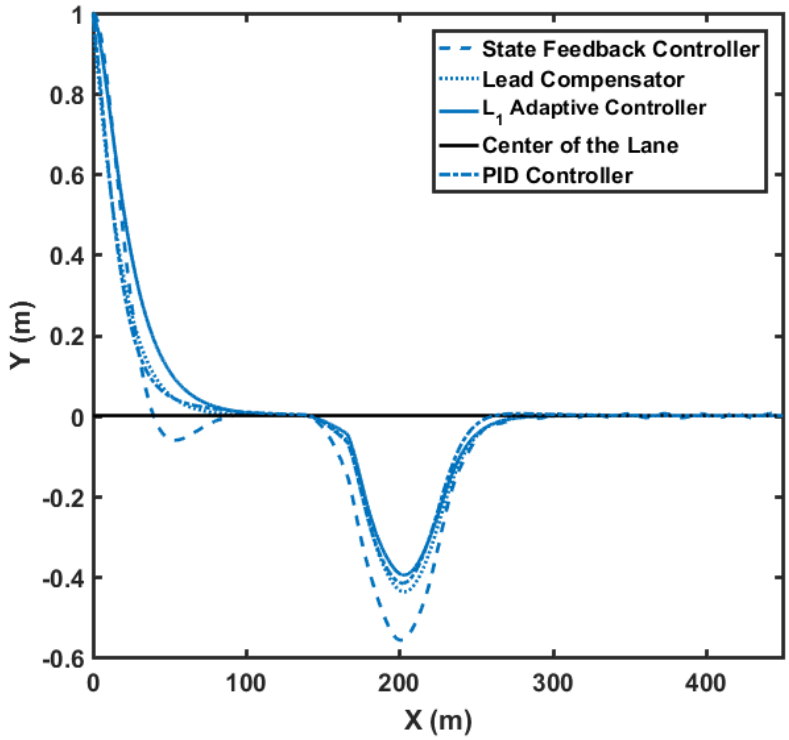

Figure 6.9. Vehicle position in the presence of the wind, road banking angle, and icy section of road controlled by four different controllers

The control signals (steering wheel angles) δ generated by the controllers are demonstrated in Figure 6.10. The control signal generated by all controllers are in the acceptable range. However, it can be seen in the zoomed section of this figure that at the beginning of the simulation, the maximum value of the steering wheel angle used by the $\mathcal{L}_1$ adaptive controller is less than a quarter of the equivalent signal generated by the lead compensator. This results in a smoother ride in the vehicle controlled by the $\mathcal{L}_1$ adaptive controller.

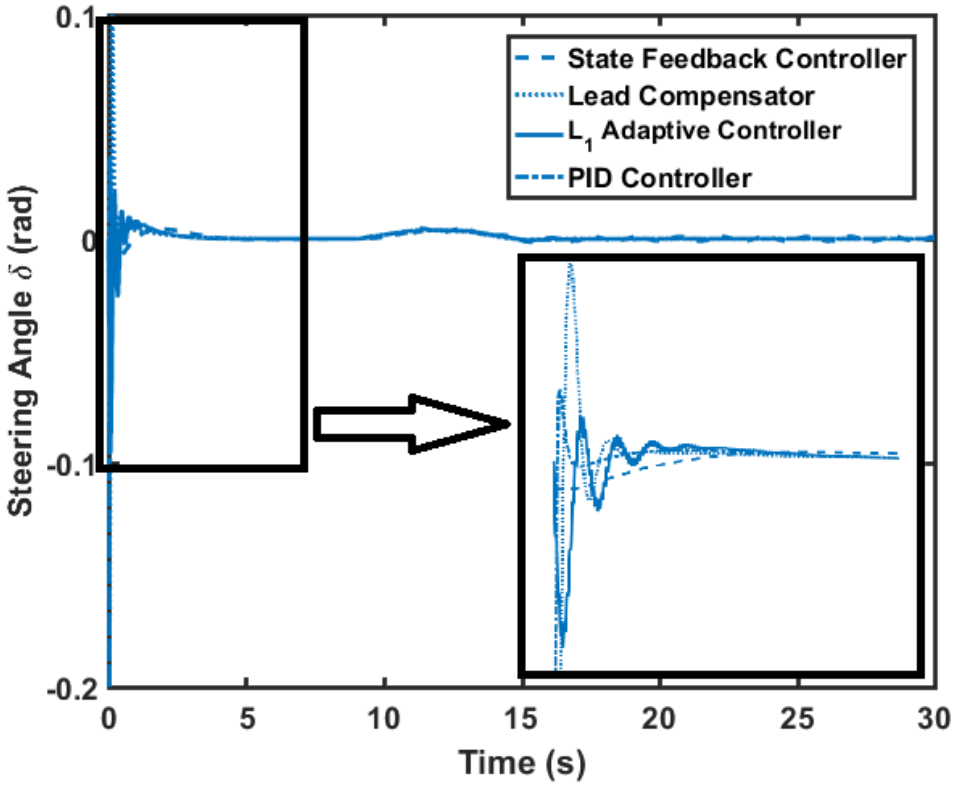

Figure 6.10. Control signal (steering wheel angle) δ of the controllers

Similar simulations were performed on a curved road. The road started with straight line section, then there was a sharp left turn, and at the end, there was a long right turn, as shown in Figure 6.11. The vehicle was one meter off the center of the road at the beginning of the simulations. All the extreme cases of the wind, icy road, and road banking angles explained before are included in this scenario too. As explained before, wind gusts and road banking angle end at $t = 15s$, but the icy section of the road (with

80% drop in the values of cornering stiffness) continues until the end of the simulation ($t = 30s$ and $X = 450m$).

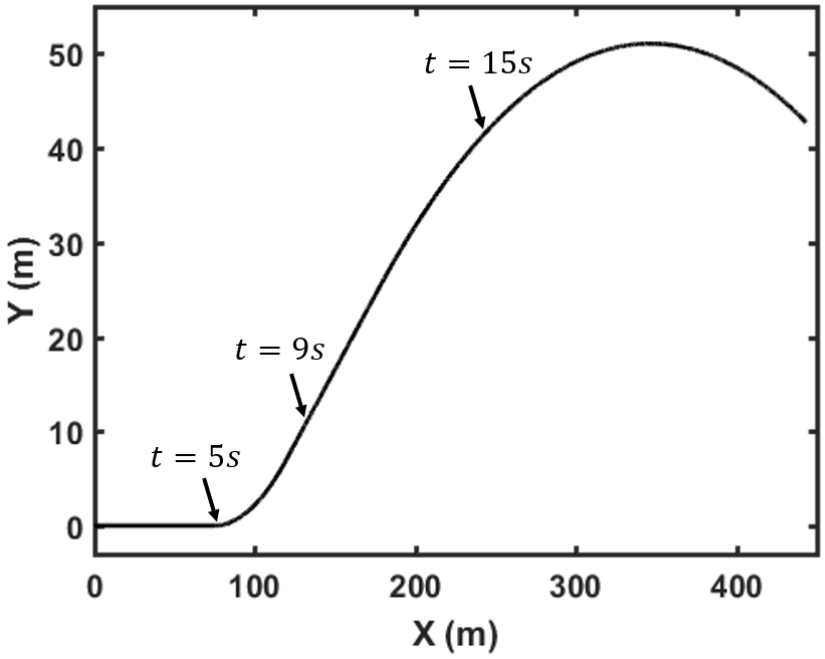

Figure 6.11. Position of the center of the lane in the curved road scenario

The results in Figure 6.12 show the successful performance of the designed $\mathcal{L}_1$ adaptive controller in the presence of all uncertainties and disturbances. The simulation results show that the $\mathcal{L}_1$ controller maintains the vehicle at the center of the lane in all sections of the road. Results shown in Figure 6.9 and Figure 6.12 might suggest that the lead compensator has a faster response. However, it should be considered the $\mathcal{L}_1$ adaptive controller can maintain the vehicle at the center of the lane during the whole simulation, whereas the vehicle controlled by the lead compensator deviates from the lane center at some points. The reader may note that based on Figure 6.5, there is a limitation on the speed of the reference model (the value of m).

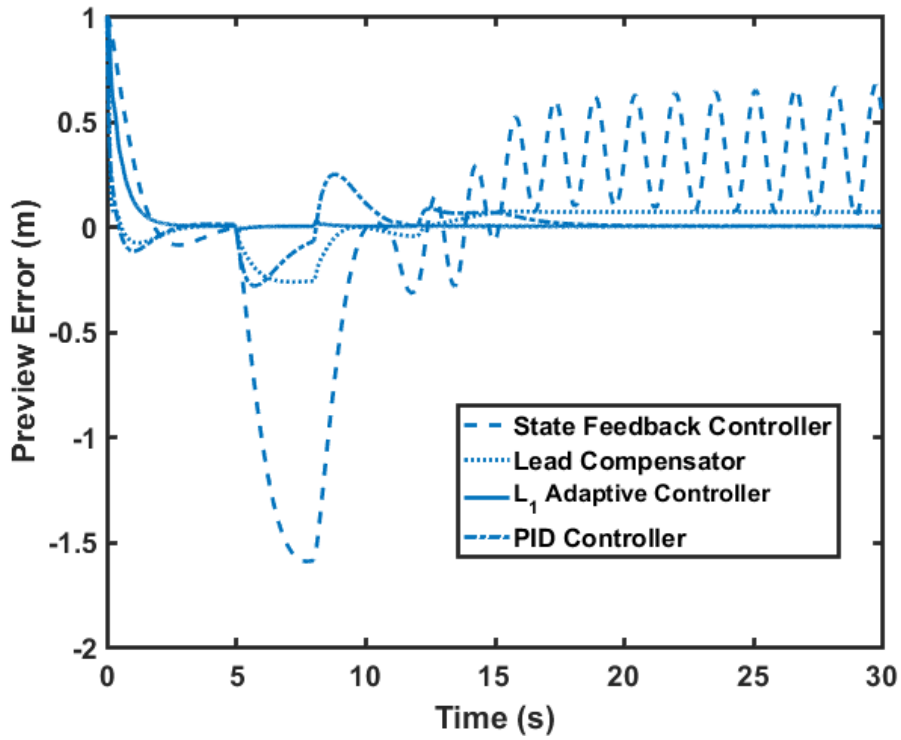

Figure 6.12. Comparison of preview error of vehicle on the curved road

The lateral error, e_1, for all the controllers are shown in Figure 6.13. This figure confirms that the $\mathcal{L}_1$ adaptive controller has the best performance when both the disturbances and the curvy section of the road are added to the simulations. The fact that at the end of simulation the error is not zero is because that section of the road is curved (see Figure 6.11) and the controller is keeping the preview error ($e_1 + d_s\, e_2$) at zero not the lateral error (e_1).

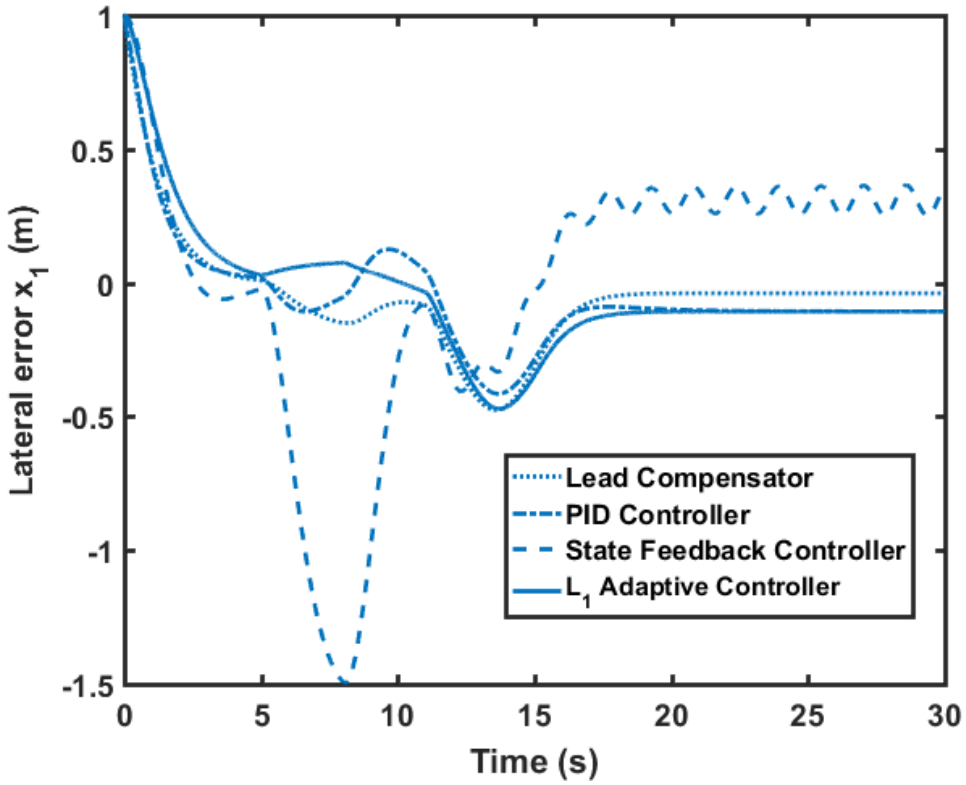

Figure 6.13. Lateral error (x_1) of the vehicle on the curved road

The steering wheel signals (δ) generated by the controllers are shown in Figure 6.14. This figure shows that control signal (steering wheel) generated by $\mathcal{L}_1$ adaptive controller is in the acceptable range. Also, in the beginning of the simulation where there is a significant initial offset from the center of the lane, the lead compensator shows an aggressive behavior which does not exist in the $\mathcal{L}_1$ adaptive controller. The maximum value of the control signal in the lead controller is more than 3.5 times the maximum value of the control signal in the $\mathcal{L}_1$ adaptive controller. In the curvy section of the road, a very small amount of chattering exists in the adaptive control signal, which is negligible compared to similar adaptive controllers. The reason that the chattering is so small in this algorithm is the existence of the low-pass filter in the controller.

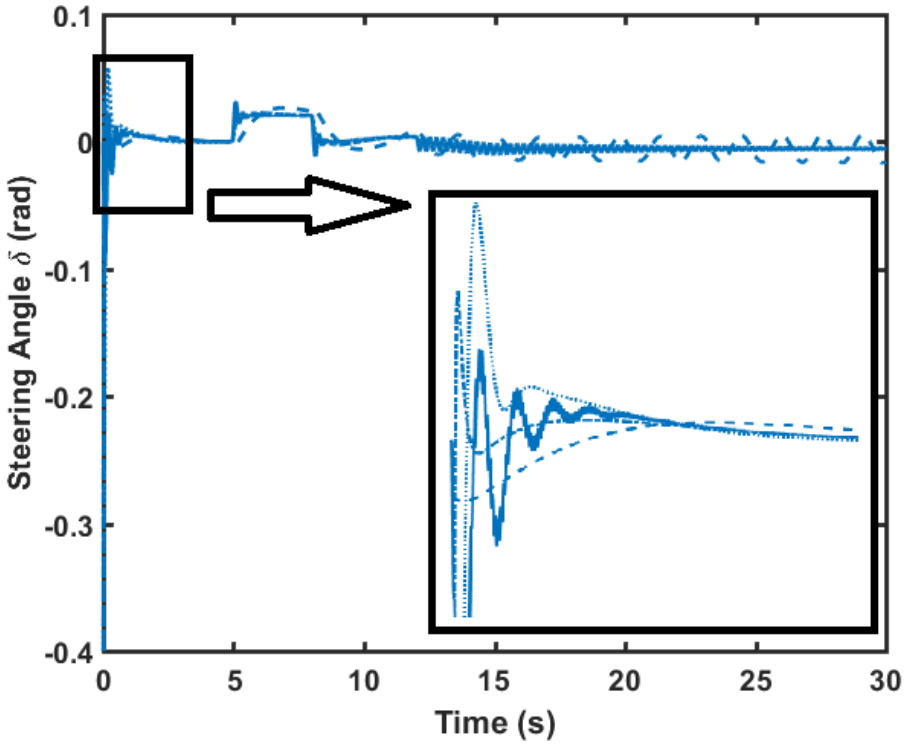

Figure 6.14. Control signal (steering wheel angle) δ on the curved road

In order to make the simulations more realistic, measurement noise is added to the simulations, and the last experiment is repeated. A normally (Gaussian) distributed random signal with zero mean and standard deviation equal to 0.05 is added to all the output/state measurements. Similar results to Figure 6.12 are obtained (see Figure 6.15). The results from the state feedback controller are not included in this figure because adding noise made the response of that controller unstable.

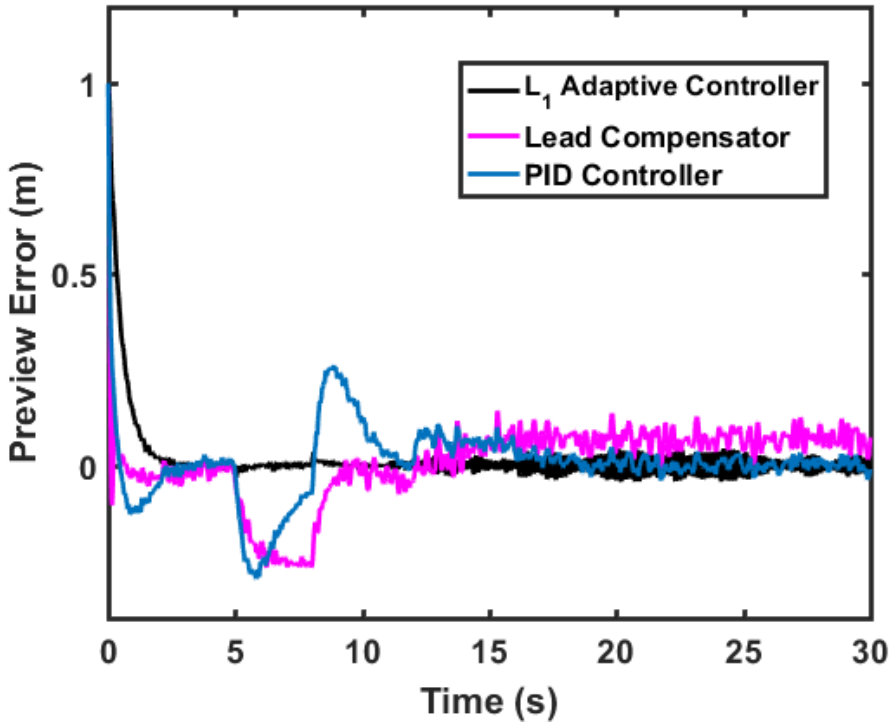

Figure 6.15. Comparison of preview error when measurement noise is added

6.4. Conclusion

$\mathcal{L}_1$ adaptive control algorithm was utilized in this chapter to design a controller for the lateral dynamics of the vehicle. Assuming the states of the system cannot be measured, an output feedback version of the algorithm was designed in this study, which makes the implementation of the controller easier. In order to test the robustness of the controller, a scenario including strong wind gusts and road banking (in the same direction of the wind) was considered. In addition, it was assumed that as soon as the wind gusts start, the road condition deteriorates and becomes icy, resulting in 80% change in the values of cornering stiffness parameters, the parameters which have the most significant effect on the vehicle dynamics. Finally, measurement noise was considered to make the simulations more realistic.

The simulation results show that the designed lateral control algorithm has excellent robustness and disturbance rejection capability. In the challenging scenarios considered here, the conventional state feedback controller failed to keep the vehicle in

the center of the lane, and the more robust lead compensator brought the lateral preview error back to zero after some deviation. However, the proposed algorithm kept error very close to zero at all simulation time, for both straight and curved roads.

Although we designed controllers to maintain the vehicle at the center of the lane in different conditions, in a fully autonomous vehicle, we need to control the longitudinal motion of the car too. Whereas vehicle lateral control only depends on each individual car and its position relative to the road reference, longitudinal control adds the complication of other vehicles driving in front of the vehicle with different speeds. In the next chapter, we design longitudinal controllers, combine them with the presented lateral controllers, and implement the overall system on our driving simulator.

Chapter 7.

Integrated Vehicle Control System

In the last two chapters, we studied and presented state-of-the-art lateral controllers for autonomous and driver-assisted vehicles. However, in any driving scenario, the driver is engaged in another fundamental control action: longitudinal control. The main aim of this chapter is to address the problem of longitudinal control and integrate it with the lateral controller. We will also implement the overall system on the driving simulator (described in Chapter 3).

7.1. Longitudinal Control

The longitudinal control is referred to a combination of control of a vehicle headway (vehicle-following) on the road, avoiding rear-end collision, and keeping safe distance with other road users. Some examples of the controlled variables are the distance from the preceding vehicle, the velocity of the vehicle, and the longitudinal acceleration. The actuating signals in these systems are accelerator (gas, throttle) and brake signals. Some of the familiar examples of the longitudinal control systems are cruise control (standard, adaptive, or cooperative), collision avoidance, and automated highway systems (platoons). Among other benefits and motivations for the longitudinal control systems studies are enhancing the ride comfort, improving highway safety, and reducing highway traffic congestions.

7.1.1. Vehicle Longitudinal Dynamics

The longitudinal forces acting on a vehicle on an inclined road are shown in Figure 7.1. These forces include gravity ($mg\sin(\theta)$), aerodynamic drag forces (F_{aero}), rolling resistance (R_{xf} and R_{xr}), and longitudinal tire forces (F_{xf} and F_{xr}). Considering m as the mass of the vehicle and θ as the angle of inclination of the road, the equation can be written as

$$m\ddot{x} = F_{xf} + F_{xr} - F_{aero} - R_{xf} - R_{xr} - mg\sin(\theta) \qquad (7\text{-}1)$$

The aerodynamic force on a vehicle can be written as

$$F_{aero} = \frac{1}{2}\rho C_d A_F (V_x + V_{wind})^2 \qquad (7\text{-}2)$$

where V_{wind} is the velocity of wind (negative for tailwind), V_x is the velocity of the car, A_F is the frontal area of the car, C_d is aerodynamic drag coefficient, and ρ is the air mass density.

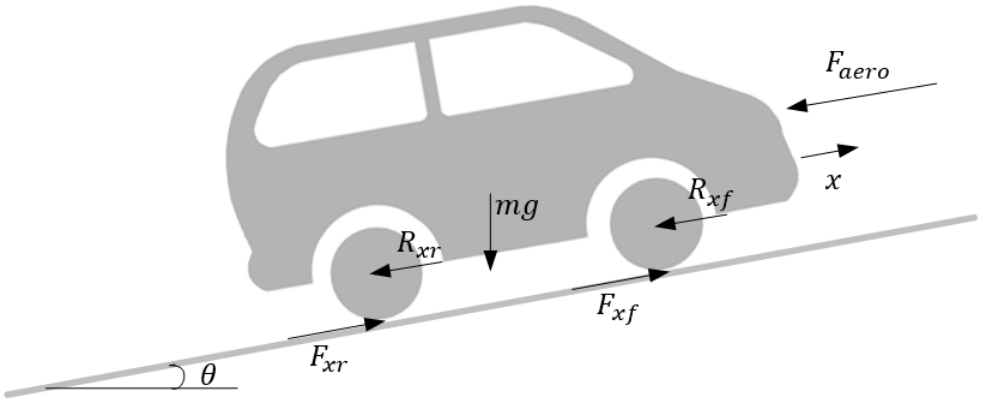

Figure 7.1. Longitudinal forces acting on a vehicle on an inclined road

At a temperature of $15°C$ and pressure of $101.32\ kPa$, the mass density can be considered as $1.225\ kg/m^3$. For a passenger car with a mass in range $800 - 2000\ kg$, the frontal area A_F can be considered as [245]:

$$A_F = 1.6 + 0.00056(m - 765) \qquad (7\text{-}3)$$

When the vehicle is moving, ground friction forces act on tires. These forces are called rear and front longitudinal tire forces F_{xr} and F_{xf}, respectively. In normal driving conditions where the slip ratio is less than 0.1 (dry roads), these forces are proportional to the slip ratio:

$$F_{xf} = C_{\sigma f}\sigma_{xf} \qquad (7\text{-}4)$$

$$F_{xr} = C_{\sigma r}\sigma_{xr} \qquad (7\text{-}5)$$

In the above equations, $C_{\sigma f}$ and $C_{\sigma r}$ are the longitudinal tire stiffness of the tires of the vehicle. Slip ratio (σ_x) is defined as the difference between equivalent rotational velocity of the tire and the actual velocity (longitudinal) of the wheel (V_x). This can be written as:

$$\sigma_x = \frac{r_{eff}\omega_w - V_x}{V_x} \qquad (7\text{-}6)$$

during breaking and

$$\sigma_x = \frac{r_{eff}\omega_w - V_x}{r_{eff}\omega_w} \qquad (7\text{-}7)$$

during acceleration. In the above equations, r_{eff} is the effective radius of the rotating tire and ω_w is the angular velocity of the wheel.

The longitudinal slip ratio in slippery road conditions is greater than 0.1 implying that a linear model may not sufficiently describe the dynamics and nonlinear tire models are employed in such conditions. Some examples of these nonlinear models can be found in [246].

As the tire rotates, due to elasticity, the material is deflected when it goes through the contact patch. Although it springs back after it leaves the contact patch, the energy spent in deforming will not be completely recovered. Rolling resistance force is defined to represent this loss of energy. This force can be modeled as

$$R_{xf} + R_{xr} = f\left(F_{zf} + F_{zr}\right) \qquad (7\text{-}8)$$

where F_z is the normal load on tire, and f is the rolling resistance coefficient. This parameter varies in the range $0.01 - 0.04$. For standard passenger cars with radial tires, it can be considered 0.015 [245].

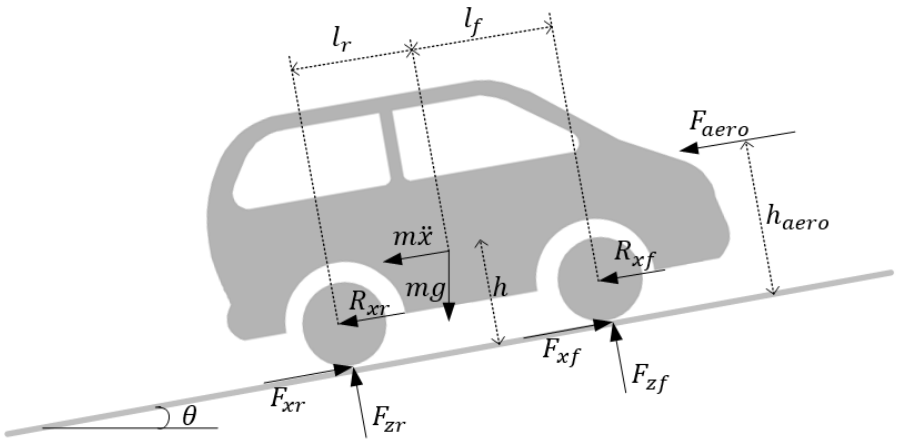

Figure 7.2. Calculation of tire loads

The load on the tire (normal tire forces) depends not only on the weight of the vehicle, but also on the acceleration of the vehicle, fore-aft location of the center of the gravity of the vehicle, aerodynamic drag forces on the car, and inclination of the road. We can write the following equation at the contact point of the rear tire in Figure 7.2:

$$F_{aero}h_{aero} + F_{zf}(l_f + l_r) + mgh\sin(\theta) - mgl_r\cos(\theta) + m\ddot{x}h = 0 \qquad (7\text{-}9)$$

where l_f and l_r are the longitudinal distances of front and rear axles from the center of gravity, respectively. Also in the above equation, h is the height of the center of gravity, and h_{aero} is the height of the point at which equivalent aerodynamics force acts. Similarly, we can write the following equation at the contact point of the front tire in Figure 7.2:

$$-F_{aero}h_{aero} + F_{zr}(l_f + l_r) - mgh\sin(\theta) - mgl_f\cos(\theta) - m\ddot{x}h = 0 \qquad (7\text{-}10)$$

Solving (7-9) and (7-10) for F_{zf} and F_{zr}, respectively, results in

$$F_{zf} = \frac{-F_{aero}h_{aero} - m\ddot{x}h - mgh\sin\theta + mgl_r\cos\theta}{l_f + l_r} \qquad (7\text{-}11)$$

and

$$F_{zr} = \frac{F_{aero}h_{aero} + m\ddot{x}h + mgh\sin\theta + mgl_f\cos\theta}{l_f + l_r} \qquad (7\text{-}12)$$

The above equations imply that when the vehicle accelerates, when the inclination of the road increases, or when the aerodynamic forces increase, the normal loads on the rear and front tires increase and decrease, respectively.

7.1.2. Cruise (Speed) Control

Standard cruise control systems regulate the speed of the vehicle. These systems have a hierarchical structure as shown in Figure 7.3. In this structure, the upper controller sets the desired acceleration. This desired acceleration is obtained by changing the throttle input by the lower controller. The lower controller uses the vehicle dynamics explained in section 7.1.1 and engine maps to determine the required throttle input [247, 248]. The job of the lower controller is to make sure that the vehicle acceleration follows the desired acceleration set by the upper controller system.

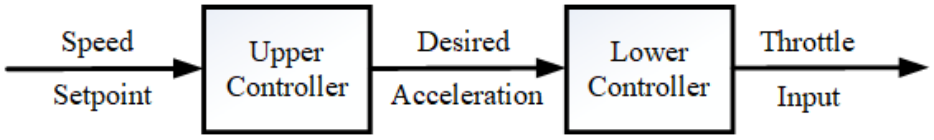

Figure 7.3. Cruise control hierarchical structure

The vehicle longitudinal model considered by the upper controller is

$$\ddot{x} = \frac{1}{\tau s+1}\ddot{x}_{des} \qquad (7\text{-}13)$$

where $\ddot{x}$ and $\ddot{x}_{des}$ are the actual and desired acceleration of the vehicle, respectively. In other words, the acceleration of the car tracks the desired acceleration following a first order system with the time constant τ. In fact, we do not expect the vehicle to track the desired acceleration perfectly. The reason is the limited bandwidth of the lower controller system. A standard value for this time constant is 0.5 which we have used in all the simulations and controller design problems [40].

Upper Level Controller

A simple strategy for the upper controller is the PI control technique. The desired speed can be considered as the set-point, and the difference between the set-point and the actual longitudinal velocity of the car can be considered as the error signal:

$$\ddot{x}_{des}(t) = k_p\left(V_{ref} - V_x\right) + k_I \int_0^t (V_{ref} - V_x)dt \qquad (7\text{-}14)$$

where V_{ref} and V_x are the desired and actual speed of the vehicle, respectively. The parameters of the PI controlller are shown by k_p and k_I. The speed control system using the above controller is depicted in Figure 7.4:

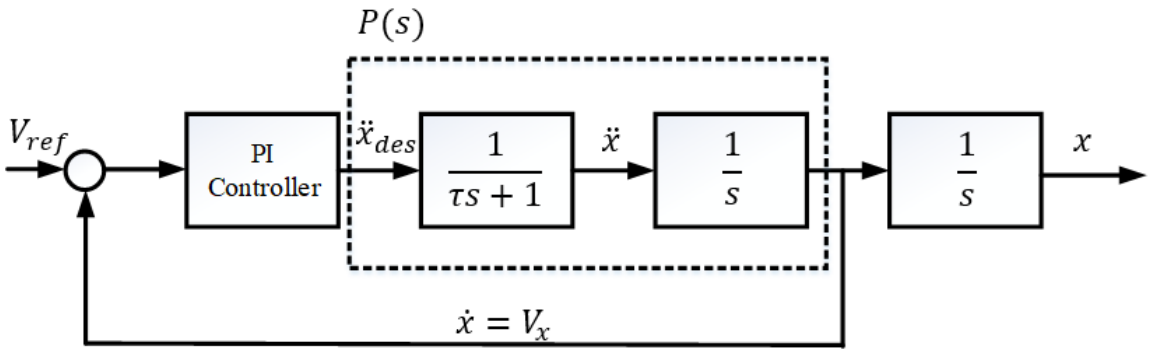

Figure 7.4. Cruise (speed) control system

Define

$$P(s) = \frac{1}{s(\tau s+1)} \qquad (7\text{-}15)$$

and

$$C(s) = k_p + \frac{k_I}{s} \qquad (7\text{-}16)$$

Then, the closed-loop transfer function is

$$\frac{V_x}{V_{ref}} = \frac{PC}{1+PC} = \frac{k_p s+k_I}{\tau s^3+s^2+k_p s+k_I} \qquad (7\text{-}17)$$

Considering $k_I = k_p/4$ (as it is suggested for tuning PI controllers in [249]), and $\tau = 0.5$, the root locus of the system described in (7-17) is plotted for varying k_p (Figure 7.5). This figure shows that the closed-loop is stable for all non-zero values of k_p. For a value of $k_p = 0.9$, the damping ratio is 0.75. The higher gains will result in a smaller damping ratio.

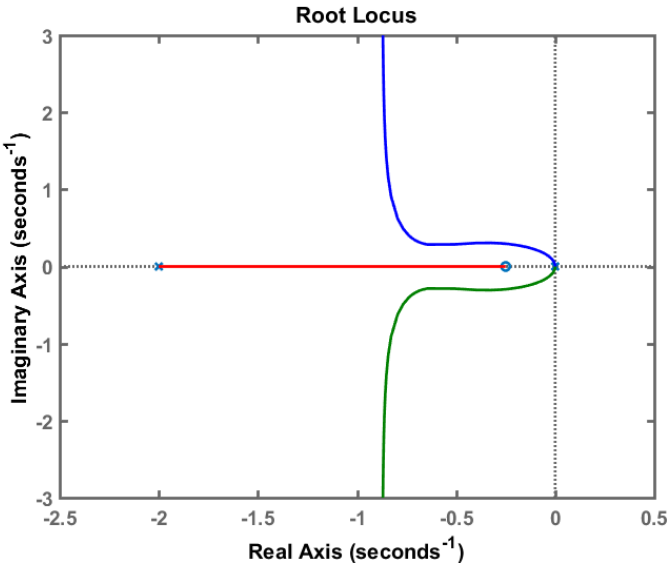

Figure 7.5. Root locus of the cruise control system

A simulation is performed to evaluate the performance of a PI controller for controlling the speed of the vehicle. In this simulation, we have considered the parameter values as $\tau = 0.5$, $k_p = 0.3$, and $k_I = 0.01$. The result of the simulation is shown in Figure 7.6. The reference speed is $20\ m/s$ ($72\ km/h$) in the beginning. It is then changed to $25\ m/s$ ($90\ km/h$). The simulation results show that the PI controller can satisfactorily control the speed of the vehicle.

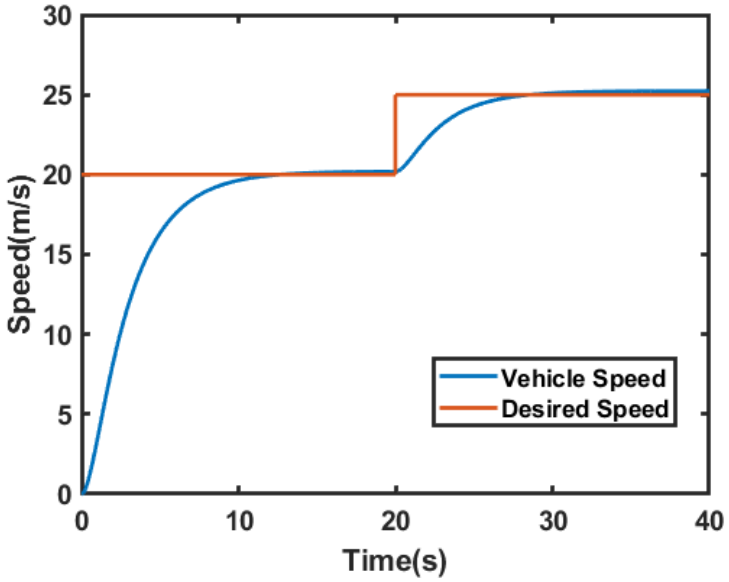

Figure 7.6. Speed control simulation

7.1.3. Adaptive Cruise Control

Adaptive cruise control (ACC) can be considered as one of the main applications of the longitudinal control in autonomous cars. It can also be considered within a driving assistance system configuration. A vehicle, which is equipped with ACC, drives at the desired speed (set by the driver in driver assistance systems, or by the supervisory control of the car in autonomous vehicles) when there is no car in front of the vehicle. If the vehicle's sensor (Radar or Lidar) detects a preceding vehicle, the ACC determines whether the current speed is safe or not. If the detected vehicle is slow or very close (it might come from another lane), the ACC will switch from speed control to spacing control. In this mode, a desired spacing from the preceding vehicle is maintained by manipulation of the accelerator and brake signals.

Based on the definition of ACC above, there will be two modes of operation: speed control which is explained and designed in section 7.1.2, and vehicle following which will be explained in this section. Also, there will be transitional maneuvers between these two modes which will be discussed in section 7.27.2.

In the vehicle following mode, two important specifications should be met: individual vehicle stability, and the string stability when there is a string of ACC vehicles [250].

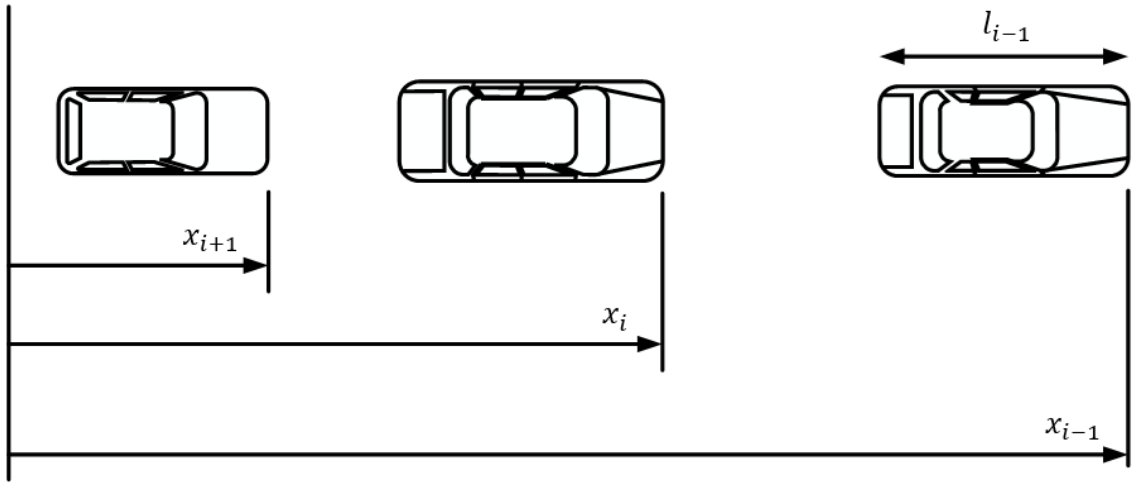

Figure 7.7. String of vehicles in adaptive cruise control

A vehicle is said to have individual vehicle stability if the spacing error converges to zero when the preceding vehicle has a constant speed. Consider the vehicles in Figure 7.7. The spacing error for vehicle i is defined as

$$\delta_i = x_i - x_{i-1} + L_{des} \qquad (7\text{-}18)$$

where L_{des} is the desired spacing. The length of the preceding vehicle l_{i-1} is included in L_{des}. The desired spacing can be constant or, preferably, a function of the longitudinal speed of the vehicle. The system has individual vehicle stability if

$$\ddot{x}_{i-1} \to 0 \Rightarrow \delta_i \to 0 \qquad (7\text{-}19)$$

However, the spacing error will be nonzero when the acceleration of the preceding vehicle is not zero. If the spacing errors of a string of ACC vehicles are guaranteed not to be amplified towards the end of the string, it is referred to as having string stability.

If we consider δ_i and δ_{i-1} as the spacing error of two consecutive cars in a string of ACC vehicles, the transfer function $H(s)$ can be defined as

$$H(s) = \frac{\delta_i}{\delta_{i-1}} \qquad (7\text{-}20)$$

It can be shown that the system has string stability if the following two conditions are satisfied [250]:

$$\|H(s)\|_\infty \leq 1 \qquad (7\text{-}21)$$

$$h(t) > 0 \ \ \forall t \geq 0 \qquad (7\text{-}22)$$

Radar, Lidar, or the other vehicle onboard sensors can only measure the spacing between vehicles, relative velocity, and the vehicle's own velocity. Assuming that the acceleration of the vehicle can be controlled without any delay (instantaneously), a linear control algorithm like

$$\ddot{x}_i = -k_p \delta_i - k_v \dot{\delta}_i \qquad (7\text{-}23)$$

results in

$$\ddot{\delta}_i = \ddot{x}_i - \ddot{x}_{i-1} = -k_p\delta_i - k_v\dot{\delta}_i + k_p\delta_{i-1} + k_v\dot{\delta}_{i-1} \qquad (7\text{-}24)$$

which yields

$$\ddot{\delta}_i + k_v\dot{\delta}_i + k_p\delta_i = k_p\delta_{i-1} + k_v\dot{\delta}_{i-1} \qquad (7\text{-}25)$$

The above closed-loop error dynamics can be shown in the following transfer function that shows how the spacing error is propagated along the string:

$$G(s) = \frac{\delta_i}{\delta_{i-1}} = \frac{k_v s + k_p}{s^2 + k_v s + k_p} \qquad (7\text{-}26)$$

Using $k_p = 1$ and $k_v = 0.5$, the Bode plot in Figure 7.8 can be obtained which shows that the magnitude of transfer function is greater than 1 in some frequencies. Considering the conditions necessary for string stability, this means that the mentioned control law is not string stable.

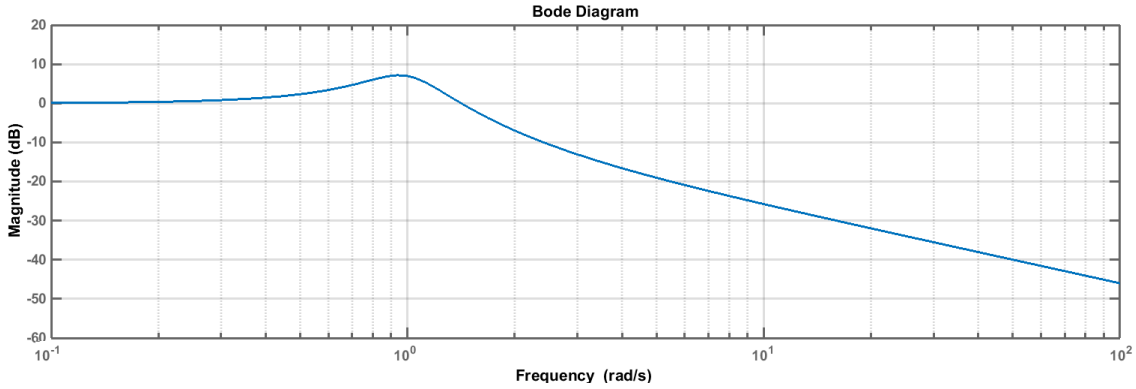

Figure 7.8. Bode plot for constant spacing policy

Although all positive values of k_p and k_v result in individual vehicle stability, no positive values of these parameters can guarantee the magnitude of $G(s)$ be less than one. In order to show this, we write $G(s)$ in (7-26) as

$$G(s) = \left(\frac{k_p}{s^2 + k_v s + k_p}\right)\left(\frac{k_v}{k_p}s + 1\right) = G_1(s)G_2(s) \qquad (7\text{-}27)$$

We know that the magnitude of $G_1(j\omega)$ is less than one if $\frac{k_v}{2\sqrt{k_p}} \geq 0.707$, or

$$k_v \geq 1.414\sqrt{k_p} \qquad (7\text{-}28)$$

The magnitude of $G_2(j\omega)$ is less than one at frequencies up to the resonant frequency $\sqrt{k_p}$, if the frequency $\sqrt{k_p}$ is smaller than the frequency $\frac{k_p}{k_v}$. Therefore, we need to have $\frac{k_p}{k_v} > \sqrt{k_p}$. This can be written as

$$\sqrt{k_p} > k_v \qquad (7\text{-}29)$$

Since the conditions in (7-28) and (7-29) cannot be satisfied at the same time, the magnitude of $G(s)$ will always be more than one at some frequencies, no matter what the values of k_p and k_v are.

The above conclusion implies that using the sensors we have (which include Radar, Lidar, and other onboard sensors that can only measure the spacing between vehicles, relative velocity, and the vehicle's own velocity), string stability cannot be guaranteed using constant spacing policy. The problem can be solved by adding wireless communication between the cars. Since this solution was not an option in this study, we considered constant time-gap policy instead of the constant spacing policy.

In constant time-gap (CTG) policy, the spacing between vehicles depends on the velocity and is not constant:

$$L_{des} = l_{i-1} + h\dot{x}_i \qquad (7\text{-}30)$$

where h is defined as time-gap. The spacing error can be written as

$$\delta_i = x_i - x_{i-1} + l_{i-1} + h\dot{x}_i \qquad (7\text{-}31)$$

The following control algorithm is presented in [251] for this problem.

$$\ddot{x}_{i_{des}} = -\frac{1}{h}(\dot{\varepsilon}_i + \lambda\delta_i) \qquad (7\text{-}32)$$

where

$$\varepsilon = x_i - x_{i-1} + l_{i-1} \qquad (7\text{-}33)$$

Considering (7-33) and differentiating (7-31) we get

$$\dot{\delta}_i = \dot{\varepsilon} + h\ddot{x}_i \qquad (7\text{-}34)$$

Assuming the acceleration of the car equals the desired acceleration ($\ddot{x}_i = \ddot{x}_{i_{des}}$), and substituting it from (7-32) in (7-34), we get the following equation for the error dynamics:

$$\dot{\delta}_i = -\lambda\delta_i \qquad (7\text{-}35)$$

This means δ_i is independent of δ_{i-1} and it approaches to zero if λ is positive. However, this result is obtained assuming that the vehicle can instantaneously follow the desired acceleration ($\tau = 0$ in (7-13)). If the effect of lower controlled is considered, τ would be nonzero in (7-13) and $\ddot{x}_i \neq \ddot{x}_{i_{des}}$. In this case, we have

$$\tau\dddot{x}_i + \ddot{x} = \ddot{x}_{i_{des}} \qquad (7\text{-}36)$$

Substituting (7-32) in (7-36) we get

$$\tau\dddot{x}_i + \ddot{x} = -\frac{1}{h}(\dot{\varepsilon}_i + \lambda\delta_i) \qquad (7\text{-}37)$$

Differentiating twice from (7-31) results in

$$\ddot{\delta}_i = \ddot{\varepsilon}_i + h\dddot{x}_i \qquad (7\text{-}38)$$

Using (7-37) and (7-38), we have

$$\ddot{\varepsilon}_i = \ddot{\delta}_i + \frac{1}{\tau}\left(\dot{\delta}_i + \lambda\delta_i\right) \qquad (7\text{-}39)$$

The term $\delta_i - \delta_{i-1}$, which is the difference between errors of two vehicles next to each other, can be written as

$$\delta_i - \delta_{i-1} = \varepsilon_i - \varepsilon_{i-1} + h(\dot{x}_i - \dot{x}_{i-1}) = \varepsilon_i - \varepsilon_{i-1} + h\dot{\varepsilon}_i \qquad (7\text{-}40)$$

Using (7-39) and (7-40), the dynamic relationship between δ_i and δ_{i-1} can be written as

$$G(s) = \frac{\delta_i}{\delta_{i-1}} = \frac{s+\lambda}{h\tau s^3 + hs^2 + (1+\lambda h)s + \lambda} \qquad (7\text{-}41)$$

It is proved in [250] that the magnitude of the above function (substituting $s = j\omega$) is less than one in all frequencies if and only if

$$h \geq 2\tau \qquad (7\text{-}42)$$

In other words, in order to have the string stability, the time gap should be at least twice the time constant of the lower controller system.

To simulate the explained constant time gap policy for two vehicles, we assume $\tau = 0.5, h = 1, \lambda = 1, l_1 = 5$ and $x_2(0) - x_1(0) = 30$. We consider the speed of the preceding vehicle ($\dot{x}_1$) as shown in Figure 7.9 to have acceleration, constant speed, and deceleration in the simulation.

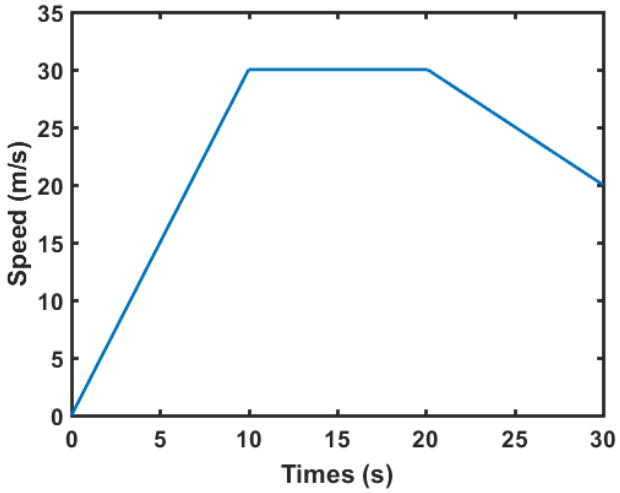

Figure 7.9. The speed of the preceding vehicle

Using the algorithm in (7-32), the spacing error of the following vehicle (δ_2) is obtained (see (7-31)) as shown in Figure 7.10. This figure shows the satisfactory

performance of the algorithm even when the preceding vehicle accelerates or decelerates. This performance can be improved by selecting a higher time-gap.

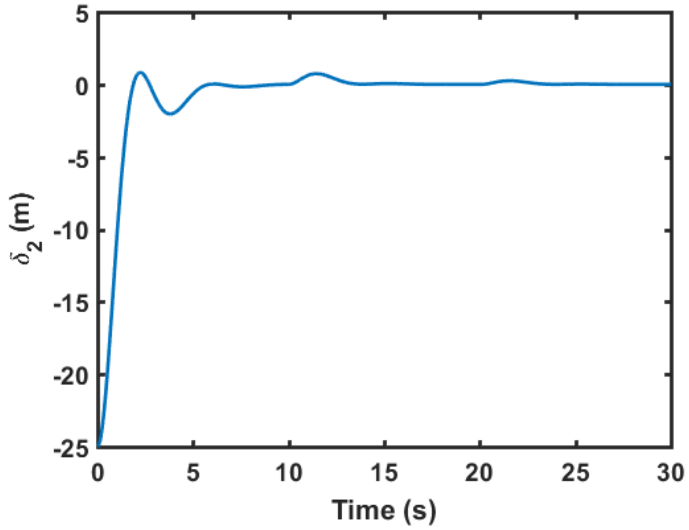

Figure 7.10. Error of longitudinal control system (spacing error) using constant time-gap policy

7.2. Transitions

The vehicle under velocity control might detect a new vehicle because either the new vehicle is slow or cuts from another lane. If ACC decides to change the mode to vehicle following, a transitional trajectory should be designed for the vehicle. On the other hand, when the car is in the vehicle following mode, it might lose the preceding vehicle because it might go faster or move to another lane. The vehicle might switch to velocity control or do a maneuver to follow another vehicle, which needs another transitional trajectory. The necessity of having this transition is explained in the following example.

Suppose the vehicle is working under speed control with the velocity 30 m/s (about 108 km/h). Consider the scenario that it encounters a preceding vehicle in 100 meters ahead which is stopped due to a technical problem. Also consider $\lambda = 1$, $h = 1\ s$ and $L = 5$. If the vehicle wants to switch to vehicle following mode, the initial spacing would be $L + h\dot{x}_i = 35\ m$. However, using (7-31), the initial spacing error is $\delta_i = -65\ m$. In this case, the initial difference between velocities is $\dot{\varepsilon}_i = 30$.

Based on the algorithm shown in (7-32), the initial desired acceleration would be $35\ m/s^2$ which is a big positive value. In other words, the vehicle speed should increase! Even if the vehicle decided to quickly stop at that speed with a braking deceleration of $5\ m/s^2$, it would have needed

$$X = \frac{30^2}{2(5)} = 90m \qquad (7\text{-}43)$$

to stop, which means it could barely prevent an accident with the stalled car. With an acceleration of 35 that was obtained by the mentioned rule, there will be a crash.

The reason for the crash in this example is the fact that ACC without transitional trajectory does not consider that preventing a crash has the highest priority. It also does not consider that a new detected vehicle is not necessary a target vehicle for constant spacing (vehicle following). Therefore, a transitional controller is required to consider these issues.

In this work, we use the transitional trajectories introduced in [252] to solve this problem. When a new target vehicle is detected by Radar/Lidar, the vehicle should decide to choose one of the following actions:

1. Speed control
2. Vehicle following (it should be performed using a well-defined transition trajectory)
3. Braking hard to avoid accident

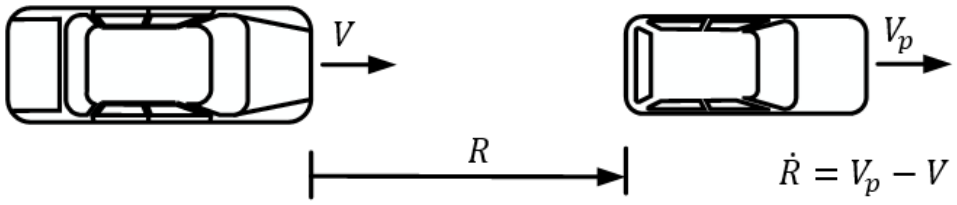

Figure 7.11. Definition of range and range-rate

The $R - \dot{R}$ diagram shown in Figure 7.12 is defined using the following equations:

$$R = x_p - x \qquad (7\text{-}44)$$

$$\dot{R} = V_p - V \qquad (7\text{-}45)$$

where x and V are, respectively, the positon and velocity of the autonomous vehicle and x_p and V_p are, respectively, the positon and velocity of the preceding vehicle. The variables R and $\dot{R}$ are demonstrated in Figure 7.11.

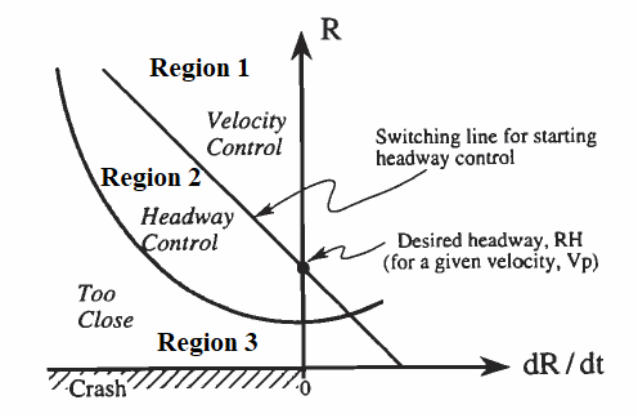

Figure 7.12. Range versus range-rate diagram [252]

When a preceding vehicle is detected, the values of R and $\dot{R}$ and the above figure determine the appropriate action that should be taken by the autonomous car. For example, if the vehicle is in speed control mode and detects a new car in front, if the values of R and $\dot{R}$ are in region 1 of the above figure, the vehicle continues the speed control. In other words, the detected vehicle will not be a target vehicle. The reason can be the high speed of the preceding vehicle (big $\dot{R}$) or considerable distance between the vehicle (big R). In region 2, headway control (vehicle following) will be used. In other words, the detected vehicle will be the target vehicle. Finally, if the values of R and $\dot{R}$ are in region 3, maximum deceleration is necessary to avoid a collision.

Since the horizontal axis is the derivative of the vertical axis in Figure 7.12, R will decrease in the left half of the diagram and it will increase in its right-half. This is shown in Figure 7.13.

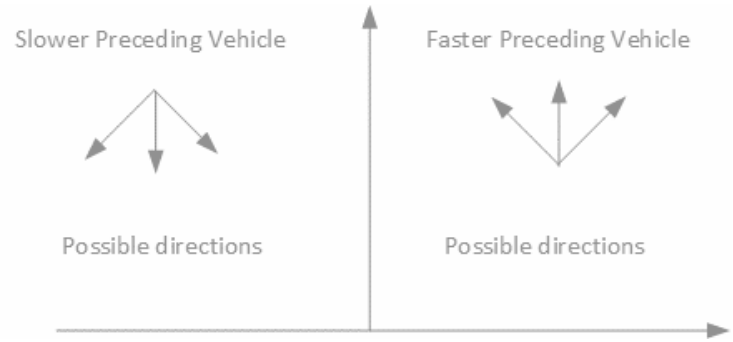

Figure 7.13. Possible motion directions

In the $R - \dot{R}$ diagram in Figure 7.12, there is a switching line which determines when the vehicle should switch from speed control to vehicle following and vice versa. Considering R_{final} as the desired distance between the vehicles, the switching line can be written as

$$R = -T\dot{R} + R_{final} \qquad (7\text{-}46)$$

where T is the slope of the line.

Whenever a new vehicle is detected, if the value of R is greater than the value given by (7-46), the speed control should be activated. In this case, vehicle following would start only when the trajectory reaches the switching line. In other words, the trajectory ABC in Figure 7.14 means that first, the distance between the vehicles is reduced with a constant $\dot{R}$. Then, the desired spacing is obtained on the switching line (7-46). Pay attention that since the value of $\dot{R}$ is negative in the ABC trajectory, R will never be less than R_{final}.

The advantage of the trajectory shown in Figure 7.14 over other trajectories, for example directly going from A to C, is that it avoids sudden braking and abrupt maneuvers as soon as the preceding vehicle is detected. The result of the proposed trajectory will enhance the drivers and passengers comfort.

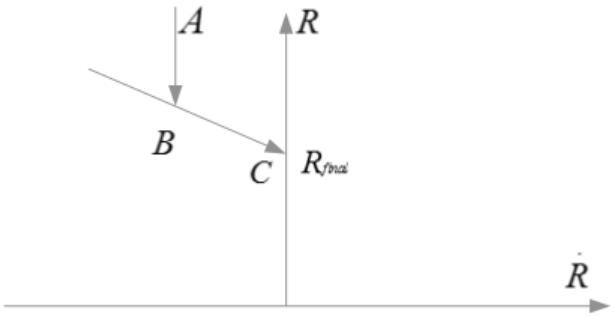

Figure 7.14. Using switching line for smooth transition from speed control to vehicle following

If the preceding vehicle is detected below the switching line, a trajectory similar to the one in Figure 7.15 can be used. When the vehicle brakes, $\dot{R}$ becomes less negative (increases) and the car slows down. The mathematical equation of this parabolic section of the trajectory is given by

$$R = \frac{\dot{R}^2}{2D} + R_{min} \qquad (7\text{-}47)$$

where D is the deceleration of the car. When the switching line is reached, the vehicle will accelerate again and reaches the desired spacing R_{final}. In this case, unlike the previous case, the distance becomes less than the desired distance for a short period of time. R_{min} is the minimum value of the distance in the constant declaration trajectory. This trajectory is shown in Figure 7.15.

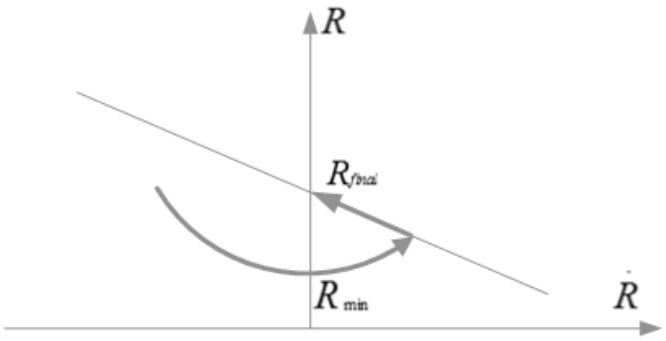

Figure 7.15. Acceleration after constant deceleration

To determine the slope of the switching line, we can use the coasting acceleration, which is the acceleration (deceleration) of the vehicle when there is no throttle and braking. In order to increase the driver comfort, we like the vehicle to reach the desired

following distance (R_{final}) without any braking. Therefore, the slope of the switching line can be calculated using Figure 7.16.

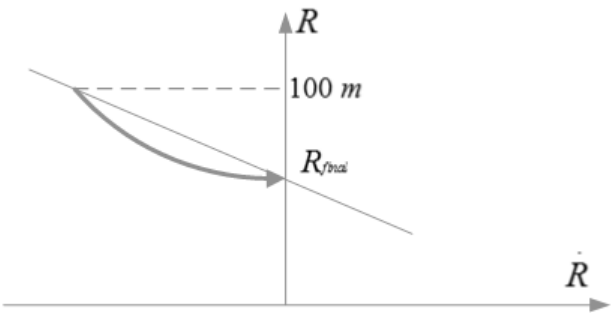

Figure 7.16. Coasting trajectory

We assume $D = 0.4\ m/s^2$ as the deceleration during coasting. We also assume that the maximum range of the sensor is $100m$. In other words, the preceding vehicle will be detected in a $100\ m$ distance. Using the parabola equation in (7-47), the point where the parabola intersects with $R = 100m$ can be obtained. The slope of the line connecting that point and R_{final}, would be the slope of the switching line. For example, if the desired distance between the vehicles is considered as $R_{final} = 30m$, using equation (7-47), we get $\dot{R} = 7.48$. Therefore the switching line passes through points $(-7.48,100)$ and $(0,30)$. This means that the slope of this line is -9.35. The same algorithm can be used for different cars with different coasting accelerations, Radar/Lidar ranges, and the desired final distances.

The reader may also note that we do not need to worry about string stability while executing these transitional maneuvers. The reason is the fact that only the lead car would perform the maneuvers. The rest of the cars in the string of the vehicles do not need to do the transitional maneuvers; they just simply follow the lead vehicle using the constant time-gap policy. The CTG guarantees the string stability of the vehicles in the string.

7.3. Implementation

The final goal of this phase of the project is to implement the designed algorithms on the simulator and, in future, on the processors of an actual autonomous vehicle prototype. The controllers designed in Chapter 5, Chapter 6, and Chapter 7 constitute the *control* subsystem in the autonomous driving system shown in Figure 7.17.

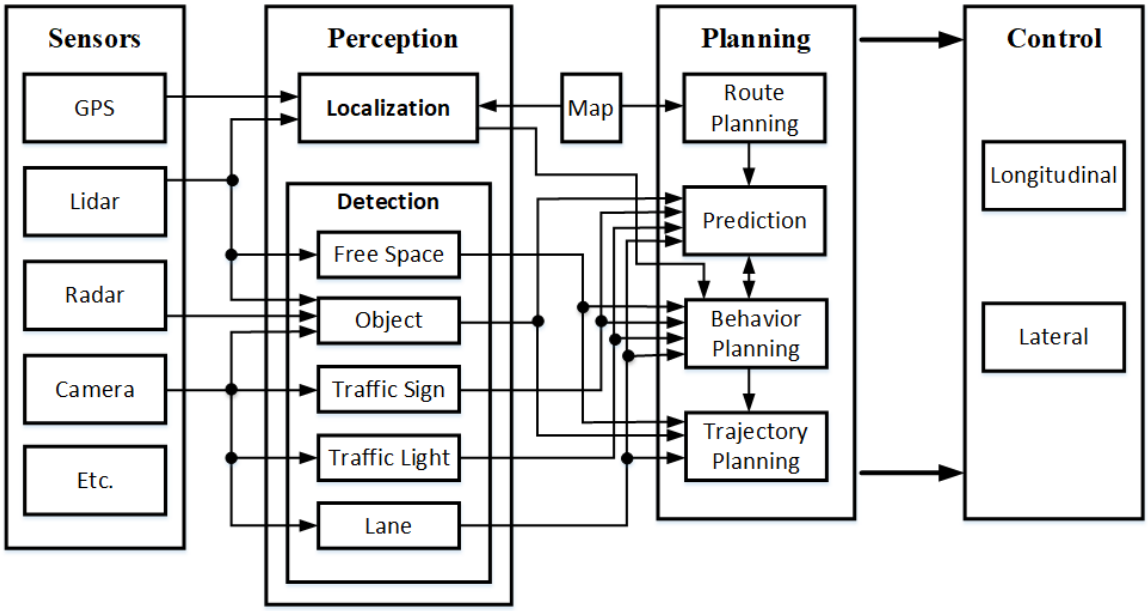

Figure 7.17. Different parts of autonomous driving system

The *sensors* subsystem in Figure 7.17 collects data from the environment. The camera(s) will be mounted on top of the vehicle (facing front), the Lidar will be installed on its roof, and the Radar will be in the bumper. GPS sensor will contribute to the localization algorithm. Other sensors like ultrasonic and inertial measurement unit (IMU) might be added to increase the accuracy of the system.

The *perception* subsystem uses the raw data obtained by the sensors and generates meaningful information from them. The localization section of this subsystem determines where in the world the vehicle is. The precision of GPS is up to a few meters which is less than the precision we need to control the vehicle. Therefore, the GPS data is combined with data coming from the Lidar, and using the map and mathematical localization algorithm the location of the car is determined with a precision of a few centimeters. The detection section of the perception subsystem detects objects in the

environment around the vehicle, traffic signs, traffic lights, free space in front of the vehicle, and road lanes.

The information coming from the perception subsystem helps the *planning* subsystem, to generate the desired trajectory of the vehicle. In this section, In the vehicle predicts the behavior of the other vehicles of the road, considers the traffic signs and lights, takes the distance from lanes into account, and uses the planned route obtained from the map and localization, to generate the desired trajectory.

The *control* subsystem uses the planned trajectory and sensor data to generate the required inputs (acceleration, brake, and steering wheel) to make the vehicle follow that trajectory. Designing this section was our contribution to the project of designing the autonomous vehicle. This task was done using the controllers designed in Chapters 5 to 7.

In order to show the effectiveness of the control algorithms presented in this section, we implemented the controllers on AISL driver simulator, explained in Chapter 3. The algorithms are written in Delphi, and the communication to the simulator is through User Datagram Protocol (UDP). The throttle and brake commands are applied to the vehicle electronically, but the steering command (lateral control) turns the steering wheel of the vehicle physically.

The application of the above control algorithms on the driving simulator is shown here through a driving scenario, as follows:

1) The autonomous vehicle (the red vehicle in the third lane from right shown in Figure 7.18) is driving in the center lane of a highway. Since no object is detected in front of the vehicle, it employs speed control (cruise) algorithms to follow the speed limit of the highway which is 80 km/h. Lateral control algorithms are in effect to keep the vehicle at the center of the lane in the presence of road curves and disturbances including wind.

Figure 7.18. Autonomous driving scenario (part 1)

2) A slower vehicle (the blue vehicle) is detected ahead. Appropriate transition maneuvers are selected by the autonomous vehicle (AV). The speed is reduced so that the constant time gap policy between the two vehicle be followed (Figure 7.19).

Figure 7.19. Autonomous driving scenario (part 2)

3) Since the adjacent lane is empty, AV initiates a lane change by signaling left and following a lane change maneuver (Figure 7.20 and Figure 7.21).

Figure 7.20. Autonomous driving scenario (part 3)

Figure 7.21. Autonomous driving scenario (part 4)

4) The vehicle does not detect any preceding vehicle in the new lane. Therefore, it returns to cruising mode by increases speed and regulating it at 80 km/h. The lane-keeping lateral controller is also back in effect to keep AV at the lane center. After reaching a safe distance ahead of the blue vehicle, AV returns to the third lane.

Figure 7.22. Autonomous driving scenario (part 5)

Figure 7.23. Autonomous driving scenario (part 6)

The diagram showing autonomous vehicle's offset from the road center is shown in Figure 7.24. Wind gusts are added to the simulations as disturbance. Measurement noise are also included to make the results more realistic. The results show that the vehicle was able to perform its task successfully in the presence of disturbances, noises, and road curvature.

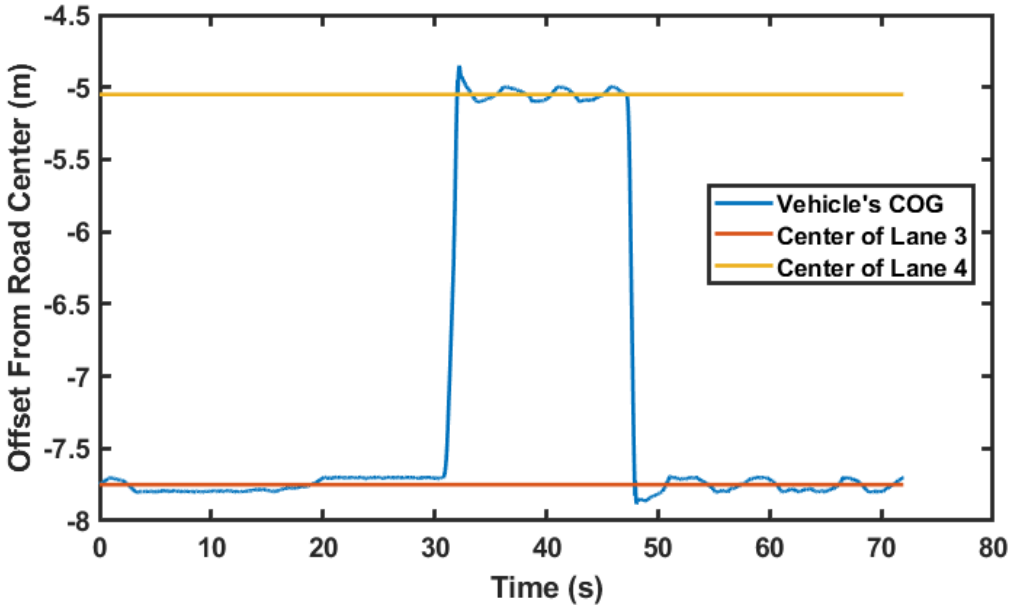

Figure 7.24. AV's offset from the road center in the autonomous driving scenario including wind disturbance and measurement noise

7.4. Conclusion

In this chapter, we presented the dynamic equations governing the longitudinal motion of the vehicle. Based on the longitudinal dynamics, we presented a controller system for the cruise (speed) control. In addition, we investigated different strategies to be considered for adaptive cruise control of the autonomous vehicle in our project and concluded that the constant time gap policy is the most appropriate one to choose. We also considered the transition between speed control and vehicle following modes. The conditions when the vehicle should apply the brake to avoid collision were also described. The designed control algorithms were successfully implemented on a high-quality driving simulator. The integrated longitudinal and lateral controllers could make the vehicle follow the desired trajectories in various scenarios satisfactorily.

Chapter 8.

Conclusion and Future Work

You might think that the first fatal car accident must have happened after Karl Benz built his famous car Patent-Motorwagen in 1886. However, Mary Ward, a scientist, writer, and artist, had the unfortunate privilege of being the first known person to be killed by a car in 1869. Depending on what your definition of a car is, the first recorded nonfatal accident could have happened almost 250 years ago when Nicolas-Joseph Cugnot built the very first 'self-propelled mechanical vehicle' capable of carrying passengers in 1771. When he wanted to show several French officials the ability of the vehicle to carry passengers and cannons for the military, the automobile went out of control and smashed into a garden wall at a speed of only 3 *kph*.

We have come a long way since Cugnot steam car. The automotive industry has significantly improved. Currently, there are more than one billion vehicles in the world. However, there is a dark side to this: the loss of human lives due to car crashes. Technology is being used to alleviate this problem: all car manufacturers have already implemented passive safety systems and active driver assistance systems. In addition, driverless cars are on the verge of becoming a reality. However, there are still many problems regarding driver assistance systems and autonomous driving that need to be addressed.

In this thesis, several vehicle lateral control algorithms are reported and compared. The driver modeling aspect of driver assistance systems is investigated, and a method to detect intoxicated driving is presented. In addition, the idea of adding serial and parallel controllers while the driver is performing the lane keeping task is proposed and discussed.

8.1. Major Contributions

In this thesis, there are six major contributions in the field of intelligent transportations, which are summarized as follows:

- We used system identification techniques and presented two models to describe the lateral control behavior of sober and drunk drivers. In these models, the preview error at 1.25 s ahead of the vehicle was considered as the input to the driver and the steering wheel angle of the vehicle was treated as the driver's output. Different linear model structures were investigated and the ARIMAX structure was chosen as the best structure to describe the behavior of drivers. The 200 sets of data collected in drthe iving simulator were split into two halves: the first half was used only for identification and the second half for validation of the models. The model validations show that the proposed models can successfully predict the behavior of both types of drivers. Also, the residual analysis was performed, and the validity of the model was confirmed.

- We introduced a novel method to detect alcohol-induced driving. We showed that if an ARIMAX model is considered for drivers, the positions of two complex conjugate poles of the models can be indicators of the intoxicated driving behavior. We used online identification techniques to identify and update the model of the drivers while they are driving. We demonstrated that this method could facilitate recognition of sober and intoxicated drivers by checking the poles of the model. This method of identifying DWI drivers not only is useful in detecting alcohol-induced driving but also can be used as a measure to evaluate the performance of the driver. It can also detect any other impairment that might have a similar effect to alcohol on driving behavior.

- The idea of improving the steering action of the driver by a serial controller was presented. In the proposed algorithm, the steering signal coming from the steering wheel is fed to a serial controller. The output of the controller becomes the actual steering of the car. The serial controller was programmed in the driving simulator, and its performance was tested using actual drivers wearing Fatal Vision Goggles. Although the results indicated that the added serial controller makes the erratic behavior of

intoxicated drivers smoother, the study of road departure percentage and lateral position standard deviation evaluation indices showed that the improvement caused by the added serial controller in these aspects is insignificant. The observations agree with driver's adaptation ability and risk homeostasis theory (RHT). The added controller modifies the steering command from the driver before it is fed to the steering wheel. As a result, the driver experiences a new *equivalent vehicle*. Because of the human driver's adaptation ability, the drivers adjust their behavior so that the overall system follows the crossover principle. In spite of what mentioned, the serial controller might have other benefits such as ease of driving, passenger comfort, reducing emissions, and less fuel consumption, which need to be further studied. Another advantage of this system is that, unlike many other driver assistance systems, it does not distract or disengage the driver, which improves safety.

- The idea of improving the steering action of the driver by a parallel controller was presented. In this algorithm, the output of an independent lateral controller is added to the control signal generated by the human driver. The parallel controller was programmed in Matlab and the driving simulator. Both simulation results and human-in-the-loop experiment results showed that the suggested parallel controller structure is effective in improving the lane keeping task when an impaired driver is controlling the vehicle. Therefore, this additional parallel controller can be added to the vehicle when an impaired driver is detected using the algorithm presented earlier in this thesis.

- A novel, simple neural-network controller, which was recently introduced by our group, was used to design a lateral controller. Unlike the most commonly used lateral controller, the new controller was not model-based. In other words, the mathematical model of the vehicle was not necessary to find the controller parameters in this algorithm. The performance of this designed controller was comparable to conventional neural network

controllers. However, the complexity of the proposed method is much less which results in a simpler design procedure and fewer function evaluations for GA optimization of the neural network weights. We also considered a 25% variation in model parameters and demonstrated the robustness of the algorithm using Monte-Carlo analysis.

- $\mathcal{L}_1$ adaptive control algorithm was utilized in this chapter to design a controller for the lateral dynamics of the vehicle. Assuming the states of the system cannot be measured, an output feedback version of the algorithm was designed in this study, which makes the implementation of the controller easier. In order to test the robustness of the controller, a scenario including strong wind gusts and road banking (in the same direction of the wind) was considered. In addition, it was assumed that as soon as the wind gusts start, the road condition deteriorates and becomes icy, resulting in 80% change in the values of cornering stiffness parameters, the parameters which have the most significant effect on the vehicle dynamics. Finally, measurement noise was considered to make the simulations more realistic. The simulation results show that the designed lateral control algorithm has excellent robustness and disturbance rejection capability. In the challenging scenarios considered here, the conventional state feedback controller failed to keep the vehicle in the center of the lane, and the more robust lead compensator brought the lateral preview error back to zero after some deviation. However, the proposed algorithm kept error very close to zero at all simulation time, for both straight and curved roads.

8.2. Suggestions for Future Work

Tackling all the problems of driver assistance systems and driverless cars in one thesis is impossible. Our intention in this work was to propose and improve some algorithms related to intoxicated driving and vehicle lateral control. The following

discussion gives a short summary of some topics that could be studied in future as the next step of this work.

- Detection of driver impairment, especially driver drunkenness, is one of the most important problems in transportation systems and it is very crucial for the safety of all drivers, passengers, and pedestrians. The proposed novel method can be used to develop a warning system for driver impairment as well. However, there is room for further improvement in the future. In this analysis, we used vehicle information (preview error) and vehicle input (steering wheel angle) to detect alcohol impairment. Accelerate and brake signals can also be added to the system to make the detection more accurate. In addition, this information can be used together with the physiological state of the driver to make the DWI detection more precise. Finally, in order to reduce the level of uncertainty, a personalized model of each driver can be used instead of generic models of sober and impaired drivers.

- We studied the performance of the proposed serial controller in maintaining the lateral position of the vehicle in the center of the lane. Preliminary results show that the suggested controller might have other benefits such as ease of driving, passenger comfort, reducing emissions, and less fuel consumption, which need to be further studied. Further studies are required to figure out what kind of serial controllers can address each of the aforementioned problems more effectively.

- The focus of the proposed parallel controller in this thesis was to address intoxicated driving, based on the model obtained in Chapter 3. However, a similar approach could be applied to target driver's fatigue, distraction, inexperience, etc. Modeling the behavior of drivers in each of these cases, and compensating it using the proposed augmented controller can be the subject of future studies.

- The performance of the fused neural network controller can be improved by online adaptation of the connection weights. Since the structure of the controller is simple and the number of connection weights is small, online adaptation is feasible. The algorithm may be enhanced to adjust the connection weights according to the vehicle speed and the tracking error.

- $\mathcal{L}_1$ adaptive control algorithm is a new control structure with guaranteed robustness and fast adaptation. In this study, we considered the *output* feedback version of this method because the sensors that measure the outputs of the lateral control system are easily available. Another version of the algorithm uses *state* feedback in the presence of unmatched uncertainties, which is the case for the lateral control problem. In case all the states of the system are available for measurement, the feasibility of applying this algorithm to the problem could be studied.

- In this study, we used the previously explained driving simulator and also detailed Matlab/Simulink simulations for testing and implementing our developed algorithms. The next logical step is the implementation of these algorithms on a real car.

References

[1] "Crashes vs. Congestion, What is the cost to the society?," American Automobile Association (AAA)2011.

[2] A. Doshi and M. M. Trivedi, "On the roles of eye gaze and head dynamics in predicting driver's intent to change lanes," *IEEE Transactions on Intelligent Transportation Systems*, vol. 10, pp. 453-465, Sep 2009.

[3] A. Amditis, M. Bimpas, G. Thomaidis, M. Tsogas, M. Netto, S. Mammar, *et al.*, "A situation-adaptive lane-keeping support system: Overview of the SAFELANE approach," *IEEE Transaction on Intelligent Transportation Systems*, vol. 11, pp. 617-629, 2010.

[4] K. Murata, E. Fujita, S. Kojima, S. Maeda, Y. Ogura, T. Kamei, *et al.*, "Noninvasive Biological Sensor System for Detection of Drunk Driving," *IEEE Transactions on Information Technology in Biomedicine*, vol. 15, pp. 19-25, 2011.

[5] L.-w. Zhu, Z.-y. Zhang, Z.-j. Bao, and Y. Sun, "Study on the drink driving behavior of drivers in beijing based on the theory of plan behavior," in *LEITS 2010*, 2010, pp. 1-5.

[6] D. Jiangpeng, T. Jin, B. Xiaole, S. Zhaohui, and X. Dong, "Mobile phone based drunk driving detection," in *4th International Conference on Pervasive Computing Technologies for Healthcare (PervasiveHealth)*, Munich, 2010, pp. 1-8.

[7] Y. C. Liu and C. H. Ho, "The effects of different breath alcohol concentration and post alcohol upon drivers driving performance," in *IEEM*, 2007, pp. 505-509.

[8] U. S. D. o. Transportation, "The visual detection of DWI motorists," National Highway Traffic Safety Administration2010.

[9] U. CDC. (2011). *Mobile vehicle safety-impaired driving*. Available: http://www.cdc.gov/motorvehiclesafety/impaired_driving/impaired-drv_factsheet.html

[10] J. Culp, M. El Gindy, and A. Haque, "Driver alertness monitoring techniques: a literature review," *International Journal of Heavy Vehicle Systems*, vol. 15, pp. 255-271, 2008.

[11] D. Das, S. Zhou, and J. D. Lee, "Differentiating Alcohol-induced driving behavior using steering wheel signals," *IEEE Transactions on Intelligent Transportation Systems*, vol. PP, pp. 1-14, 2012.

[12] M. Sakairi, "Water-cluster-detecting breath sensor and applications in cars for detecting drunk or drowsy driving," *IEEE Sensors Journal*, pp. 1078 - 1083, 2011.

[13] Y. Liang, M. L. Reyes, and J. D. Lee, "Real-time detection of driver cognitive distraction using support vector machines," *IEEE Transactions on Intelligent Transportation Systems*, vol. 8, pp. 340-350, 2007.

[14] L. M. Bergasa, J. Nuevo, M. A. Sotelo, R. Barea, and M. E. Lopez, "Real-time system for monitoring driver vigilance," *IEEE Transactions on Intelligent Transportation Systems*, vol. 7, pp. 63-77, 2006.

[15] R. N. Khushaba, S. Kodagoda, S. Lal, and G. Dissanayake, "Driver drowsiness classification using fuzzy wavelet-packet-based feature-extraction algorithm," *IEEE Transactions on Biomedical Engineering,* vol. 58, pp. 121-131, 2011.
[16] T. Toledo, H. N. Koutsopoulos, and M. Ben-Akiva, "Integrated driving behavior modeling," *Transportation Research Part C: Emerging Technologies,* vol. 15, pp. 96-112, 2007.
[17] S. Sekizawa, S. Inagaki, T. Suzuki, S. Hayakawa, N. Tsuchida, T. Tsuda, *et al.*, "Modeling and recognition of driving behavior based on stochastic switched ARX model," *IEEE Transactions on Intelligent Transportation Systems,* vol. 8, pp. 593-606, 2007.
[18] X. Ma and I. Andreasson, "Behavior measurement, analysis, and regime classification in car following," *IEEE Transactions on Intelligent Transportation Systems,* vol. 8, pp. 144-156, 2007.
[19] A. V. Desai and M. A. Haque, "Vigilance monitoring for operator safety: A simulation study on highway driving," *Journal of safety research,* vol. 37, pp. 139-147, 2006.
[20] S. Cherng, C. Y. Fang, C. P. Chen, and S. W. Chen, "Critical Motion Detection of Nearby Moving Vehicles in a Vision-Based Driver-Assistance System," *IEEE Transactions on Intelligent Transportation Systems,* vol. 10, pp. 70-82, 2009.
[21] M. Staubach, "Factors correlated with traffic accidents as a basis for evaluating Advanced Driver Assistance Systems," *Accident Analysis and Prevention,* vol. 41, pp. 1025-1033, 2009.
[22] E. Adell, A. Varhelyi, M. Alonso, and J. Plaza, "Developing human-machine interaction components for a driver assistance system for safe speed and safe distance," *Intelligent Transport Systems (IET),* vol. 2, pp. 1-14, 2008.
[23] A. Doshi, S. Y. H. Cheng, and M. M. Trivedi, "A Novel Active Heads-Up Display for Driver Assistance," *IEEE Transactions on Systems Man and Cybernetics Part B-Cybernetics,* vol. 39, pp. 85-93, 2009.
[24] E. J. Rossetter, J. R. Switkes, and J. C. Gerdes, "Experimental validation of the potential field lanekeeping system," *International Journal of Automotive Technology,* vol. 5, pp. 95-108, 2004.
[25] FHWA, "Roadway Departure Safety," U.S. Department of Transportation 2011.
[26] D. Bevly, X. Cao, M. Gordon, G. Ozbilgin, D. Kari, B. Nelson, *et al.*, "Lane Change and Merge Maneuvers for Connected and Automated Vehicles: A Survey," *IEEE Transactions on Intelligent Vehicles,* vol. 1, pp. 105-120, 2016.
[27] N. Hovakimyan and C. Cao, *L1 Adaptive Control Theory: Guaranteed Robustness with Fast Adaptation* vol. 21: Siam, 2010.
[28] C. Cao and N. Hovakimyan, "Design and analysis of a novel L1 adaptive control architecture with guaranteed transient performance," *IEEE Transactions on Automatic Control,* vol. 53, 2008.
[29] C. Cao and N. Hovakimyan, "adaptive controller for systems with unknown time-varying parameters and disturbances in the presence of non-zero trajectory initialization error," *International Journal of Control,* vol. 81, pp. 1147-1161, 2008/07/01 2008.
[30] M. M. Shirazi and A. B. Rad, "Modeling the steering behavior of intoxicated drivers," in *ITSC*, 2012, pp. 648-653.

[31] M. M. Shirazi and A. B. Rad, "Detection of Intoxicated Drivers Using Online System Identification of Steering Behavior," *Intelligent Transportation Systems, IEEE Transactions on,* vol. 15, pp. 1738-1747, 2014.
[32] M. M. Shirazi, A. B. Rad, and O. Mohareri, "An overriding controller for vehicle lateral control system," in *ICM 2011*, 2011, pp. 128-133.
[33] M. L. Ho, P. T. Chan, A. B. Rad, M. Shirazi, and M. Cina, "A novel fused neural network controller for lateral control of autonomous vehicles," *Applied Soft Computing,* vol. 12, pp. 3514-3525, 11// 2012.
[34] M. M. Shirazi and A. B. Rad, "${{mathcal L}_1}$ Adaptive Control of Vehicle Lateral Dynamics," *IEEE Transactions on Intelligent Vehicles,* vol. 3, pp. 92-101, 2018.
[35] L. Saxton, "Mobility 2000 and the Roots of IVHS," *IVHS review,* pp. 11-26, 1993.
[36] L. Saxton, "PROCEEDINGS OF A NATIONAL WORKSHOP ON IVHS, DALLAS 1990," 1990.
[37] S. E. Shladover, "PATH at 20—History and Major Milestones," *IEEE Transactions on Intelligent Transportation Systems,* vol. 8, pp. 584-592, 2007.
[38] I. Catling, *Advanced Technology for Road Transport: IVHS and Att*: Artech House, Inc., 1993.
[39] R. French and I. America, "A comparison of IVHS progress in the United States, Europe, and Japan," 1993.
[40] A. Eskandarian, *Handbook of intelligent vehicles*. London: Springer, 2012.
[41] S. Singh, "Critical reasons for crashes investigated in the national motor vehicle crash causation survey," 2015.
[42] E. D. Dickmanns and V. Graefe, "Dynamic monocular machine vision," *Machine vision and applications,* vol. 1, pp. 223-240, 1988.
[43] E. D. Dickmanns, "Vehicles capable of dynamic vision," in *IJCAI*, 1997, pp. 1577-1592.
[44] M. Bertozzi, A. Broggi, and A. Fascioli, "Vision-based intelligent vehicles: State of the art and perspectives," *Robotics and Autonomous Systems,* vol. 32, pp. 1-16, 2000/07/31/ 2000.
[45] Q. Chen, U. Ozguner, and K. Redmill, "Ohio State University at the 2004 DARPA Grand Challenge: developing a completely autonomous vehicle," *IEEE Intelligent Systems,* vol. 19, pp. 8-11, 2004.
[46] M. Buehler, K. Iagnemma, and S. Singh, *The 2005 DARPA grand challenge: the great robot race* vol. 36: Springer Science & Business Media, 2007.
[47] S. Thrun, M. Montemerlo, H. Dahlkamp, D. Stavens, A. Aron, J. Diebel, *et al.*, "Stanley: The robot that won the DARPA Grand Challenge," *Journal of field Robotics,* vol. 23, pp. 661-692, 2006.
[48] M. Buehler, K. Iagnemma, and S. Singh, *The DARPA urban challenge: autonomous vehicles in city traffic* vol. 56: springer, 2009.
[49] A. Broggi, P. Cerri, M. Felisa, M. C. Laghi, L. Mazzei, and P. P. Porta, "The VisLab Intercontinental Autonomous Challenge: an extensive test for a platoon of intelligent vehicles," *International Journal of Vehicle Autonomous Systems,* vol. 10, pp. 147-164, 2012.

[50] P. Cerri, G. Soprani, P. Zani, J. Choi, J. Lee, D. Kim, *et al.*, "Computer vision at the Hyundai autonomous challenge," in *Intelligent Transportation Systems (ITSC), 2011 14th International IEEE Conference on*, 2011, pp. 777-783.
[51] F.-Y. Wang, "AI and Intelligent Vehicles Future Challenge (IVFC) in China: From cognitive intelligence to parallel intelligence," in *ITU Kaleidoscope: Challenges for a Data-Driven Society (ITU K), 2017*, 2017, pp. 1-2.
[52] J. Ziegler, P. Bender, M. Schreiber, H. Lategahn, T. Strauss, C. Stiller, *et al.*, "Making Bertha drive—An autonomous journey on a historic route," *IEEE Intelligent Transportation Systems Magazine,* vol. 6, pp. 8-20, 2014.
[53] A. C. Madrigal, "Inside waymo's secret world for training self-driving cars," *The Atlantic,* 2017.
[54] R. Bradley, "Tesla autopilot, the electric-vehicle maker sent its cars a software update that suddenly made autonomous driving a reality," ed: MIT Technology Review. https://www. technologyreview. com/s/600772/10-breakthrough-technologies-2016-teslaautopilot/[Accessed 2016-07-10], 2016.
[55] S. O.-R. A. V. S. Committee, "Taxonomy and definitions for terms related to on-road motor vehicle automated driving systems," *SAE International,* 2014.
[56] A. Simoes, "Older Drivers and Driving Automation," in *International Conference on Applied Human Factors and Ergonomics*, 2017, pp. 1082-1094.
[57] R. Isermann, R. Schwarz, and S. Stolzl, "Fault-tolerant drive-by-wire systems," *Control Systems Magazine, IEEE,* vol. 22, pp. 64-81, 2002.
[58] J. Broughton and C. Baughan, "The effectiveness of antilock braking systems in reducing accidents in Great Britain," *Accident Analysis & Prevention,* vol. 34, pp. 347-355, 2002.
[59] A. Lie, C. Tingvall, M. Krafft, and A. Kullgren, "The effectiveness of ESP (electronic stability program) in reducing real life accidents," *Traffic Injury Prevention,* vol. 5, pp. 37-41, 2004.
[60] R. Isermann, "Diagnosis methods for electronic controlled vehicles," *Vehicle System Dynamics,* vol. 36, pp. 77-117, 2001.
[61] S. E. Shladover, "Review of the State of Development of Advanced Vehicle Control Systems (AVCS)," *Vehicle System Dynamics,* vol. 24, pp. 551-595, 1995/07/01 1995.
[62] S. Tsugawa, M. Aoki, A. Hosaka, and K. Seki, "A survey of present IVHS activities in Japan," *Control Engineering Practice,* vol. 5, pp. 1591-1597, 1997.
[63] A. Vahidi and A. Eskandarian, "Research advances in intelligent collision avoidance and adaptive cruise control," *Intelligent Transportation Systems, IEEE Transactions on,* vol. 4, pp. 143-153, 2003.
[64] R. Bishop and I. ebrary, *Intelligent vehicle technology and trends*: Artech House Norwood, MA,, USA, 2005.
[65] R. Rajamani, *Vehicle Dynamics and Control*: Springer, 2006.
[66] P. Venhovens, J. Bernasch, J. Löwenau, H. Rieker, and M. Schraut, "The application of advanced vehicle navigation in BMW driver assistance systems," *SAE transactions,* vol. 108, pp. 936-945, 1999.
[67] N. H. T. S. A. The U.S. Department of Transportation, "Automotive Collision Avoidance System Field Operational Test," DOT HS 809 886, 2009.

[68] T. Watanabe, N. Kishimoto, K. Hayafune, K. Yamada, and N. Maede, "Development of an Intelligent Cruise Control System," 1995.
[69] O. Carsten and F. Tate, "Intelligent speed adaptation: accident savings and cost-benefit analysis," *Accident Analysis & Prevention*, vol. 37, pp. 407-416, 2005.
[70] K. Isomoto, T. Niibe, T. Suetomi, and T. Butsuen, "Development of a lane-keeping system for lane departure avoidance," 1995.
[71] S. Tokoro, K. Moriizumi, T. Kawasaki, T. Nagao, K. Abe, and K. Fujita, "Sensor fusion system for pre-crash safety system," 2004, pp. 945-950.
[72] R. Moritz, "Pre-crash sensing-functional evolution based on short range radar sensor platform," 2000.
[73] F. R. D. P. o. R.-T. T. I. A. Ministry of Transport and Communications Finland. *Impacts of an automatic emergency call system on accident consequences*. Available: http://www.ecall.fi/eCall_Safety_Effects_Finland_Summary_final_06.pdf
[74] S. E. Shladover, J. VanderWerf, M. Miller, N. Kourjanskaia, and H. Krishnan, "Development and Performance Evaluation of AVCSS Deployment Sequences to Advance from Today's Driving Environment to Full Automation," INSTITUTE OF TRANSPORTATION STUDIES, CALIFORNIA PATH PROGRAM UCB-ITS-PRR-2001-18, 2005.
[75] T. A. Seder, J. F. Szczerba, and D. Cui, "Night vision on full windshield head-up display," ed: Google Patents, 2012.
[76] A. M. Kirson, "Land vehicle multiple navigation route apparatus," ed: Google Patents, 1993.
[77] K. A. Redmill, M. P. Fitz, S. Nakabayashi, T. Ohyama, F. Ozguner, U. Ozguner, *et al.*, "An incident warning system with dual frequency communications capability," in *IEEE IV2003 Intelligent Vehicles Symposium. Proceedings (Cat. No.03TH8683)*, 2003, pp. 552-557.
[78] S. E. Shladover, "Recent international activity in cooperative vehicle–highway automation systems," 1055-1425, 2012.
[79] J. A. Fax and R. M. Murray, "Information flow and cooperative control of vehicle formations," *IEEE transactions on automatic control*, vol. 49, pp. 1465-1476, 2004.
[80] R. H. Miller and A. L. Tascillo, "Blind spot warning system for an automotive vehicle," ed: Google Patents, 2005.
[81] E. Dagan, O. Mano, G. P. Stein, and A. Shashua, "Forward collision warning with a single camera," in *Intelligent Vehicles Symposium, 2004 IEEE*, 2004, pp. 37-42.
[82] C.-W. Lo, S.-H. Lin, and H.-C. Wei, "Lane departure warning system," ed: Google Patents, 2013.
[83] O. H. Dagci, D. K. Grimm, V. Sadekar, D. J. Bartz, S. Y. Hermiz, and W. E. Hamilton, "Vehicle speed monitoring system," ed: Google Patents, 2009.
[84] A. Lie, C. Tingvall, M. Krafft, and A. Kullgren, "The effectiveness of electronic stability control (ESC) in reducing real life crashes and injuries," *Traffic injury prevention*, vol. 7, pp. 38-43, 2006.
[85] M. Braennstroem, L. Helgesson, and M. Christiansson, "Brake assist system," ed: Google Patents, 2012.
[86] B. O. Hall, "Collision avoidance system," ed: Google Patents, 2001.

[87] P. Nilsson, P. Harda, A. Axelson, and S. Berge, "Method and system of a vehicle for reversible seat belt retraction," ed: Google Patents, 2016.
[88] M. Segata and R. L. Cigno, "Automatic emergency braking: realistic analysis of car dynamics and network performance," *IEEE Transactions on Vehicular Technology*, vol. 62, pp. 4150-4161, 2013.
[89] K. J. Pavlov and S. M. Stachowski, "Adaptive seat belt tensioning system," ed: Google Patents, 2004.
[90] K. Mori, A. Nagata, Y. Sato, and Y. Mizuno, "Pedestrian airbag system," ed: Google Patents, 2008.
[91] A. Tanaka, Y. Masuda, and Y. Matsuzaki, "Pedestrian airbag apparatus," ed: Google Patents, 2015.
[92] J. A. Musiol, L. M. Norgan-Curtiss, and M. D. Wilkins, "Control and application of intelligent restraint systems," SAE Technical Paper 0148-7191, 1997.
[93] H. Kurtaran, A. Eskandarian, D. Marzougui, and N. Bedewi, "Crashworthiness design optimization using successive response surface approximations," *Computational mechanics*, vol. 29, pp. 409-421, 2002.
[94] B. Witte, "Side airbag safety arrangement for vehicle occupants," ed: Google Patents, 1994.
[95] X. Zhang, X. Jin, Y. Li, and G. Li, "Improved design of the main energy-absorbing automotive parts based on traffic accident analysis," *Materials & Design*, vol. 29, pp. 403-410, 2008.
[96] R. Oorni and A. Goulart, "In-Vehicle Emergency Call Services: eCall and Beyond," *IEEE Communications Magazine*, vol. 55, pp. 159-165, 2017.
[97] A. Montague, "Direct dispatcherless automatic vehicle-to-vehicle and non-vehicle to vehicle police/emergency medical service notification system for life threatening accidents, hijackings, thefts and medical emergencies," ed: Google Patents, 2003.
[98] S.-A. R. Databases. (2011). *Driver assistance systems report*. Available: http://www.supplierbusiness.com/reportpublish/reports_endpoint.aspx?id=202
[99] J. Zhang, F. Y. Wang, K. Wang, W. H. Lin, X. Xu, and C. Chen, "Data-Driven Intelligent Transportation Systems: A Survey," *IEEE Transactions on Intelligent Transportation Systems*, vol. 12, pp. 1624-1639, 2011.
[100] S. h. An, B. H. Lee, and D. R. Shin, "A Survey of Intelligent Transportation Systems," in *2011 Third International Conference on Computational Intelligence, Communication Systems and Networks*, 2011, pp. 332-337.
[101] K. N. Qureshi and A. H. Abdullah, "A survey on intelligent transportation systems," *Middle-East Journal of Scientific Research*, vol. 15, pp. 629-642, 2013.
[102] K. Bengler, K. Dietmayer, B. Farber, M. Maurer, C. Stiller, and H. Winner, "Three decades of driver assistance systems: Review and future perspectives," *IEEE Intelligent Transportation Systems Magazine*, vol. 6, pp. 6-22, 2014.
[103] R. Okuda, Y. Kajiwara, and K. Terashima, "A survey of technical trend of ADAS and autonomous driving," in *Proceedings of Technical Program - 2014 International Symposium on VLSI Technology, Systems and Application (VLSI-TSA)*, 2014, pp. 1-4.

[104] B. Paden, M. Čáp, S. Z. Yong, D. Yershov, and E. Frazzoli, "A Survey of Motion Planning and Control Techniques for Self-Driving Urban Vehicles," *IEEE Transactions on Intelligent Vehicles,* vol. 1, pp. 33-55, 2016.
[105] J. Elkind, "A Survey of the Development of Models for the Human Controller," *Progress in Astronautics and Aeronautics,* vol. 13, pp. 623-643, 1964.
[106] D. T. McRuer, "New approaches to human-pilot/vehicle dynamic analysis," DTIC Document1968.
[107] G. Ornstein, "The automatic analog determination of human transfer function coefficients," *Medical and Biological Engineering and Computing,* vol. 1, pp. 377-387, 1963.
[108] A. V. Phatak and G. A. Bekey, "Model of the adaptive behavior of the human operator in response to a sudden change in the control situation," *Man-Machine Systems, IEEE Transactions on,* vol. 10, pp. 72-80, 1969.
[109] J. R. Mclean and E. R. Hoffmann, "Analysis of drivers control movements," *Human Factors: The Journal of the Human Factors and Ergonomics Society,* vol. 13, pp. 407-418, 1971.
[110] P. Sweatman and P. Joubert, "Automobile directional characteristics and driver steering performance," *Vehicle System Dynamics,* vol. 5, pp. 155-170, 1976.
[111] D. H. Weir and D. T. McRuer, "Dynamics of driver vehicle steering control," *Automatica,* vol. 6, pp. 87-98, 1970.
[112] D. H. Weir and D. T. McRuer, "Measurement and Interpretation of DriverVehicle System Dynamic Response," *Human Factors: The Journal of the Human Factors and Ergonomics Society,* vol. 15, pp. 367-378, 1973.
[113] M. Good, "Sensitivity of driver-vehicle performance to vehicle characteristics revealed in open-loop tests," *Vehicle System Dynamics,* vol. 6, pp. 245-277, 1977.
[114] L. D. Reid, "A survey of recent driver steering behavior models suited to accident studies," *Accident Analysis & Prevention,* vol. 15, pp. 23-40, 1983.
[115] K. Guo and H. Guan, "Modelling of Driver/Vehicle Directional Control System," *Vehicle System Dynamics,* vol. 22, pp. 141-184, 1993/01/01 1993.
[116] C. C. MacAdam, "Understanding and modeling the human driver," *Vehicle System Dynamics,* vol. 40, pp. 101-134, 2003.
[117] J. A. Michon, "A critical view of driver behavior models: What do we know, what should we do," *Human behavior and traffic safety,* pp. 485–520, 1985.
[118] R. C. Miall and D. M. Wolpert, "Forward models for Physiological motor control," *Neural Networks,* vol. 9, pp. 1265-1279, 1996.
[119] J. Rix and D. Cole, "Models of human learning applicable to the vehicle steering task," 2002, pp. 683–688.
[120] R. Sutton, "Linear Models," in *Modeling Human Operators In Control System Design,* ed: John Wiley & Sons, 1990, pp. 47-84.
[121] M. Kondo, A. Ajimine, and S. o. A. Engineers, *Driver's Sight Point and Dynamics of the Driver-vehicle-system Related to it*: Society of Automotive Engineers, 1968.
[122] T. Jürgensohn, "Control Theory Models of the Driver," in *Modelling Driver Behaviour in Automotive Environments*, P. C. Cacciabue, Ed., ed: Springer London, 2007, pp. 277-292.

[123] T. Legouis, A. Laneville, P. Bourassa, and G. Payre, "Characterization of dynamic vehicle stability using two models of the human pilot behaviour," *Vehicle System Dynamics,* vol. 15, pp. 1-18, 1986.
[124] T. Legouis, A. Laneville, P. Bourassa, and G. Payre, "Vehicle/pilot system analysis: a new approach using optimal control with delay," *Vehicle System Dynamics,* vol. 16, pp. 279-295, 1987.
[125] M. Mitschke, "Driver-Vehicle-Lateraldynamics under Regular Driving Conditions," *Vehicle System Dynamics,* vol. 22, pp. 483-492, 1993.
[126] A. Apel and M. Mitschke, "Adjusting vehicle characteristics by means of driver models," *International journal of vehicle design,* vol. 18, pp. 583-96, 1997.
[127] D. T. McRuer and E. S. Krendel, "The human operator as a servo system element* 1," *Journal of the Franklin Institute,* vol. 267, pp. 381-403, 1959.
[128] D. T. McRuer, "Mathematical models of human pilot behavior," DTIC Document1974.
[129] D. T. McRuer, R. W. Allen, D. H. Weir, and R. H. Klein, "New results in driver steering control models," *Human Factors: The Journal of the Human Factors and Ergonomics Society,* vol. 19, pp. 381-397, 1977.
[130] E. Donges, "A two-level model of driver steering behavior," *Human Factors: The Journal of the Human Factors and Ergonomics Society,* vol. 20, pp. 691-707, 1978.
[131] M. Mitschke and E. Ahring, "Control loop for driver-vehicle with four wheel steering," *JSAE Review,* vol. 16, pp. 211-211, 1995.
[132] M. Plochl and P. Lugner, "A 3-level driver model and its application to driving simulations," 2000.
[133] J. Edelmann, M. Plochl, W. Reinalter, and W. Tieber, "A passenger car driver model for higher lateral accelerations," *Vehicle System Dynamics,* vol. 45, pp. 1117-1129, 2007.
[134] A. Savkoor and S. Ausejo, "Analysis of driver's steering and speed control strategies in curve negotiation," *Vehicle System Dynamics,* vol. 33, pp. 94-109, 2000.
[135] C. C. MacAdam, "Application of an optimal preview control for simulation of closed-loop automobile driving," *IEEE Transactions on Systems, Man and Cybernetics,* vol. 11, pp. 393-399, 1981.
[136] G. Zadeh, "Neural network and fuzzy logic applications to vehicle systems: literature survey," *International journal of vehicle design,* vol. 18, pp. 132-93, 1997.
[137] Y. Zeyada, E. El-Beheiry, M. El-Arabi, and D. Karnopp, "Driver modeling using Fuzzy Logic controls for human-in-the-loop vehicle simulations," in *Current Advances in Mechanical Design and Production VII*, F. H. Mohamed and M. M. Said, Eds., ed Oxford: Pergamon, 2000, pp. 85-94.
[138] T. Hessburg and M. Tomizuka, "Fuzzy logic control for lateral vehicle guidance," *Control Systems Magazine, IEEE,* vol. 14, pp. 55-63, 1994.
[139] G. Xi and Y. Qun, "Driver—Vehicle—Environment Closed—Loop Simulation of Handling and Stability Using Fuzzy Control Theory," *Vehicle System Dynamics,* vol. 23, pp. 172-181, 1994.

[140] I. Kageyama, "On a new driver model with fuzzy control," *Dynamics of vehicles on roads and on railway tracks,* vol. 23, p. 314, 1992.
[141] U. Kramer and G. Rohr, "A fuzzy model of driver behaviour: computer simulation and experimental results," 1982, p. 31.
[142] F. Di Puccio, P. Forte, M. Guiggiani, and D. Rotti, "Modelling and Simulation of Driver's Control on 4-wheeled Vehicle Dynamics."
[143] J. S. Shim, Y. S. Yoon, S. J. Heo, and Y. M. Yoo, "Closed-loop simulation of a vehicle system with an artificial driver," *Mechanics of Structures and Machines, vol. 23, no. 1,* pp. 87-113, 1995.
[144] C. C. MacAdam and G. E. Johnson, "Application of elementary neural networks and preview sensors for representing driver steering control behaviour," *Vehicle System Dynamics, vol. 24, no. 1,* pp. 3-30, 1996.
[145] T. Fujioka and N. Takubo, "Driver model obtained by neural network system," *JSAE Review,* vol. 12, pp. 82–85, 1991.
[146] A. L. Kornhauser, "Neural network approaches for lateral control of autonomous highway vehicles," in *Vehicle Navigation and Information Systems Conference, 1991,* 1991, pp. 1143-1151.
[147] S. Neusser, J. Nijhuis, L. Spaanenburg, B. Hoefflinger, U. Franke, and H. Fritz, "Neurocontrol for lateral vehicle guidance," *IEEE MICRO,* pp. 57-66, 1993.
[148] D. James, F. Boehringer, K. Burnham, and D. Copp, "Adaptive driver model using a neural network," *Artificial Life and Robotics,* vol. 7, pp. 170-176, 2004.
[149] U. S. NHTSA, "The Visual Detection of DWI Motorists," U.S. Department of Transportation.
[150] J. W. Gardner and P. N. Bartlett, "A brief history of electronic noses," *Sensors and Actuators B: Chemical,* vol. 18, pp. 210-211, 1994.
[151] N. Paulsson, E. Larsson, and F. Winquist, "Extraction and selection of parameters for evaluation of breath alcohol measurement with an electronic nose," *Sensors and Actuators A: Physical,* vol. 84, pp. 187-197, 2000.
[152] W. Yue-cheng, X. Yun-qing, X. Pei, and J. Xiao-wei, "The Design of an Automotive Anti-Drunk Driving System to Guarantee the Uniqueness of Driver," in *Information Engineering and Computer Science, 2009. ICIECS 2009. International Conference on*, 2009, pp. 1-4.
[153] Q. Wu and W. Yu, "A driver abnormality recondition model based on dynamic Bayesian network for ubiquitous computing," in *Advanced Computer Theory and Engineering (ICACTE), 2010 3rd International Conference on*, 2010, pp. V1-320-V1-324.
[154] K. Sakakibara, T. Taguchi, A. Nakashima, T. Wakita, S. Yabu, and B. Atsumi, "Development of a new breath alcohol detector without mouthpiece to prevent alcohol-impaired driving," in *ICVES'08*, 2008, pp. 299-302.
[155] W. Gao, "Design of an Electronic Alcohol Nose Based on MSP430," in *Image and Signal Processing, 2008. CISP '08. Congress on*, 2008, pp. 145-147.
[156] B. Carswell and V. Chandran, "Automated recognition of drunk driving on highways from video sequences," in *ICIP-94.*, 1994, pp. 306-310.
[157] S. Aravind, T. Karthick, and U. Sakthivel, "E-Eyanthra perspiration based drunken driving prevention system," in *4th NISS Conference, 2010*, 2010, pp. 270-274.

[158] J. W. Lee, "A Machine Vision System for Lane-Departure Detection," *Computer Vision and Image Understanding,* vol. 86, pp. 52-78, 2002.
[159] C. R. Jung and C. R. Kelber, "A lane departure warning system based on a linear-parabolic lane model," in *Intelligent Vehicles Symposium, 2004 IEEE,* 2004, pp. 891-895.
[160] C. R. Jung and C. R. Kelber, "A lane departure warning system using lateral offset with uncalibrated camera," in *Intelligent Transportation Systems, 2005. Proceedings. 2005 IEEE,* 2005, pp. 102-107.
[161] C. R. Jung and C. R. Kelber, "Lane following and lane departure using a linear-parabolic model," *Image and Vision Computing,* vol. 23, pp. 1192-1202, 2005.
[162] D. Pomerleau, "RALPH: rapidly adapting lateral position handler," in *Intelligent Vehicles '95 Symposium., Proceedings of the*, 1995, pp. 506-511.
[163] Y. Pan, T. Acarman, and U. Ozguner, "Non-standard safety technology," in *Intelligent Transportation Systems, 2001. Proceedings. 2001 IEEE*, 2001, pp. 1126-1131.
[164] E. J. D. Ogden and H. Moskowitz, "Effects of Alcohol and Other Drugs on Driver Performance," *Traffic Injury Prevention,* vol. 5, pp. 185-198, 2004/09/01 2004.
[165] H. Moskowitz and D. Fiorentino, "A review of the literature on the effects of low doses of Alcohol in driving-related skills," National Highway Traffic Safety Administration2000.
[166] K. Gardels, "Automatic car controls for electronic highways," 1960.
[167] R. E. Fenton and R. J. Mayhan, "Automated highway studies at the Ohio State University-an overview," *Vehicular Technology, IEEE Transactions on,* vol. 40, pp. 100-113, 1991.
[168] J. Guldner, H. S. Tan, and S. Patwardhan, "Analysis of automatic steering control for highway vehicles with look-down lateral reference systems," *Vehicle System Dynamics, vol. 26,* pp. 243-269, 1996.
[169] W.-b. Zhang and R. E. Parsons, "Intelligent roadway reference system for vehicle lateral guidance and control," ed: Google Patents, 1994.
[170] J. Guldner, H.-S. Tan, and S. Patwardhan, *On fundamental issues of vehicle steering control for highway automation*: California PATH Program, Institute of Transportation Studies, University of California, Berkeley, 1997.
[171] D. Farkas, J. Young, B. Baertlein, and U. Ozguner, "Forward-looking radar navigation system for 1997 AHS demonstration," in *Intelligent Transportation System, 1997. ITSC'97., IEEE Conference on*, 1997, pp. 672-675.
[172] J. Manigel and W. Leonhard, "Vehicle control by computer vision," *IEEE Transactions on industrial electronics,* vol. 39, pp. 181-188, 1992.
[173] S. Tsugawa, "Vision-based vehicles in Japan: Machine vision systems and driving control systems," *IEEE Transactions on industrial electronics,* vol. 41, pp. 398-405, 1994.
[174] A. Eidehall, J. Pohl, F. Gustafsson, and J. Ekmark, "Toward autonomous collision avoidance by steering," *IEEE Transactions on Intelligent Transportation Systems,* vol. 8, pp. 84-94, 2007.
[175] U. Lee, J. Jung, S. Jung, and D. H. Shim, "Development of a self-driving car that can handle the adverse weather," *International journal of automotive technology,* vol. 19, pp. 191-197, 2018.

[176] N. Y. Ershadi, J. M. Menéndez, and D. Jiménez, "Robust vehicle detection in different weather conditions: Using MIPM," *PLoS one,* vol. 13, p. e0191355, 2018.
[177] B. G. Rajagopal, N. Vishakraj, N. U. Kumar, and P. Jothivenkatesh, "Vision-based system for counting of moving vehicles in different weather conditions," in *2017 International conference of Electronics, Communication and Aerospace Technology (ICECA)*, 2017, pp. 86-91.
[178] S. Gehrig, N. Schneider, R. Stalder, and U. Franke, "Stereo vision during adverse weather — Using priors to increase robustness in real-time stereo vision," *Image and Vision Computing,* vol. 68, pp. 28-39, 2017/12/01/ 2017.
[179] H. Kawazoe, T. Murakami, O. Sadano, K. Suda, and H. Ono, "Development of a lane-keeping support system," SAE Technical Paper 0148-7191, 2001.
[180] M. Nagai, H. Mouri, and P. Raksincharoensak, "Vehicle lane-tracking control with steering torque input," *Vehicle System Dynamics,* vol. 37, pp. 267-278, 2002.
[181] M. Montiglio, S. Martini, and V. Murdocco, "Development of a lane keeping support system for heavy trucks," in *13th ITS World Congress*, 2006.
[182] S. Ishida and J. E. Gayko, "Development, evaluation and introduction of a lane keeping assistance system," in *Intelligent Vehicles Symposium, 2004 IEEE*, 2004, pp. 943-944.
[183] J. Pohl and J. Ekmark, "Development of a haptic intervention system for unintended lane departure," SAE Technical Paper 0148-7191, 2003.
[184] M. Donath, V. Morellas, T. Morris, and L. Alexander, "Preview Based Control of a Tractor Trailer Using DGPS for Preventing Road Departure Accidents," in *Proceedings of the IEEE Conference on Intelligent Transportaion Stystems*, Boston, MA, 1997.
[185] C. Thorpe, M. Hebert, T. Kanade, and S. Shafer, "The new generation system for the CMU Navlab," in *Vision-based vehicle guidance*, M. Ichiro, Ed., ed: Springer-Verlag New York, Inc., 1992, pp. 30-82.
[186] C. J. Taylor, J. Kosecka, R. Blasi, and J. Malik, "A Comparative Study of Vision-Based Lateral control strategies for Autonomous highway driving," *International Journal of Robotic research,* pp. Vol. 18, No. 5, pp. 442-453, 1999.
[187] J. K. Hedrick, M. Tomizuka, and P. Varaiya, "Control issues in automated highway systems," *Control Systems, IEEE,* vol. 14, pp. 21-32, 1994.
[188] M. L. Ho, P. T. Chan, and A. B. Rad, "Lane change algorithm for autonomous vehicles via virtual curvature method," *Journal of Advanced Transportation,* vol. 43, pp. 47-70, 2009.
[189] M. Tideman, M. C. Van der Voort, B. Van Arem, and F. Tillema, "A Review of Lateral Driver Support Systems," in *Intelligent Transportation Systems Conference, 2007. ITSC 2007. IEEE*, 2007, pp. 992-999.
[190] J. Leonard, J. How, S. Teller, M. Berger, S. Campbell, G. Fiore, *et al.*, "A perception-driven autonomous urban vehicle," in *The DARPA Urban Challenge*, ed: Springer, 2009, pp. 163-230.
[191] H. Mouri and H. Furusho, "Automatic path tracking using linear quadratic control theory," in *Intelligent Transportation System, 1997. ITSC '97., IEEE Conference on*, 1997, pp. 948-953.

[192] C. Ching-Yao and T. Han-Shue, "Feasibility analysis of steering control as a driver-assistance function in collision situations," *Intelligent Transportation Systems, IEEE Transactions on,* vol. 2, pp. 1-9, 2001.
[193] H. Peng and M. Tomizuka, "Preview Control for Vehicle Lateral Guidance in Highway Automation," *Journal of Dynamic Systems, Measurement, and Control,* vol. 115, pp. 679-686, 1993.
[194] M. Canale, L. Fagiano, A. Ferrara, and C. Vecchio, "Vehicle Yaw Control via Second-Order Sliding-Mode Technique," *IEEE Transactions on Industrial Electronics,* vol. 55, pp. 3908-3916, 2008.
[195] M. Schorn, U. Stahlin, A. Khanafer, and R. Isermann, "Nonlinear trajectory following control for automatic steering of a collision avoiding vehicle," in *American Control Conference, 2006,* 2006, p. 6 pp.
[196] M. Nagai, M. Onda, and T. Katagiri, "Simulation of emergency obstacle avoidance situations using genetic algorithm," *JSAE Review,* vol. 18, pp. 158-160, 1997.
[197] X. Wang, M. Fu, H. Ma, and Y. Yang, "Lateral control of autonomous vehicles based on fuzzy logic," *Control Engineering Practice,* vol. 34, pp. 1-17, 1// 2015.
[198] L. Bi, M. Wang, C. Wang, and Y. Liu, "Development of a Driver Lateral Control Model by Integrating Neuromuscular Dynamics Into the Queuing Network-Based Driver Model," *IEEE Transactions on Intelligent Transportation Systems,* vol. 16, pp. 2479-2486, 2015.
[199] S. J. Qin and T. A. Badgwell, "A survey of industrial model predictive control technology," *Control Engineering Practice,* vol. 11, pp. 733-764, 2003.
[200] P. Falcone, F. Borrelli, J. Asgari, H. E. Tseng, and D. Hrovat, "Predictive Active Steering Control for Autonomous Vehicle Systems," *Control Systems Technology, IEEE Transactions on,* vol. 15, pp. 566-580, 2007.
[201] J.-H. Lee and W.-S. Yoo, "An improved model-based predictive control of vehicle trajectory by using nonlinear function," *Journal of Mechanical Science and Technology,* vol. 23, pp. 918-922, 2009/04/01 2009.
[202] S. J. Anderson, S. C. Peters, T. E. Pilutti, and K. Iagnemma, "An optimal-control-based framework for trajectory planning, threat assessment, and semi-autonomous control of passenger vehicles in hazard avoidance scenarios," *International Journal of Vehicle Autonomous Systems,* vol. 8, pp. 190-216, 2010.
[203] I. M. Gregory, E. Xargay, C. Cao, and N. Hovakimyan, "Flight test of L1 adaptive controller on the NASA AirSTAR flight test vehicle," in *AIAA Guidance, Navigation and Control Conference*, 2010, pp. 6.2010-8015.
[204] T. J. Leman, E. Xargay, G. Dullerud, N. Hovakimyan, and T. Wendel, "L1 adaptive control augmentation system for the X-48B aircraft," University of Illinois, 2010.
[205] J. Wang, N. Hovakimyan, and C. Cao, "L1 adaptive augmentation of gain-scheduled controller for racetrack maneuver in aerial refueling," in *AIAA Guidance, Navigation, and Control Conference*, 2009.
[206] J. Wang, C. Cao, N. Hovakimyan, R. Hindman, and D. B. Ridgely, "L1 adaptive controller for a missile longitudinal autopilot design," in *AIAA Guidance, Navigation and Control Conference*, 2008.

[207] Z. Li, N. Hovakimyan, C. Cao, and G.-O. Kaasa, "Integrated estimator and L 1 adaptive controller for well drilling systems," in *American Control Conference, 2009. ACC'09.*, 2009, pp. 1958-1963.
[208] M. A. Ralph, "L1-Adaptive Control for Anesthesia Delivery," 2011.
[209] D. Li, Y. Song, W. Cai, P. Li, and H. R. Karimi, "Wind Turbine Pitch Control and Load Mitigation Using an Adaptive Approach," *Mathematical Problems in Engineering*, vol. 2014, 2014.
[210] Available: http://www.forum8.com/idrive_simulator.htm
[211] D. McCartney, B. Desbrow, and C. Irwin, "Using alcohol intoxication goggles (Fatal Vision® goggles) to detect alcohol related impairment in simulated driving," *Traffic Injury Prevention*, vol. 18, pp. 19-27, 2017/01/02 2017.
[212] J. Jewell and S. Hupp, "Examining the effects of fatal vision goggles on changing attitudes and behaviors related to drinking and driving," *The Journal of Primary Prevention*, vol. 26, pp. 553-565, 2005.
[213] J. C. Fell and R. B. Voas, "The effectiveness of reducing illegal blood alcohol concentration (BAC) limits for driving: Evidence for lowering the limit to .05 BAC," *Journal of Safety Research*, vol. 37, pp. 233-243, 2006/01/01/ 2006.
[214] F. Vision. (2011, 13 Sept. 2013). *Drunk driving prevention*. Available: http://fatalvision.com/
[215] D. L. Strayer, F. A. Drews, and D. J. Crouch, "A comparison of the cell phone driver and the drunk driver," *Human Factors*, vol. 48, pp. 381-391, 2006.
[216] T. Pilutti and A. G. Ulsoy, "Identification of driver state for lane-keeping tasks," *IEEE Transactions on Systems, Man and Cybernetics, Part A: Systems and Humans*, vol. 29, pp. 486-502, 1999.
[217] L. K. Chen and A. G. Ulsoy, "Identification of a driver steering model, and model uncertainty, from driving simulator data," *Journal of Dynamic Systems Measurement and Control-Transactions of the Asme*, vol. 123, pp. 623-629, 2001.
[218] L. Ljung, "Models Of Linear Time-Invariant Systems," in *System Identification : Theory For The User*, 2nd ed Upper Saddle River, NJ: Prentice Hall PTR, 1999, pp. 79-120.
[219] H. Akaike, "A new look at the statistical model identification," *Automatic Control, IEEE Transactions on*, vol. 19, pp. 716-723, 1974.
[220] J. Rissanen, "Modeling by shortest data description," *Automatica*, vol. 14, pp. 465-471, 1978.
[221] L. Ljung, *System identification (2nd ed.): theory for the user*: Prentice Hall PTR, 1999.
[222] R. S. Sharp, D. Casanova, and P. Symonds, "A mathematical model for driver steering control, with design, tuning and performance results," *Vehicle System Dynamics*, vol. 33, pp. 289-326, 2000.
[223] H. Peng and M. Tomizuka, "Lateral control of front-wheel-steering rubber-tire vehicles," *California Partners for Advanced Transit and Highways (PATH)*, 1990.
[224] R. Rajamani, *Vehicle dynamics and control*: Springer Science & Business Media, 2011.
[225] K. J. Åström and T. Hägglund, *PID controllers: theory, design, and tuning* vol. 2: Instrument society of America Research Triangle Park, NC, 1995.

[226] F. Sagberg, S. Fosser, and I.-A. F. Sætermo, "An investigation of behavioural adaptation to airbags and antilock brakes among taxi drivers," *Accident Analysis & Prevention,* vol. 29, pp. 293-302, 1997.
[227] H. Ohno, "Analysis and modeling of human driving behaviors using adaptive cruise control," *Applied Soft Computing,* vol. 1, pp. 237-243, 2001.
[228] R. SUTTON, "Modelling human operators in control system design(Book)," *Taunton, England/New York, Research Studies Press, Ltd./John Wiley & Sons, Inc., 1990, 223,* 1990.
[229] G. J. Wilde, "The theory of risk homeostasis: implications for safety and health," *Risk analysis,* vol. 2, pp. 209-225, 1982.
[230] H. Summala, "Accident risk and driver behaviour," *Safety Science,* vol. 22, pp. 103-117, 1996.
[231] T. W. Hoyes, N. A. Stanton, and R. Taylor, "Risk homeostasis theory: A study of intrinsic compensation," *Safety science,* vol. 22, pp. 77-86, 1996.
[232] C. T. Chen, *Linear System Theory and Design*: Oxford University Press, 2013.
[233] A. V. Oppenheim, A. S. Willsky, and S. H. Nawab, *Signals \& systems (2nd ed.)*: Prentice-Hall, Inc., 1996.
[234] V. Panwar, N. Kumar, N. Sukavanam, and J.-H. Borm, "Adaptive neural controller for cooperative multiple robot manipulator system manipulating a single rigid object," *Applied Soft Computing,* vol. 12, pp. 216-227, 2012/01/01/ 2012.
[235] R. E. Jenkins and B. P. Yuhas, "A simplified neural network solution through problem decomposition: the case of the truck backer-upper," *IEEE Transactions on Neural Networks,* vol. 4, pp. 718-720, 1993.
[236] E. Onieva, J. E. Naranjo, V. Milanés, J. Alonso, R. García, and J. Pérez, "Automatic lateral control for unmanned vehicles via genetic algorithms," *Applied Soft Computing,* vol. 11, pp. 1303-1309, 2011/01/01/ 2011.
[237] A. Moura, R. Rijo, P. Silva, and S. Crespo, "A multi-objective genetic algorithm applied to autonomous underwater vehicles for sewage outfall plume dispersion observations," *Applied Soft Computing,* vol. 10, pp. 1119-1126, 2010/09/01/ 2010.
[238] D. Lawrence, "Handbook of genetic algorithms," *Van No strand Reinhold, New York,* 1991.
[239] S. Huang, K. K. Tan, and K. Z. Tang, *Neural Network Contrl: Theory and Applications (Csi, Control and Signal/Image Processing Series, 3)*: Research Studies Pr, 2004.
[240] A. B. Rad and W. L. Lo, "Predictive PI controller," *International Journal of Control,* vol. 60, pp. 953-975, 1994/11/01 1994.
[241] H. E. Tseng, "Dynamic estimation of road bank angle," *Vehicle System Dynamics,* vol. 36, pp. 307-328, 2001.
[242] C. Cao and N. Hovakimyan, "L1 Adaptive Output Feedback Controller for Systems of Unknown Dimension," *IEEE Transactions on Automatic Control,* vol. 53, pp. 815-821, 2008.
[243] K. J. Åström and B. Wittenmark, *Adaptive control*: Courier Corporation, 2013.
[244] R. Hindman, C. Cao, and N. Hovakimyan, "Designing a High Performance, Stable L1 Adaptive Output Feedback Controller," in *AIAA Guidance, Navigation*

and Control Conference and Exhibit, ed: American Institute of Aeronautics and Astronautics, 2007.
[245] J. Y. Wong, *Theory of ground vehicles*: John Wiley & Sons, 2001.
[246] H. Pacejka, *Tire and vehicle dynamics*: Elsevier, 2005.
[247] S.-B. Choi and P. Devlin, "Throttle and brake combined control for intelligent vehicle highway systems," SAE Technical Paper1995.
[248] J. K. Hedrick, D. Mcmahnon, and D. Swaroop, "Vehicle modeling and control for automated highway systems," *California Partners for Advanced Transit and Highways (PATH)*, 1993.
[249] K. J. Åström and T. Hägglund, *Advanced PID control*: ISA-The Instrumentation, Systems, and Automation Society; Research Triangle Park, NC 27709, 2006.
[250] D. Swaroop and J. K. Hedrick, "String stability of interconnected systems," *Automatic Control, IEEE Transactions on*, vol. 41, pp. 349-357, 1996.
[251] P. A. Ioannou and C. C. Chien, "Autonomous intelligent cruise control," *Vehicular Technology, IEEE Transactions on*, vol. 42, pp. 657-672, 1993.
[252] P. Fancher and Z. Bareket, "Evaluating Headway Control Using Range Versus Range-Rate Relationships," *Vehicle System Dynamics*, vol. 23, pp. 575-596, 1994/01/01 1994.
[253] S. Boyd and L. Vandenberghe, *Convex optimization*: Cambridge university press, 2004.
[254] J.-B. Pomet and L. Praly, "Adaptive nonlinear regulation: estimation from the Lyapunov equation," *Automatic Control, IEEE Transactions on*, vol. 37, pp. 729-740, 1992.

Appendix A.

Projection Operator

Projection based adaptation laws in adaptive control theory are used to prevent parameter drift. The projection operator is explained in this appendix. First, we need to define the convex set and convex function [253]:

A set $\Omega \subseteq \mathbb{R}^n$ is a convex set if for $\forall x, y \in \Omega$, we have

$$\lambda x + (1-\lambda)y \in \Omega, \qquad \forall \lambda \in [0,1].$$

An example of convex and nonconvex sets is shown in Figure A.1.

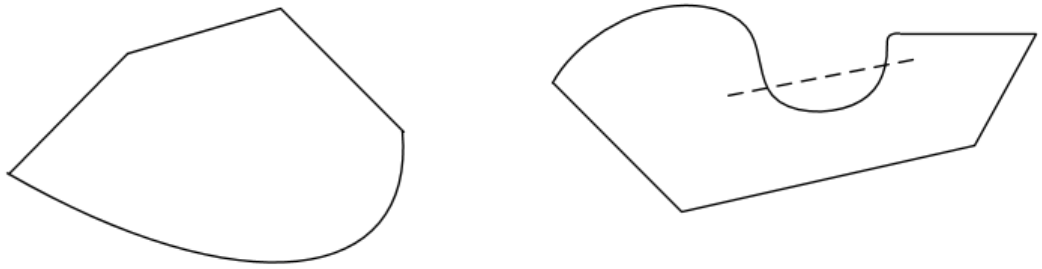

Figure A.1. An example of a convex set (left) and nonconvex set (right)

A function $f: \mathbb{R}^n \to \mathbb{R}$ is a convex function, if for $\forall x, y \in \mathbb{R}^n$, we have

$$f(\lambda x + (1-\lambda)y) \leq \lambda f(x) + (1-\lambda) f(y), \qquad \forall \lambda \in [0,1].$$

An example of a convex function is shown in Figure A.2.

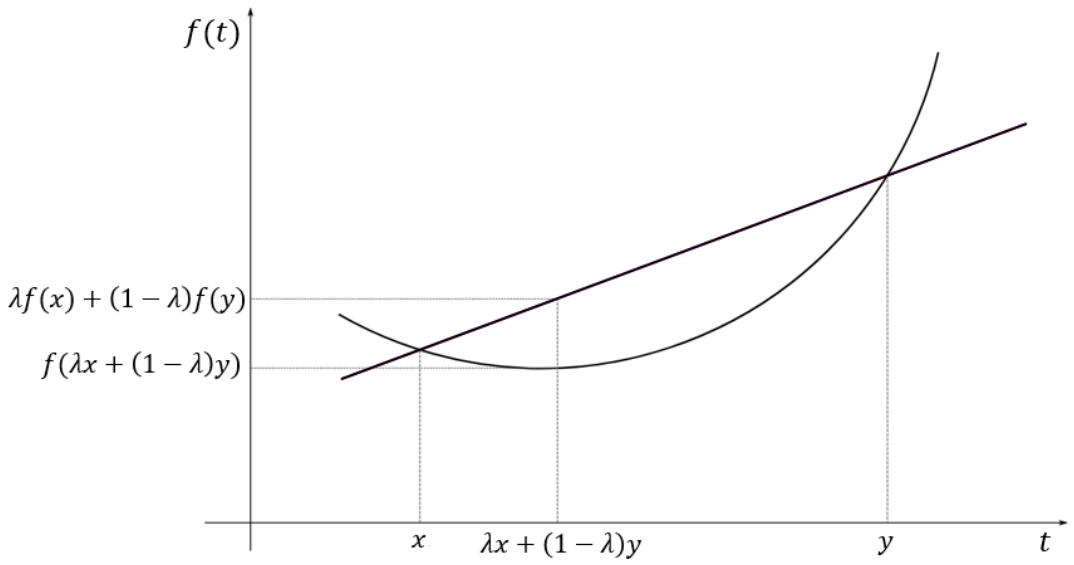

Figure A.2. A sketch of a convex function

Consider a convex set with the following smooth boundary:

$$\Omega_c \triangleq \{\theta \in \mathbb{R}^n | f(\theta) \leq c\}, \qquad 0 \leq c \leq 1$$

where $f: R^n \to R$ is defined as the following convex function

$$f(\theta) = \frac{(\epsilon_\theta + 1)\theta^T\theta - \theta_{max}^2}{\epsilon_\theta \theta_{max}^2}$$

where $\epsilon_\theta > 0$ is the projection tolerance bound and θ_{max} is the norm bound we impose on θ. The definition of the projection operator follows [254]:

$$\text{Proj}(\theta, y) \triangleq \begin{cases} y & \text{if } f(\theta) < 0 \\ y & \text{if } f(\theta) \geq 0 \text{ and } \nabla f^T y \leq 0 \\ y - \frac{\nabla f}{\|\nabla f\|} \langle \frac{\nabla f}{\|\nabla f\|}, y \rangle f(\theta) & \text{if } f(\theta) \geq 0 \text{ and } \nabla f^T y > 0 \end{cases}$$

This definition means that the projection operator does not change y if θ is inside the set $\Omega_0 = \{\theta \in \mathbb{R}^n | f(\theta) \leq 0\}$. However, in $\{\theta \in \mathbb{R}^n | 0 \leq f(\theta) \leq 1\}$, if $\nabla f^T y > 0$, the projection operator subtracts a vector normal to the boundary $\bar{\Omega}_{f(\theta)}\{\bar{\theta} \in \mathbb{R}^n | f(\bar{\theta}) = f(\theta)\}$ so that a smooth transformation from the original vector field y to an inward or

tangent vector field for Ω_1 is obtained. The projection operator is illustrated in Figure A.3.

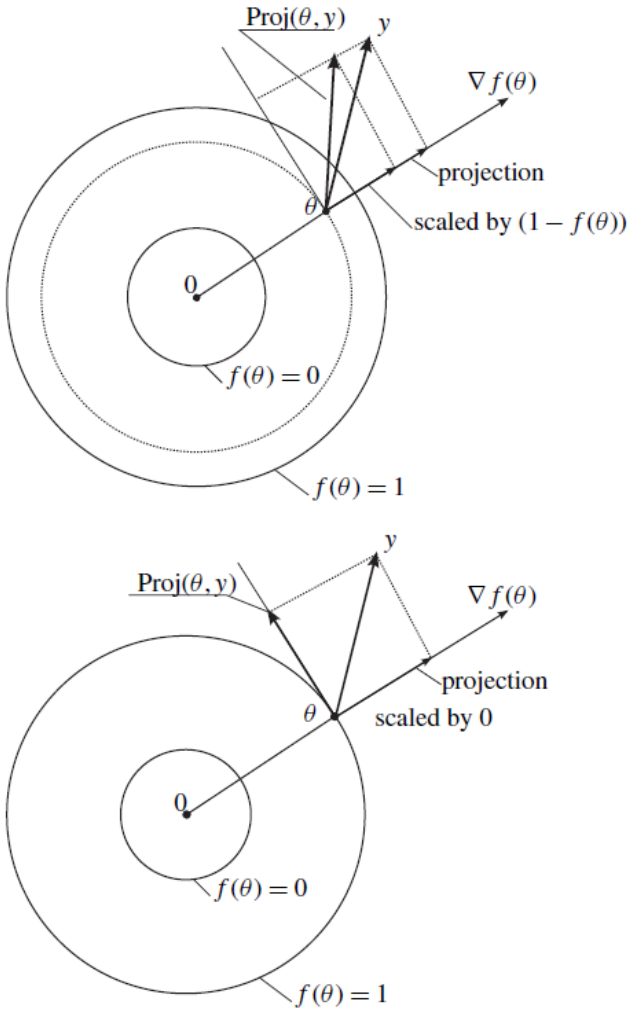

Figure A.3. Projection operator [27]

In adaptive control theory, using this projection operator guarantees the boundedness of adaptive parameters, which is $\hat{\sigma}(t)$ in this work.